UC San Diego

UC San Diego Electronic Theses and Dissertations

Title

The search for quantum criticality near the convergence of hidden order and ferromagnetism

Permalink

https://escholarship.org/uc/item/4gm12483

Author

Butch, Nicholas Patrick

Publication Date

2008

Peer reviewed|Thesis/dissertation

eScholarship.org Powered by the California Digital Library
University of California

UNIVERSITY OF CALIFORNIA, SAN DIEGO

The Search for Quantum Criticality near the Convergence of Hidden Order and Ferromagnetism

A dissertation submitted in partial satisfaction of the
requirements for the degree Doctor of Philosophy
in
Physics

by

Nicholas Patrick Butch

Committee in charge:

Professor M. Brian Maple, Chair
Professor Dimitri N. Basov
Professor Michael M. Fogler
Professor David N. Hendrickson
Professor John C. Wheeler

2008

Copyright
Nicholas Patrick Butch, 2008
All rights reserved.

The dissertation of Nicholas Patrick Butch is approved, and it is acceptable in quality and form for publication on microfilm:

_____

_____

_____

_____

_____

Chair

University of California, San Diego

2008

This manuscript is dedicated to Elizabeth Eileen Butch,
for her patience, support, and optimism.

If we are uncritical we shall always find what we want:
we shall look for, and find, confirmations,
and we shall look away from, and not see,
whatever might be dangerous to our pet theories.
– Karl Popper

The first principle is that you must not fool yourself,
and you are the easiest person to fool.
– Richard Feynman

It is better, of course, to know useless things than to know nothing.
– Lucius Annaeus Seneca

TABLE OF CONTENTS

LIST OF FIGURES

ACKNOWLEDGEMENTS

Many people have contributed to the work presented herein and their assistance is greatly appreciated. First and foremost, the members of the Maple laboratory must be recognized for their collaboration and friendship. I thank my advisor Brian Maple for not just direction in research but exposure to all those other things that a professional physicist has to deal with, and for everything I know about herding cats and keepin' on. Many thanks to everyone else, in particular: Jason Jeffries, for being a congenial sounding board, both on- and off-topic, and on- and off-beer; Ben Taylor, for all those rambling discussions on scaling and superconductivity, and our many trips to Quantum Design; Todd Sayles, for being a great officemate and commiserator over these seven long years; Ryan Baumbach, for sharing my coffee addiction and proclivity for venting; Neil Frederick, for his wit and wisdom; Diego Zocco, for his passionate approach to everything; Dan Scanderbeg, for his cheer and sunny disposition; Johnpierre Paglione, whose enthusiasm for physics inspired me to approach my own research with the same attitude; Pei-Chun Ho, for sharing the frustrations of low-temperature research; Tatsuya Yanagisawa and Bill Yuhasz, for too much of those filled skutterudites; Vivien Zapf and Eric Bauer, for breaking me in; and James Hamlin, for his fresh perspectives on pressure measurements. I've also had the pleasure of working with some talented undergraduates, who have gone on to greater things: many, many thanks to Ben Yukich, without whose able efforts this dissertation would have been much longer and more painful - I could not have found a more affable and talented sample grower if I tried; Columbine Robinson, for enduring my long-winded explanations; Stella Kim, for her friendship during my early years; Colin McElroy, for our weekly banter; and to Eileen Gonzalez and Kevin Huang, who make the best human quasiparticle I've ever met. I wish to also thank our administrative support: Carolyn Rosado and Audrey Morris, whose efforts as Brian's assistant have made it possible to focus on research, and Gary Doran, who fixes all money matters, always has a kind word to say, and some candy stashed somewhere. Oth-

ers around the department have provided invaluable assistance and good advice: physics facilities - Paul Redgate, Jeff Phillips, and Lester Brooks; physics computing - Kevin Smith, Bryan Hill, Chris Camacho, and Lee Davenport; the physics electronics shop - Allen White, Clem Demmitt, George Kassabian, and Mike Rezin; and the physics machine shop - the late Andy Pommer and Bob Parker. Outside of the department, my job was made easier by many people, but particular thanks go to Tad Linfesty and Don Johnson in the Campus Research Machine Shop, and Joe Sullivan at the Isotope Lab. I would also like to thank Sonia Francoual, now at the NHMFL in Los Alamos, for many insightful discussions during our pulsed-field measurements.

A special thanks to my family for believing in me for all these years. Of course, I owe the most to my wife, who has tolerated me through graduate school, and continues to provide support and sympathy in the most trying of times.

Certain parts of this dissertation would not have been possible without the cooperation of generous colleagues. Ben Yukich was responsible for an astounding amount of high-quality sample preparation, and I think we all lament ever letting him leave the laboratory. Todd Sayles performed all of the specific heat measurements and readily provided assistance during the subsequent analysis. Pei-Chun Ho and Tatsuya Yanagisawa performed low-temperature electrical resistivity measurements to determine the superconducting upper critical field curves for some intermediate concentrations. Countless discussions with Jason Jeffries during our pressure studies of URu_2Si_2 have shaped my knowledge and understanding of this material and its history.

Funding for this research was provided by the United States Department of Energy (DOE) and the National Science Foundation. Part of this work overlaps with a project partially funded by the National Nuclear Security Administration under the auspices of the Stewardship Stockpile Academic Alliances program.

VITA

1997-2001	Research Assistant, H. Kojima Group Department of Physics Rutgers University Henry Rutgers Thesis: "Metallic Behavior in Two-Dimensional Electron Systems"
2000	Research Assistant, Bell Laboratories Lucent Technologies, Murray Hill, NJ
2000-2001	Research Assistant, S. H. Garofalini Group Department of Ceramic and Materials Engineering Rutgers University
2001	Bachelor of Science, Ceramic & Materials Engineering Rutgers University
2001	Bachelor of Science, Physics Rutgers University
2001-2002, 2004	Teaching Assistant, Department of Physics University of California, San Diego
2001-2008	Research Assistant, M. B. Maple Group Department of Physics University of California, San Diego
2003	Master of Science, Physics University of California, San Diego
2008	Doctor of Philosophy, Physics University of California, San Diego

PUBLICATIONS

V. V. Krishnamurthy, D. T. Adroja, N. P. Butch, R. Osborn, S. K. Sinha, J. L. Robertson, M. C. Aronson, S. E. Nagler, M. B. Maple,"Magnetic short range correlations and ω/T scaling in the non-Fermi liquid regime of $URu_{2-x}Re_xSi_2$ ($x = 0.2 - 0.6$)," in preparation (2008).

N. P. Butch, J. R. Jeffries, D. A. Zocco, and M. B. Maple, "Hydrostaticity and Hidden Order: Pressure Media in Electrical Transport Studies of URu_2Si_2," submitted to Phys. Rev. B (2008).

Nicholas P. Butch, Todd A. Sayles, Benjamin T. Yukich, and M. Brian Maple, "Suppression of Hidden Order and Emergence of Ferromagnetism in $URu_{2-x}Re_xSi_2$," submitted to MRS Proceedings Sping 2008.

M. Brian Maple, Jason R. Jeffries, Nicholas P. Butch, and Benjamin T. Yukich, "Evolution of Superconducting and Hidden Order Phases in URu_2Si_2 under Applied Pressure," submitted to MRS Proceedings Spring 2008.

P.-C. Ho, N. P. Butch, V. S. Zapf, T. Yanagisawa, N. A. Frederick, S. K. Kim, W. M. Yuhasz, and M. B. Maple, "High field ordered phase and upper critical field of the filled skutterudite system $Pr(Os_{1-x}Ru_x)_4Sb_{12}$," J. Phys.: Condens. Matter 20, 215226 (2008).

P.-C. Ho, T. Yanagisawa, N. P. Butch, W. M. Yuhasz, C. C. Robinson, A. A. Dooraghi and M. B. Maple, "A comparison of the normal and superconducting state properties of $Pr(Os_{1-x}Ru_x)_4Sb_{12}$ and $Pr_{1-x}Nd_xOs_4Sb_{12}$," Physica B 403, 1038 (2008).

J. R. Jeffries, N. P. Butch, B. T. Yukich, M. B. Maple, "The Evolution of the Ordered States of Single Crystal URu_2Si_2 under Pressure," J. Phys.: Condens. Matter 20, 095225 (2008); IOP Select.

N. P. Butch, M. C. de Andrade, and M. B. Maple, "Resource Letter Scy-3: Superconductivity," Am. J. Phys.76, 106 (2008); Virtual Journal of Applications of Superconductvity 14(2), (2008).

J. R. Jeffries, N. P. Butch, B. T. Yukich, M. B. Maple, "Competing Ordered Phases in URu_2Si_2: Hydrostatic Pressure and Re-substitution," Phys. Rev. Lett. 99, 217207 (2007).

R. Wawryk, O. Zogal, A. Pietraszko, S. Paluch, T. Cichorek, W. M. Yuhasz, T. A. Sayles, P. -C. Ho, T. Yanagisawa, N. P. Butch, M. B. Maple, Z. Henkie, "Crystal structure, ^{139}La NMR and transport properties of the As-based filled skutterudites $LaOs_4As_{12}$ and $PrOs_4As_{12}$," J. Alloy. Compd. - in press (2007).

M. B. Maple, Z. Henkie, W. M. Yuhasz, P.-C. Ho, T. Yanagisawa, T. A. Sayles, N. P. Butch, J. R. Jeffries, A. Pietraszko, "Strongly correlated electron phenomena

in Pr-based filled skutterudite compounds." J. Magn. Magn. Mater. 310, 182-187 (2007).

Nicholas P. Butch, Jason R. Jeffries, Benjamin T. Yukich, M. Brian Maple, "Tuning of Hidden Order and Superconductivity in URu_2Si_2 by Applied Pressure and Re Substitution," in Actinides 2006 - Basic Science, Applications and Technology, edited by K. J. M. Blobaum, E. Chandler, L. Havela, M. B. Maple, M. Neu (Mater. Res. Soc. Symp. Proc. 986, Warrendale, PA, 2007), 0986-OO02-03.

M. B. Maple, N. P. Butch, N. A. Frederick, P.-C. Ho, J. R. Jeffries, T. A. Sayles, T. Yanagisawa, W. M. Yuhasz, Songxue Chi, H. J. Kang, J. W. Lynn, Pengcheng Dai, S. K. McCall, M. W. McElfresh, M. J. Fluss, Z. Henkie, and A. Pietraszko, "Field-Dependent Ordered Phases and Kondo Phenomena in the Filled Skutterudite Compound $PrOs_4As_{12}$," Proc. Natl. Acad. Sci. 103, 6783 (2006).

W. M. Yuhasz, N. P. Butch, T. A. Sayles, P.-C. Ho, J. R. Jeffries, T. Yanagisawa, N. A. Frederick, M. B. Maple, Z. Henkie, A. Pietraszko, S. K. McCall, M. W. McElfresh, and M. J. Fluss, "Multiple ordered phases and heavy fermion behavior in the filled skutterudite compound $PrOs_4As_{12}$," Phys. Rev. B 73, 144409 (2006).

M. B. Maple, N. P. Butch, E. D. Bauer, V. S. Zapf, P. C. Ho, S. D. Wilson, P. C. Dai, D. T. Adroja, S. H. Lee, J. H. Chung, J. Lynn, "Non-Fermi liquid behavior and quantum criticality in $Sc_{1-x}U_xPd_3$ and $URu_{2-x}Re_xSi_2$," Physica B: Physics of Condensed Matter 378-380, 911 (2006).

D. E. MacLaughlin, M. S. Rose, J. E. Anderson, O. O. Bernal, R. H. Heffner, G. J. Nieuwenhuys, R. E. Baumbach, N. P. Butch and M. B. Maple, "Effect of annealing on glassy dynamics and non-Fermi liquid behavior in UCu_4Pd," Physica B 374-375, 177 (2006).

M. B. Maple, N. A. Frederick, P.-C. Ho, W. M. Yuhasz, T. A. Sayles, N. P. Butch, J. R. Jeffries and B. J. Taylor, "Novel strongly correlated electron states in filled skutterudite lanthanide osmium antimonides," Physica B 359-361, 830 (2005).

P.-C. Ho, W. M. Yuhasz, N. P. Butch, N. A. Frederick, T. A. Sayles, J. R. Jeffries, M. B. Maple, J. B. Betts, A. H. Lacerda, P. Rogl, G. Giester, "Ferromagnetism and possible heavy-fermion behavior in single crystals of $NdOs_4Sb_{12}$," Phys. Rev. B 72, 94410 (2005).

K. S. Burch, A. Schafgans, N. P. Butch, T. A. Sayles, M. B. Maple, B. C. Sales, D. Mandrus, and D. N. Basov, "Optical Study of Interactions in a d-Electron Kondo Lattice with Ferromagnetism," Phys. Rev. Lett. 95, 046401 (2005).

N. P. Butch, W. M. Yuhasz, P.-C. Ho, J. R. Jeffries, N. A. Frederick, T. A. Sayles, X. G. Zheng, M. B. Maple, J. B. Betts, A. H. Lacerda, F. M. Woodward, J. W. Lynn, P. Rogl, and G. Giester, "Ordered magnetic state in $PrFe_4Sb_{12}$ single crystals," Phys. Rev. B 71, 214417 (2005).

S. D. Wilson, P. Dai, D. T. Adroja, S.-H. Lee, J.-H. Chung, J. W. Lynn, N. P. Butch, and M. B. Maple, "Quantum Critical Scaling and the Origin of Non-Fermi-Liquid Behavior in $Sc_{1-x}U_xPd_3$," Phys. Rev. Lett. 94, 056402 (2005).

E. D. Bauer, V. S. Zapf, P.-C. Ho, N. P. Butch, E. J. Freeman, C. Sirvent, and M. B. Maple, "Non-Fermi-Liquid Behavior within the Ferromagnetic Phase in $URu_{2-x}Re_xSi_2$," Phys. Rev. Lett. 94, 046401 (2005).

W. M. Yuhasz, N. A. Frederick, P.-C. Ho, N. P. Butch, B. J. Taylor, T. A. Sayles, M. B. Maple, J. B. Betts, A. H. Lacerda, P. Rogl, and G. Giester, "Heavy-fermion behavior, crystalline electric field effects, and weak ferromagnetism in $SmOs_4Sb_{12}$," Phys. Rev. B 71, 104402 (2005).

B.-L. Young, D. E. MacLaughlin, M. S. Rose, K. Ishida, O. O. Bernal, H. G. Lukefahr, K. Heuser, G. R. Stewart, N. P. Butch, P.-C. Ho, and M. B. Maple, "Disorder effects near a magnetic instability in $CePtSi_{1-x}Ge_x$ $(x = 0, 0.1)$," Phys. Rev. B 70, 024401 (2004).

N. A. Frederick, T. D. Do, P.-C. Ho, N. P. Butch, V. S. Zapf, and M. B. Maple, "Superconductivity and crystalline electric field effects in the filled skutterudite series $Pr(Os_{1-x}Ru_x)_4Sb_{12}$," Phys. Rev. B 69, 024523 (2004).

R. E. Walstedt, H. Kojima, N. Butch, and N. Bernhoeft, "^{63}Cu nuclear relaxation in the quantum critical point system $CeCu_{5.9}Au_{0.1}$," Phys. Rev. Lett. 90, 067601 (2003).

V. M. Pudalov, M. E. Gershenson, H. Kojima, N. Butch, E. M. Dizhur, G. Brunthaler, A. Prinz, and G. Bauer, "Low-density spin susceptibility and effective mass of mobile electrons in Si inversion layers," Phys. Rev. Lett. 88, 196404 (2002).

M. E. Gershenson, V. M. Pudalov, H. Kojima, N. Butch, E. M. Dizhur, G. Brunthaler, A. Prinz, and G. Bauer, "Crossed magnetic fields technique for studying spin and orbital properties of 2d electrons in the dilute regime," Physica E 12, 585 (2002).

FIELDS OF STUDY

Major Field: Physics

Studies in Strongly Correlated Electron Materials
M. Brian Maple, Bernd T. Matthias Professor of Physics,
University of California, San Diego

ABSTRACT OF THE DISSERTATION

The Search for Quantum Criticality
near the
Convergence of Hidden Order and Ferromagnetism

by

Nicholas Patrick Butch
Doctor of Philosophy in Physics
University of California, San Diego, 2008
Professor M. Brian Maple, Chair

The properties of the heavy fermion superconductor URu_2Si_2 have been investigated as a function of Re substitution. Single crystals of $URu_{2-x}Re_xSi_2$, for $0 \leq x \leq 0.6$, were synthesized via the Czochralski technique and studied through measurements of x-ray diffraction, electrical resistivity, specific heat, and dc magnetization. In accord with previous studies, it has been found that superconductivity is quickly suppressed, while the hidden order state persists up to about $x = 0.1$. Ferromagnetic behavior is observed at intermediate concentrations, for $x > 0.15$, and its properties are consistent with itinerant ferromagnetism. The magnetic ordering transitions, interpreted via a scaled Arrott analysis, are characterized by unconventional exponents, strongly suggesting proximity to a quantum critical point. It is argued that in this system, low-temperature divergence in the specific heat divided by temperature and power-law temperature-dependence of the electrical resistivity, both archetypal characteristics of non-Fermi liquid behavior, may not be related to the ferromagnetic quantum criticality. The x-dependence of these properties and the evolution of the heavy fermion state is discussed in relation to the ordered phases in the $URu_{2-x}Re_xSi_2$ phase diagram.

I

Introduction

I.A Magnetism in Metals

Magnetism in materials is usually attributed to unpaired spins in partially-filled d- or f-electron orbitals of ions, but it can also arise from conduction electrons in a metal. The simplest cases of long-range magnetic order are ferromagnetic (FM) order, with all spins parallel, or antiferromagnetic (AFM) order, with neighboring spins antiparallel. Above the Curie temperature T_C for FM order or the Néel temperature T_N for AFM order, a material is paramagnetic and its magnetic susceptibility $\chi(T)$ is usually well-described by a Curie-Weiss (CW) law, where $\chi = (T - \theta_{CW})^{-1}$ and $\theta_{CW} \approx T_C$ or T_N, depending on its sign. In the absence of magnetic order, the sign of θ_{CW} from a high-T CW fit is used to gauge whether paramagnetic spins experience FM or AFM correlations.

In a pure nonmagnetic metal, the electrical resistivity $\rho(T)$ decreases monotonically with decreasing T as the phonon modes are depopulated, extrapolating to a small residual value at 0 K that arises due to scattering off of impurities and defects. The addition of small concentrations of magnetic impurity ions to the metal can lead to the Kondo effect, in which $\rho(T)$ develops a low-T minimum, below which $\rho \sim -\ln(T)$. At lowest T, $\rho(T)$ saturates as $-T^2$.The Kondo temperature T_K is a characteristic temperature that separates high T behavior, where

$\chi(T)$ follows a CW law, from low T nonmagnetic behavior, where $\chi(T)$ saturates to a constant value. A physical picture of this nonmagnetic ground state involves the gradual formation of a many-body singlet for $T < T_K$, in which the spin of the impurity ion is screened by antiferromagnetically coupled spins of the conduction electrons. In terms of $\mathcal{J}$, the AFM exchange between the conduction electrons and the local moment, and the density of states at the Fermi energy $N(E_F)$,

$$k_B T_K \propto E_F e^{(-1/|\mathcal{J}N(E_F)|)}. \tag{I.1}$$

The presence of a magnetic impurity also induces damped spin oscillations in the conduction electrons that serve to screen the moment over long distances, much in the same manner that Friedel charge oscillations in the conduction electrons screen impurity charges. Two sufficiently close magnetic impurity ions in a metal can thus couple via the conduction electron spin polarization through the Rudermann-Kittel-Kasuya-Yosida RKKY interaction, which goes as

$$\mathcal{J}_{RKKY} \propto -\mathcal{J}^2 N(E_F) \frac{\cos(2k_F r)}{r^3}, \tag{I.2}$$

where k_F is the Fermi wavevector and r is the position in real space. Because the sign of $\mathcal{J}_{RKKY}$ oscillates with r, the RKKY interaction can lead to either FM or AFM coupling between neighboring impurities. Note that both Kondo and RKKY interactions are still present when the concentration of magnetic ions in a metal is increased to the point where the ions occupy regular crystal sites and form a Kondo lattice. Because the energy scales of the two interactions depend differently on $\mathcal{J}N(E_F)$, this quantity is a useful conceptual tuning parameter, which forms the basis for the popular Doniach phase diagram that describes the magnetic ground state of a Kondo lattice [1]. At low $\mathcal{J}N(E_F)$, the RKKY interaction dominates and a magnetically ordered ground state is expected (usually denoted as being AFM), whereas at high $\mathcal{J}N(E_F)$, the Kondo energy scale dominates and the ground state is a lattice of nonmagnetic Kondo singlets. For some real materials, it is possible to tune the system from one regime to the other via the application of pressure

or chemical substitution [2]. The Doniach description is commonly applied to the heavy fermion compounds described in the next section.

I.B Heavy Fermion Compounds

Heavy fermion compounds are metallic materials in which strong electronic interactions result in dramatically enhanced electronic effective masses m^*, proportional to the enhanced $N(E_F)$ in these systems. Despite the strong interactions, these systems display physical properties that can be adequately described within the Landau Fermi liquid framework. Fermi liquid theory posits that the low-energy collective excitations of a strongly interacting system of fermions can be treated as single particle excitations with renormalized properties, such as the effective mass m^*, which can reach values as large as several hundred times the bare electron mass. In the low-T limit, the specific heat divided by temperature C/T, χ, and ρ have the following T-dependence:

$$C(T)/T \sim \gamma_0, \tag{I.3}$$

$$\chi(T) \sim \chi_0, \tag{I.4}$$

and

$$\rho(T) \sim \rho_0 + AT^2. \tag{I.5}$$

Because both the electronic specific heat and the magnetic susceptibility depend on $N(E_F)$, γ_0 can be related to χ_0 via the Wilson-Sommerfeld ratio $\frac{\pi^2 k_B^2}{\mu_{\text{eff}}^2}\frac{\chi_0}{\gamma_0} \approx 1$ and the empirically determined Kadowaki-Woods ratio $\frac{A}{\gamma_0^2} = 10^{-5}\mu\Omega \text{ cm } (\text{mole K mJ}^{-1})^2$ [4]. The vast majority of the heavy fermion compounds contain rare earth or actinide elements [3], often obeying a full-moment CW law at high T. The Kondo effect is evident in many of these compounds, but in contrast to the conventional single-ion Kondo effect, in these Kondo lattice compounds, $\rho(T)$ not only exhibits a local minimum, it also goes through a local maximum at $T \sim 50 - 100$ K, and then decreases rapidly to low T as it would in a conventional metal. In analogy to

the single-ion Kondo effect, at high T the highly-concentrated magnetic ions act as independent local moments, while at lower T the conduction electrons screen the moments. Below a coherence temperature $T_{\rm coh}$, the regular distribution of the ions in the crystal lattice leads to coherent Kondo scattering, which results in the formation of narrow conduction bands at the Fermi energy, which are responsible for the heavy quasiparticle masses. Localized electron phenomena other than the Kondo effect can also lead to large effective masses. Some examples include valence fluctuations, inelastic exchange scattering involving crystalline electric field-split energy levels, and scattering off of ions in off-center potential wells.

I.C Quantum Critical Points

An important phenomenon often observed in heavy fermion systems is the quantum critical point (QCP). While conceptually similar to the classical critical point commonly observed at finite temperature, the QCP is a zero-temperature phase transition, which can be experimentally accessed via the laboratory tuning parameters of applied magnetic field, pressure, or chemical substitution. In practice, the QCP often forms the endpoint of a line of classical phase transitions, commonly occurring at the value of some tuning parameter at which a magnetic phase transition is suppressed to 0 K. Because they occur at zero temperature, critical order parameter fluctuations are quantum mechanical in nature instead of thermally driven, which can significantly affect the statistical and scaling properties at the phase transition in relation to the classical counterpart. In addition, it is sometimes found that new ordered states, such as superconductivity, occupy the region of parameter space where a QCP is extrapolated to occur. Were the quantum effects strictly limited to zero temperature, QCP's would be nothing more than an intellectual curiosity. Fortunately, the quantum fluctuations can affect the physical properties of a system at finite, but usually low T. One manifestation of this behavior is the occurrence of non Fermi liquid (NFL) behavior, which is

literally the absence of Fermi liquid behavior, ie., a regime where the independent quasiparticle description breaks down. That this effect is named is a testament to the success and ubiquity of the independent quasiparticle Fermi liquid picture for metallic compounds. Experimentally, NFL behavior is recognized as:

$$C(T)/T \sim -\ln T \text{ or } -T^a \text{ or } T^{-a}, \tag{I.6}$$

$$\chi(T) \sim -\ln T \text{ or } T^{-a}, \tag{I.7}$$

and

$$\rho(T) \sim \rho_0 + A'T^n, \tag{I.8}$$

where usually $a < 1$ and $n < 2$. It should be noted that NFL behavior is also observed in the absence of quantum criticality, and may be associated with unconventional Kondo phenomena [5, 6] or other exotic physical mechanisms [7] in addition to proximity to QCP's. An additional class of NFL behavior has been identified via inelastic neutron scattering experiments: the energy-temperature scaling of the magnetic response [8]. Much of the pioneering work on NFL systems was conducted in this laboratory [9, 10]. While NFL behavior is now being identified in a staggeringly large number of systems [11], there are not many broadly applicable NFL models.

I.D URu_2Si_2 Hidden Order and Superconductivity

Some 20 years since its discovery, the ordered phase below $T_0 \approx 17$ K of the heavy fermion superconductor URu_2Si_2 remains a mystery, the nature of its order parameter still a matter of controversy, for which it has been since dubbed hidden order (HO). The superconducting (SC) phase occurs below $T_{SC} \approx 1.5$ K, and URu_2Si_2 was the first heavy fermion compound known to exhibit both magnetic and superconducting order [12, 13]. URu_2Si_2 crystallizes in the tetragonal $ThCr_2Si_2$ structure with lattice constants $a = 4.13$ Å and $c = 9.58$ Å. Its structural anisotropy is reflected in the bulk physical properties, such as the electrical resistivity and magnetic susceptibility [14, 15]. The HO phase transition is marked by

a large specific heat anomaly at 17 K characterized by a BCS-like exponential temperature dependence, which, along with the resistive anomaly, is reminiscent of the spin density wave transition [16, 17] in elemental Cr [18]. Based on this evidence, the transition has been associated with a Fermi surface instability since the earliest days [19]. Evidence in favor of a spin or charge density wave was also found in early inelastic neutron scattering measurements [20], Raman scattering measurements [21], and thermopower and elasticity measurements [22], and in later point-contact spectroscopy and infrared spectroscopy studies [23, 24]. Large anomalies at T_0 were identified in thermal expansion measurements and a minimum in c/a at 60 K [25], which corresponds to the maximum in magnetic susceptibility, and the onset of Fermi liquid behavior, determined via ^{29}Si NMR [26]. It was found that the Hall effect also has features similar to magnetic susceptibility, and high temperature electrical resistivity measurements yielded an estimated single-ion Kondo temperature of 370 K [27].

In the HO phase, a staggered moment aligned with the c direction was identified via neutron diffraction but it was noted that the small moment of 0.03 μ_{B} could not account for the large entropy associated with the feature in specific heat [28], leading to speculation that the entropy is associated with some *hidden* order parameter. Subsequent μSR measurements identified an internal field even smaller than one attributable to 0.03 μ_{B}, and it was suggested that the muon site might be located symmetrically between AFM sublattices [29]. Further inelastic neutron scattering measurements on polycrystalline samples identified the persistence of strong spatial correlations up to 50 K [30], but it was found in later neutron scattering studies on single crystals that the correlations persist to 100 K, which coincides with the maximum in electrical resistivity [31]. Broholm and coworkers also presented an argument strongly in favor of a localized moment interpretation, which has figured heavily in subsequent discussions. The small ordered moment was also observed in x-ray magnetic scattering measurements, which found that the moment is intrinsic to the sample and that it persists unchanged into the SC

region [32]. Although the authors of a nonlinear susceptibility study argued that the HO phase involves quadrupolar order [33], the results of a polarized neutron scattering study found that the HO order parameter breaks time-reversal symmetry and excluded the possibility of any multipolar order other than spin dipole [34], and elastic neutron scattering measurements in magnetic field ruled out symmetric multispin order parameters [35]. A clear discussion of the order parameter controversy at the time is given in Ref. [36], where it is noted that quadrupolar order is only a possible candidate if the measured moment arises from defects. The authors of a point contact spectroscopy report found the splitting of a peak in the HO phase to be consistent with the onset of quadrupolar order [37].

Indications that the entire sample does not order in the HO phase came from μSR measurements that were interpreted as indicating that the volume fraction of magnetically ordered sample increases with decreasing temperature [38]. Evidence for phase inhomogeneity was also found in measurements of ^{29}Si NMR [39]. It was also suggested that an isotropic ^{29}Si NMR signal below T_0 was due to the HO parameter, which was suggested to be orbital AFM [40, 41]. However, neutron scattering experiments found no evidence for orbital AFM, instead identifying quasielastic scattering at incommensurate wavevectors, which below T_0 by a gap of $\sim$ 100 K [42]. A follow-up study found that this gap accounts for the entropy released at T_0, that spin correlations persist to 100 K, and that the HO transition is itinerant in nature, finding no evidence for crystal field excitations [43]. The authors of a ^{101}Ru NQR study argued in favor of quadrupolar order [44]. Measurements of ^{29}Si NMR imply that there is no internal field associated with HO at the ^{29}Si site [45].

Recently, transport studies have reopened discussions of the gapping phenomenon associated with the HO transition. A giant Nernst signal was observed below T_0, along with an increase in the entropy per charge carrier inferred from Seebeck and Hall measurements [46]. A discovery that the lattice thermal conductivity is enhanced dramatically below T_0 was linked to the disappearance of most

of the charge carriers resulting in an increase in the electronic and phononic mean free path [47]. This conclusion was supported by a study of the thermal Hall effect [48].

Meanwhile, the unconventional nature of the SC state was being established. Electrical resistivity measurements in field demonstrated the anisotropy of the SC state, with the upper critical field $H_{c2} \approx 2$ T for $H||c$ and > 8 T for $H||a$ [49]. Low-temperature thermal conductivity measurements suggested anomalous superconductivity [50]. Point contact spectroscopy identified the opening of a gap at T_0 that persisted into the SC phase, which was interpreted as having d-wave symmetry [51]. In addition, an irreversibility line tentatively associated with the flux-line lattice was identified via ac magnetic susceptibility measurements [52]. The anisotropy of H_{c2} was more carefully determined, with a value of 3.5 T for $H||c$ and 14 T for $H||a$ [53, 54]. An anisotropic and hysteretic magnetostriction was found in the SC state as well [55]. The existence of line nodes in the SC energy gap was inferred from ^{101}Ru NQR measurements [56]. Magnetization measurements mapped out H_{c2} for $H||c$ [57].

Recently, attention has returned to the SC state. Electrical and thermal transport measurements on "ultraclean" samples show evidence for unprecedented magnetoresistance at low temperatures, a first order transition at the SC upper critical field, and a nodal gap topology [58]. A study of the specific heat in field found no nodes in-plane, but suggestions of nodes along the c-axis [59], and possible evidence for a first-order transition at the upper critical field [60]. Thermal conductivity measurements in the "ultraclean" samples have mapped out a flux line liquid transition line [61].

It was noted that many of the physical properties of URu_2Si_2 exhibit sample dependence. An early study reported the observation of a second SC transition in specific heat [62], after which Hasselbach and coworkers claimed that only one transition exists, [63], and Ramirez and coworkers put the issue to rest by demonstrating that SC transitions occurred in different macroscopic sections of single

crystals [64]. Indications were reported that low-field temperature irreversibility in the magnetic susceptibility may have arisen from metallurgical defects [65, 66]. A thorough study described differences in magnetic properties due to sample quality, although this amounted to mostly differences in neutron scattering intensity as a function of temperature [67]. Measurements up to 20 T found no annealing dependence of the HO transition [68]. Effects of disorder were also observed in ^{29}Si NMR spectra [69].

Over the years, much theoretical effort has been put into describing the HO parameter. Here is a short list of some of these ideas: local multipole order [70, 71, 72], orbital antiferromagnetism [73, 74, 75], spin-density wave [76], and helicity order [77].

I.E URu_2Si_2 Pressure Studies

Shortly after the discovery of URu_2Si_2, the material's behavior under pressure was investigated. Electrical resistivity [78, 79, 80] and specific heat [81] measurements established that T_0 is enhanced by applied hydrostatic pressure and that the rate of increase $\frac{\partial T_0}{\partial P}$ becomes larger at a critical pressure $P_c \approx 12$ kbar [19, 82, 83, 84, 85]. In contrast, T_{SC} was found to extrapolate to 0 K at a similar P_c, which led to the suggestion that HO and SC order compete for the same portion of the Fermi surface [19, 82]. Studies of electrical resistivity under applied uniaxial stress found that stress applied along the a axis suppressed T_{SC} and enhanced T_0, while the opposite effect occurred for stress applied along the c axis: enhanced T_{SC} and suppressed T_0 [86, 87].

Interest renewed once a neutron diffraction study found that the small staggered moment associated with HO grew by an order of magnitude, becoming large-moment AFM order at 15 kbar [88]. However, this was soon reinterpreted when ^{29}Si NMR measurements found evidence for the heterogeneous coexistence of the HO and AFM states below 15 kbar, with the coexistence eventually yielding

to homogeneous AFM order above 15 kbar [89, 90]. Measurements of μSR support this model; they indicate that the AFM volume fraction starts to increase from 0 at approximately 5 kbar (extrapolated to $T = 0$ K) and that the HO-AFM transition is first order [91, 92]. More support was offered by a study of dilation under pressure, which showed that thermal expansion is sensitive to the paramagnetic (PM)-HO, PM-AFM, and HO-AFM phase boundaries [93]. Measurements of ac magnetic susceptibility on the same samples from the thermal expansion study found that SC is suppressed abruptly at the boundary of the HO-AFM transition [94, 95]. Studies pertaining to the detailed nature of the HO-AFM transition have been undertaken to test a model describing the coexistence of the HO and AFM order parameters [96, 76]. Data from neutron scattering under hydrostatic pressure support the first-order nature of the HO-AFM transition, but find that the transition is separate from the PM-HO/AFM curve [96, 97]. Further support for a first-order transition has been provided by a study of neutron scattering under uniaxial stress [98]. Measurements of dc magnetization under hydrostatic pressure found that increasing pressure was accompanied by a dramatic change in the magnetocaloric effect at T_0, but were insensitive to the HO-AFM transition [99]. Similarly, a study of ac calorimetry under pressure was not able to track the HO-AFM transition [100].

A consensus seems to be forming regarding the pressure phase diagram of URu_2Si_2. A hydrostatic pressure study of neutron scattering and ac susceptibility found evidence that supports the SC phase boundary reported in Ref. [94], and a sharp HO-AFM transition at 7 kbar consistent with a first order transition [101, 102]. These reports also concluded that SC and AFM are mutually exclusive, with the respective decrease/increase in volume fraction occurring over a very narrow pressure range. In contrast to the insensitivity to the HO-AFM transition reported in Ref. [100], recent measurements of electrical resistivity and ac calorimetry have successfully tracked the PM-HO, PM-AFM, HO-AFM, and HO-SC phase transitions [103], and the phase diagram generated from these data

agrees with the those based upon NMR, μSR, neutron scattering, and thermal expansion measurements [89, 90, 91, 92, 94, 97, 101, 102].

However, all data do not support this phase diagram, and it is important to note that many experimental probes cannot confirm the HO-AFM phase separation. A study of the de Haas-van Alphen effect under pressure was unable to find changes in Fermi surface across the HO-AFM transition [104]. Measurements of the magnetization in the SC state under pressure indicate that SC persists to at least 11 kbar and that the critical field curve shows no sensitivity to the HO-AFM transition at 5 kbar [105]. Measurements of the SC critical field curve in electrical resistivity measurements [106, 107] also found no signature of a 5 kbar transition.The additional observation that the ordered phases in high magnetic field do not change appreciably between 1 bar and 11 kbar also has been taken as evidence against HO/AFM phase separation [108].

The sensitivity of URu_2Si_2 to pressure inhomogeneities during measurements has been studied extensively. From studies of uniaxial stress, a strong dependence on the direction of applied stress has been established [86], which is corroborated by the fact that the small ambient-pressure moment increases only when stress is applied along the basal plane, not along the c axis [98]. During measurements the loss of hydrostaticity often occurs due to the solidification of the pressure medium above its critical pressure, which generates shear stresses that do not exist when the medium is fluid. For instance, a study of neutron scattering measurements performed in He, which was limited to less than 5 kbar because of experimental constraints, showed no sign of AFM moment, while measurements performed in Fluorinert in order to access higher pressures detected a moment at the lower pressure of 4.5 kbar [97]. A comparison of neutron scattering and ac susceptibility measurements in Fluorinert FC70/FC77 and Daphne oil 7373 was reported, which determined that the HO-AFM transition and disappearance of SC both occurred at slightly higher pressure in the Fluorinert, [109]. Most recently, a comparison was made of electrical resistivity measurements performed in two

Fluorinert mixtures and isoamyl alcohol/n-pentane mixture, which found that the commonly used Fluorinert yields a hysteretic pressure phase diagram, while the isoamyl alcohol/n-pentane measurements show no sign of hysteresis in pressure [110].

I.F URu_2Si_2 in High Magnetic Fields

Studies of the high-field properties of URu_2Si_2 date back to early magnetization measurements that found two transitions at 36 T and 40 T [78]. A subsequent study of magnetization and electrical resistivity found a third transition at 38 T and magnetoresistance jumps that indicated Fermi surface gapping [111]. Studies of the Hall coefficient identified its suppression at 40 T [112]. Measurements of magnetization over a range of temperatures and high fields found a sharp metamagnetic transition with three steps is found below 14 K that evolved into two steps from $14-17$ K, and then into a broad metamagnetic transition above 17.5 K, persisting up to 55 K which coincides with the maximum in the magnetic susceptibility [113]. An electrical resistivity study up to 1 GPa found that the 36 T transition survives, while the higher temperature transitions broaden [114]. A neutron scattering investigation found an inflection in the field-dependence of the ordered moment at 10 T, and that the size of the excitation gap at commensurate wavevectors grew with field, while the gap at incommensurate wavevectors stayed constant to 17 T [115].

Measurements of the specific heat in both pulsed and constant high fields established that multiple phases exist at low temperatures in the vicinity of 36 T [116, 117]. This phase diagram was corroborated by magnetization measurements that found evidence in favor of reentrant HO and a possible QCP [118, 119] and ultrasound measurements [120]. A subsequent study of high-field electrical resistivity found evidence of no less than five ordered phases in the vicinity of the QCP [121]. When resistivity measurements were extended to lightly Rh-substituted

compounds, it was found that the quantum critical point remained at the same field, protected by an ordered phase, and was seemingly unrelated to the suppression of HO [122]. Specific heat measurements of a Rh-substituted sample found that the QCP was associated with a the breakup of a heavy Fermi liquid [123], which was supported by Hall effect measurements [124, 125]. Recently, measurements of the Re-substituted system have been performed, and are currently being analyzed [126].

I.G URu_2Si_2 Electronic Structure

Because the unusual properties of URu_2Si_2 seem so strongly tied to the conduction electrons, determination of the electronic structure has been pursued for many years. Measurements of the de Haas-van Alphen (dHvA) effect can help to define the Fermi surface. An early study found URu_2Si_2 to be a compensated metal with closed Fermi surfaces, and tracked the persistence of a spherical Fermi surface into the SC phase [127], while another noted that only moderately massive branches were found, in contrast to the sister compound $CeRu_2Si_2$ [128]. The Fermi surface was more carefully mapped in Ref. [129], and it was found that there is no change in dHvA frequency, but a reduction of effective mass, in the SC phase. Based on the angular dependence of the dHvA signal in the mixed state, a line node in the SC gap was suggested [130]. Most significantly, angle-resolved photoemission (ARPES) studies mapped out the Fermi surface, finding evidence for mixing of d- and renormalized f-states, while temperature-dependent data were consistent with $5f$ Kondo physics [131].

I.H URu_2Si_2 Chemical Substitution

Very early on, in an attempt to investigate the HO phase via perturbations of the Fermi surface, transition metal M substitutions $URu_{2-x}M_xSi_2$ were pursued. Most of the neighboring elements of Ru: Mn, Tc, Th, Re, Os, Rh, and

Ir had been substituted onto the Ru site, and in all cases except Os, the HO and SC phases were suppressed by $x = 0.1$ [132, 133, 134]. Despite the fact that the Mn, Tc and Re substitutions resulted in the first known heavy fermion FM instability, historically Rh substitution has been the most popular transition metal substituent.

Rhodium substitution at high concentrations was reported by Miyako and coworkers, who found from bulk property measurements that three different magnetic phases existed as x was varied [135]. A ^{29}Si NMR study found that the HO transition becomes less pronounced as Rh is added and that large-moment AFM order appears for $x > 0.3$ [136]. Early neutron scattering measurements identified a complex magnetic structure at $x = 0.3$ [137]. Later, the low x phase part of the phase diagram was investigated via neutron scattering, where it was found that from $x = 0.02 - 0.04$, HO transitioned to AFM, while at higher concentrations no magnetism was observed [138]. It was also found that the inelastic peaks associated with HO vanish in the Rh-induced AFM phase [139].

Doping with Re, Tc, or Mn results in suppression of the HO and SC phases, and leads to FM order at intermediate concentrations [134], with a maximum $T_C \approx 40$ K at $x = 0.8$ (Re). It was found that the FM is itinerant in nature, with a maximum ordered moment of $\sim 0.45\mu_B$, while the paramagnetic effective moment is $\sim 1.5\mu_B$ [132] and that the electronic contribution to the specific heat peaks at $x = 0.6$ (Re). The long range nature of the FM phase in $URu_{2-x}Re_xSi_2$ was established via neutron scattering for $x = 0.8$ [140] and ^{29}Si NMR for $x = 0.4$ [141]. A systematic study of bulk magnetization established that the FM instability exists at $x = 0.3$, while measurements of specific heat and electrical resistivity provided evidence for the occurrence of NFL behavior far within the FM state [142, 143]. Inelastic neutron scattering measurements found indications of magnetic frustration for intermediate x and a further manifestation of NFL behavior in the appearance of energy-temperature scaling in the dynamic susceptibility [144].

The present study was carried out in order to establish and characterize

the presence of NFL behavior in $URu_{2-x}Re_xSi_2$ using nominally purer and better-ordered samples, to account for magnetic and transport anisotropy, and to more precisely trace the HO and FM phase transitions.

II

Experimental Details

II.A Polycrystalline Sample Synthesis

The single-crystalline samples of $URu_{2-x}Re_xSi_2$ investigated in this study were synthesized using the Czochralski technique [145, 146, 147]. Samples were first prepared as polycrystalline boules or buttons, which were melted together in a conventional single-arc furnace under a purified argon atmosphere in the presence of a zirconium oxygen getter on a water-cooled copper hearth. Starting materials consisted of raw elements: uranium (U), ruthenium (Ru), rhenium (Re), and silicon (Si), which were weighed and mixed in stoichiometric ratio. Elemental U (3N, New Brunwick Lab) was obtained in ingot form and had to be sectioned with bolt cutters, after which selected pieces were etched for five minutes in 1 : 1 HNO_3/H_2O to remove the oxide layer. Both Ru (3N8, Colonial Metals; 4N, Englehard Corp.; 4N, ESPI) and Re (4N, Johnson Mathey; 3N, Colonial Metals) were initially melted into balls from sponge in an arc furnace, which served to reduce their surface area, remove any oxide layer, and, by increasing their mass, make them more convenient to work with. Si (8N, Alfa Aesar) flakes or slivers were mechanically removed from a large solid chunk.

It was noticed earlier that inhomogeneous Re distribution can occur in $URu_{2-x}Re_xSi_2$, resulting from difficulties in preparation related to the high melting

temperature of Re (3455 K) relative to U (1408 K), Ru (2610 K), and Si (1683 K). This was previously addressed via a two-step synthesis of polycrystalline samples: after the raw elements were initially melted together and reacted, the boule was crushed into small pieces, which were melted together to form a homogenized final product [143]. This approach did result in chemical homogeneity, as determined via electron probe microanalysis [142]. However, this technique was not used in the present study because of concerns that the act of crushing could introduce impurities (at levels below the sensitivity of the electron microprobe). Instead, before combining all of the elements, the Ru and Re were first alloyed [148]. Because the Ru-Re alloys were Ru-rich, their melting points were significantly lower than that of pure Re. This method lead to better Ru/Re mixing in $URu_{2-x}Re_xSi_2$ after the U and Si were combined with the initial Ru-Re alloy. Mass loss after arcing was less than 1%, within acceptable limits. The tendency of URu_2Si_2 and its alloys to form large grains on cooling resulted in polycrystalline boules with large reflective facets on the surface, mimicking the general appearance of a disco ball, as in Fig. II.1. These facets, which are oriented normal to the tetragonal [001] direction, are of sufficient quality that they have been used in lieu of single crystals [21, 52]. This growth habit probably facilitated the synthesis of large single crystals.

Figure II.1: Photograph of a polycrystalline sample of $URu_{1.65}Re_{0.35}Si_2$, with a diameter of approximately 2 cm, formed in an arc furnace. The large facets on the surface that give the sample its disco ball appearance are oriented perpendicular to the [001] direction.

II.B Single Crystal Synthesis

The homogenized polycrystalline samples were placed in a water-cooled tri-arc furnace (Centorr) equipped with a Czochralski pulling assembly, shown in Fig. II.2. Under flowing argon, the boules were melted with the three arcs, which were spaced evenly to provide the most homogeneous heating. A cold, rotating tungsten tip was inserted into the melt and removed, and $URu_{2-x}Re_xSi_2$ solidified in a cone shape on the tip as it was withdrawn, forming a seed. Despite the polycrystalline nature of this solid, at the tapered end near the tip, a large grain was inevitably found, which was used to seed the single crystal growth. The tip of the seed was reinserted a shallow depth into the melt, and withdrawn at a slow rate, ranging from $2 - 4$ cm/hr, for the duration of the growth.

To homogenize the temperature in the pulled sample, the pulling rod was rotated at approximately 10 rpm. Rotation of the pulling rod was important because the melt remained stationary with respect to the electric arcs, forming hot and cold spots in the melt. Rotation of the growing crystal also ensured that the pulled crystal was exposed evenly to the bulk of the melt and promoted mixing in the liquid. The latter is arguably more important in the case of $URu_{2-x}Re_xSi_2$, for which the maintenance of a homogeneous Ru/Re distribution throughout was crucial. It was found that rotation of the pulling rod promoted a cylindrical symmetry for the pulled single crystal that maintained the best concentricity with the melt. These were critical to stability of the growth, ensuring that the liquid-solid interface inside the melt, where crystal growth occurs, did not move.

The three electric arcs could be positioned about the melt with a great degree of freedom. It was important to space them evenly around the melt, but their height with respect to the melt was critical. Note that even when molten, the metal boule maintained a round shape due to surface tension, although the maximal cross-section sat lower than half of the height of the melt. The electric arcs were generated by electrodes inserted and controlled from the top of the

furnace, which introduced a mechanical bias against the ideal growth conditions. Through trial and error, it was found that the ideal growth environment required the electrodes to sit approximately $1 - 2$ mm off of the hearth, roughly at the height of the maximal cross-section.

This requirement can be understood based on the following description. Bear in mind that the melt sits on a water-cooled copper hearth, so it is being both heated and cooled at the same time, leading to the existence of rather large temperature gradients, the description of which may be further complicated by the rotation of the pulled sample and stirring of the melt. Additional cooling is provided by the pulling rod and the crystallizing sample being slowly removed from the melt. Thus the melt is hottest in the middle, coldest at the bottom, and cool at the top where the crystal is being grown. Successful single crystal growth relies on maintaining the growth interface and its immediate environment at a stable temperature. As the hottest parts of the melt are in the vicinity of the arcs' incidence, if these hot spots occur too close to the top of the melt, they are too near the growth interface and limit the diameter of the single crystal. In this configuration, the bottom of the molten boule is colder and is at least more viscous, if not solid. Thus moving the arcs' hot spots to a lower height provides three benefits: a larger volume at the bottom of the melt is hotter, the vertical temperature gradient between the growth interface and the hot spots is smaller (assuming constant hot spot and interface temperatures), and a large volume of liquid near the interface is cooler.

Stabilizing the liquid-solid interface is the goal of steady-state crystal growth, but the entire process involved much more than just this. In an arc furnace, temperature is not controlled or even monitored; instead, the position of and current flowing through the electrodes are adjusted, and temperature is inferred from the appearance of the melt and crystal (note that UV filters are necessary to avoid retinal damage). To begin with, it was necessary to take a submillimeter diameter seed crystal and create a bulk crystal with a diameter of

several millimeters, if not larger. Before the growth, current was adjusted such that the boule was entirely molten. The seed was deposited with the electrodes in a relatively high position so that the top of the melt was hotter, less material solidified on the tungsten tip, and the solid tapered down over a relatively short distance. The electrodes were then lowered, and current was increased as necessary to keep the boule molten. In their lower positions, the arcs may have also been close enough to the hearth to heat it also, reducing the efficiency with which they heat the sample. With the seed reinserted and slowly retracting, a small diameter crystal began to emerge. By very carefully reducing the current in the arcs further, it was possible to cool the melt further and encourage an increase in crystal diameter. There were limitations on how quickly the diameter could be forced to increase and doing this too quickly reduced crystal quality. Over a length of about $4-5$ mm it was safe to increase the diameter of the crystal to the target size of $5-6$ mm. Through experience, it was determined that the stable crystal diameter was a function of mainly the position and currents of the arcs, for a roughly constant volume and shape of melt. In other words, a crystal would increase its radius if it were too small or decrease its radius if it were too large to reach an equilibrium size in response to the operator's adjustments. Over a short period of time, the arcs' position and current could be held steady once growth stability was established. However, the melt volume decreased as the crystal grew, necessitating periodic decrease of arc current to compensate for a smaller volume and the adjustment of electrode position to bring them closer to the melt as its radius decreased. As mentioned earlier, the appearance of the crystal and melt were monitored. Specifically, during most of the growth, current and position of the electrodes were adjusted to keep the crystal diameter and the shape of the liquid meniscus on the retracting solid constant. Inevitably, the melt diameter decreased to slightly larger than that of the crystal, forcing a decrease in crystal diameter. It was decided when the diameter was too small, and the crystal was pulled out of the melt quickly, sometimes with an increase in arc current, to finally

separate it.

Following the growth, each sample was annealed at high temperature. The samples were wrapped in tantalum foil and sealed in a quartz tube under 150 Torr of argon along with a piece of zirconium foil, which acted as a getter. The samples were placed in a box furnace and held at 900 °C for 7 days.

At the time of this writing, the tri-arc furnace has been retired and replaced by a tetra-arc furnace (Techno-Search) that features several improvements (Fig. II.3). First, the furnace chamber is cleaner: many joints are welded, metal bellows are used instead of ball joints for the arcs, the system has a diffusion pump instead of just a mechanical roughing pump, and the pulling rod is sealed inside the chamber via long bellows, instead of being fed through an o-ring seal. Temperature homogeneity in the melt is improved with four arcs with individual current control and a rotating cooled hearth. The system has a fifth electrode dedicated to continuously arcing a zirconium getter during the entire crystal growth. Despite these upgrades, the general growth procedure remains the same, with the same demand for an operator's constant attention and intervention. Several single crystals have been grown using this system, including one crystal of $URu_{2-x}Re_xSi_2$, $x = 0.12$, reported herein. A single crystal of $URu_{1.9}Re_{0.1}Si_2$, which was featured in the August 2007 volume of Physics Today, is shown in Fig. II.4.

Figure II.2: Photograph of the tri-arc furnace used in the Czochralski growth of $URu_{2-x}Re_xSi_2$ single crystals. The pulling rod is inserted into the chamber through an o-ring assembly at the top. A motor rotates the rod while a separate drive translates the rod upward. During operation of the arcs, a UV filter is placed between the operator and the furnace.

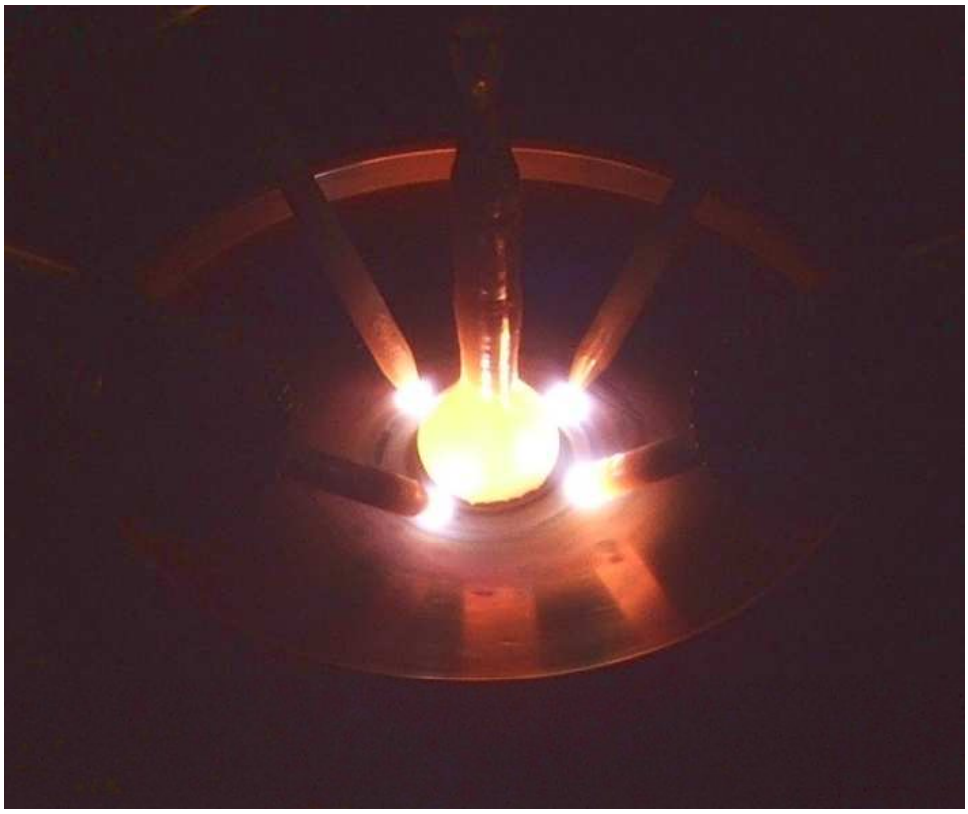

Figure II.3: Photograph of the tetra-arc furnace during the Czochralski growth of $URu_{1.88}Re_{0.12}Si_2$ single crystals. Here the four arcs are seen heating the molten boule on a rotating copper hearth as the counter-rotating single crystal is extracted from the melt.

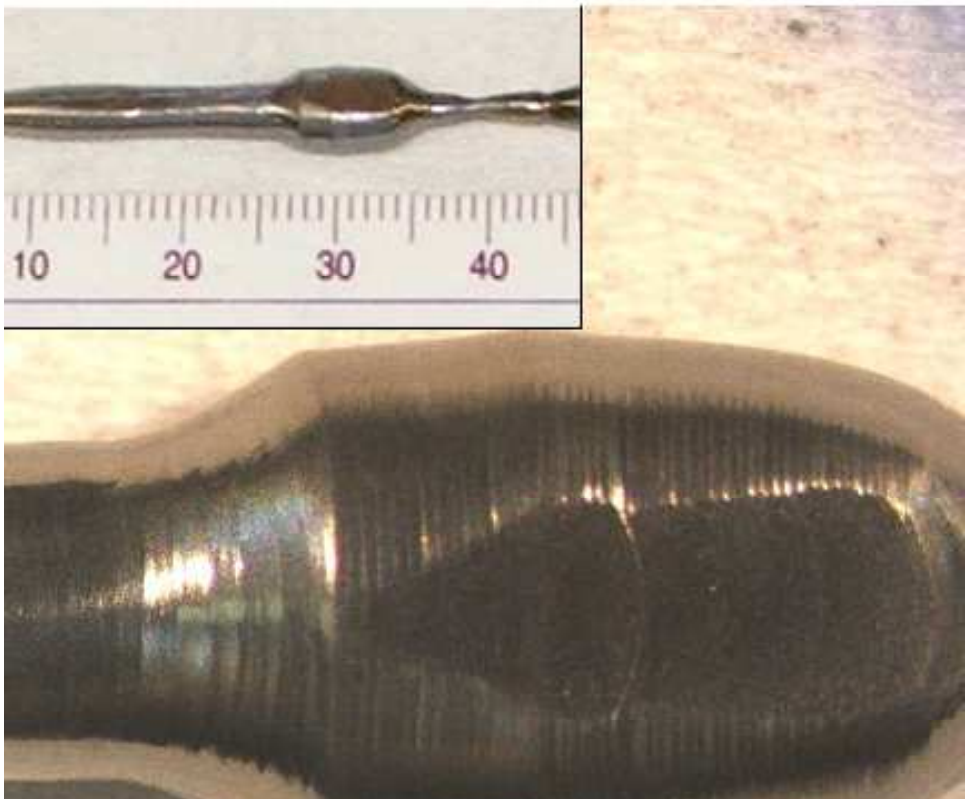

Figure II.4: Photograph of a single crystal of $URu_{1.9}Re_{0.1}Si_2$ grown in a tri-arc furnace. The large flat face was determined to be perpendicular to the [001] direction (Fig. II.5), a condition almost always true in our single crystal growth.

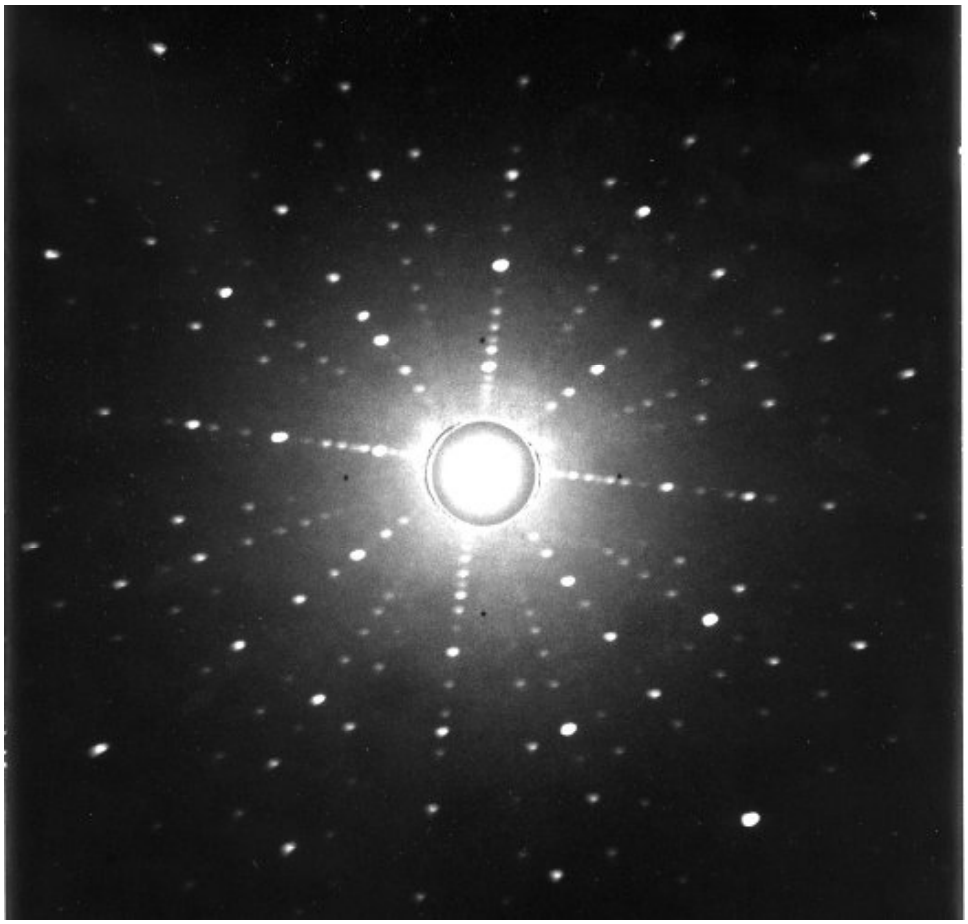

Figure II.5: Laue pattern from the sample of $URu_{1.9}Re_{0.1}Si_2$ shown in Fig. II.4. This image shows that the sample face is perpendicular to the [001] direction.

II.C Measurements

In order to verify sample composition, material from each growth was powdered and $\theta - 2\theta$ x-ray diffraction measurements were performed using a commercial Rigaku Rotaflex rotating anode x-ray machine. Peaks in the powder diffraction pattern were used to establish the lack of impurity phases and to calculate lattice constants [149, 150]. Single crystal samples were oriented via the Laue backscattering technique, using a GE x-ray generator equipped with a Polaroid land camera [151]. An example Laue pattern of a sample oriented along the [001] direction is shown in Fig. II.5. In rare cases, the Laue technique provided evidence for the existence of multiple crystallites in a sample presumed to be a single crystal.

Single crystals were initially cut up using a diamond wheel saw (South Bay Tech Model 650), which both cut the large sample into more manageable pieces, but had the added benefit (in hindsight) of cleaving the samples through the inevitable gentle mechanical vibration arising from slight warping of the cutting blade. For precision cutting, samples were cut using an abrasive wire saw (South Bay Tech Model 850), an Agie electric discharge machine (EDM or spark cutter), and/or a Hylozoic Products micro-EDM. Where specimen thickness was critical, further shaping of samples was achieved by sanding using a Buehler Ecomet 3 Variable Speed Grinder-Polisher or simple sanding by hand.

Measurements of bulk magnetization M as a function of magnetic field H and temperature T were performed using a Quantum Design Magnetic Properties Measurement System (MPMS) superconducting quantum Interference device (SQUID) magnetometer. The cryostat had a working temperature range of $1.8-300$ K, while the superconducting magnet provided applied magnetic fields up to 5.5 T. Samples were typically attached via diluted Scotch glue or Duco cement to a Delrin disk mounted in a plastic drinking straw.

The specific heat C was measured using a custom-built ^{3}He refrigerator-

based calorimeter with a base temperature of 600 mK. Apiezon N-Grease was used to attach samples to a suspended sapphire disk. Cernox chips were used for both the heater and thermometer.

Electrical resistance measurements were performed using two models of Linear Research ac resistance bridge: the LR-201 and the more modern LR-700, operating at 16 Hz. Sample resistivity ρ was calculated using measured sample dimensions, with an absolute uncertainty of $5 - 10\%$. Excitation currents ranged from $10-100\mu$A. Measurements in the temperature range $1-300$ K were performed in a a pumped ^{4}He cryostat (Captain America custom-built). Measurements at temperatures down to 25 mK were performed in ^{3}He-^{4}He dilution refrigerators (SHE Minifridge, Oxford Kelvinox 300, and Oxford Kelvinox MX100) equipped with superconducting magnets capable of generating magnetic fields as large as 9 T.

III

X-ray Diffraction

URu_2Si_2 crystallizes in the tetragonal $ThCr_2Si_2$ structure, illustrated in Fig. III.1. The lattice constants are $a = 4.13$ Å in the basal plane and $c = 9.58$ Å perpendicular to the basal plane. When Re is substituted for Ru in $URu_{2-x}Re_xSi_2$, it is assumed to occupy the Ru site in the lattice. Substituting Re for Ru removes one electron and adds a $5d$ shell. The U atoms form a body-centered tetragonal lattice. The structure is rather planar, or two-dimensional, which is reflected in the observed anisotropy in magnetic and transport properties.

Powder x-ray diffraction measurements confirmed the absence of bulk impurity phases, at no more than 5% volume fraction, and provided information about the variation of the crystal structure with x. The results are summarized in Figs. III.2 and III.3. In both figures, the electronic phase diagram, which will be discussed in greater detail, is superimposed for reference. Note that x-ray diffraction was performed at room temperature, while the electronic order occurs at much lower T. For $x \leq 0.1$, the lattice constants a and c are roughly independent of x. For $0.1 < x \leq 0.6$, c lengthens noticeably. In contrast, a increases slightly over $0.1 > x > 0.3$, while for higher x, a contracts appreciably. Because of this behavior, the lattice volume remains constant to $x = 0.1$, and increases with x, leveling off slightly by $x = 0.6$. The aspect ratio c/a is also constant up to $x = 0.1$, after which it increases substantially. These values deviate slightly from those

published for polycrystalline samples in Ref. [132].

Thus, the crystal lattice of $URu_{2-x}Re_xSi_2$ not only increases in volume, but also elongates with increasing Re concentration. Ultimately, the U atoms, which contribute most strongly to the magnetic properties, experience an in-plane contraction and out-of-plane separation, as x increases. It is telling that the dramatic changes in the lattice coincide with the disappearance at low temperature of the HO phase. In addition, the strengthening of the ferromagnetic moment at intermediate x follows the increasing value of c. Because the AFM order observed in URu_2Si_2 involves antiferromagnetically coupled FM planes, the increased interplanar spacing could weaken the AFM coupling.

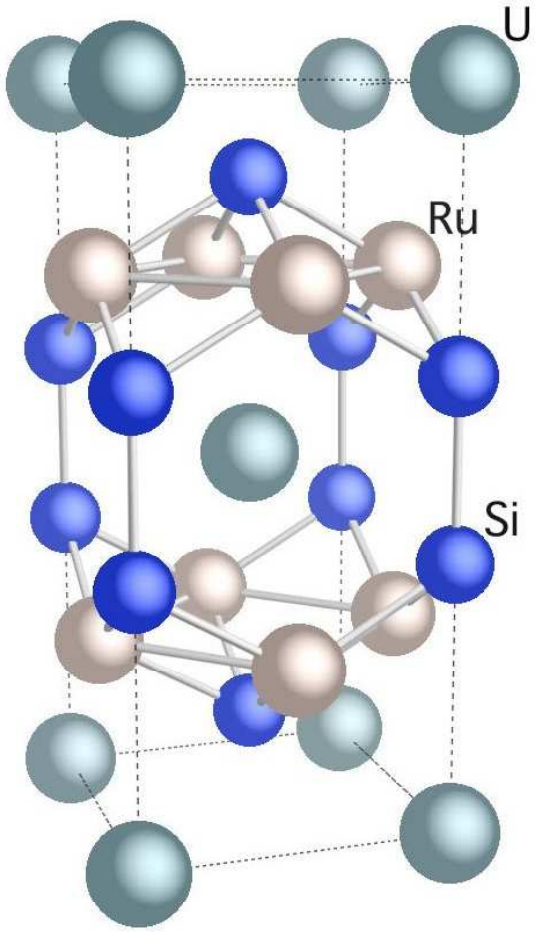

Figure III.1: Crystal structure of URu_2Si_2, which forms in the tetragonal $ThCr_2Si_2$ structure, with lattice constants $a = 4.13$ Å and $c = 9.58$ Å. Substituted Re is assumed to occupy the Ru sites.

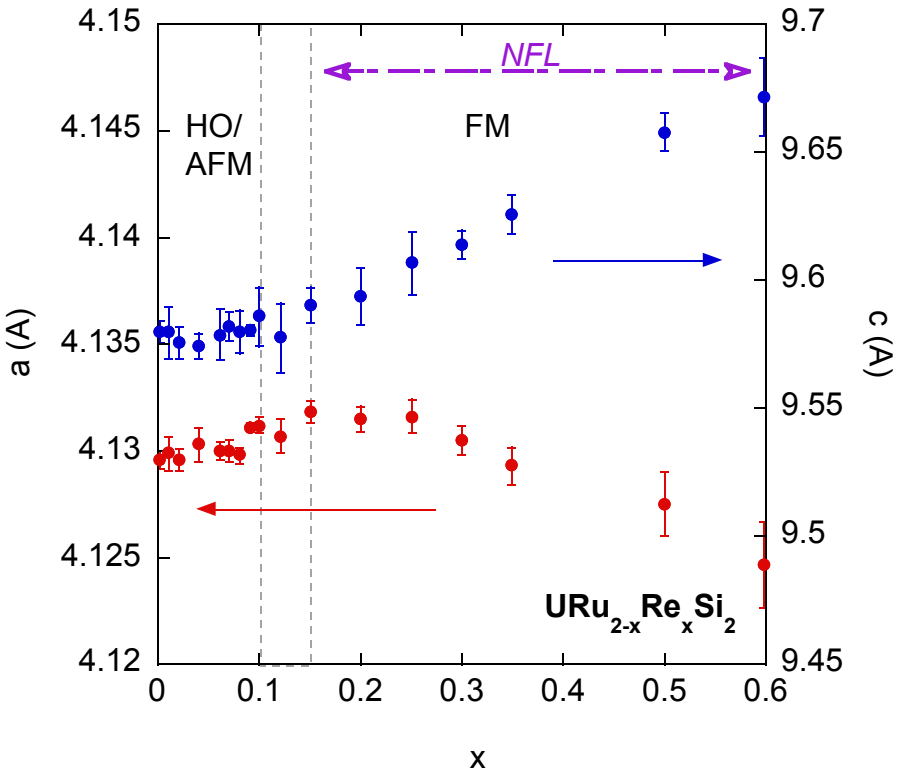

Figure III.2: Lattice constants of $URu_{2-x}Re_xSi_2$. The electronic phase diagram is superimposed for reference.

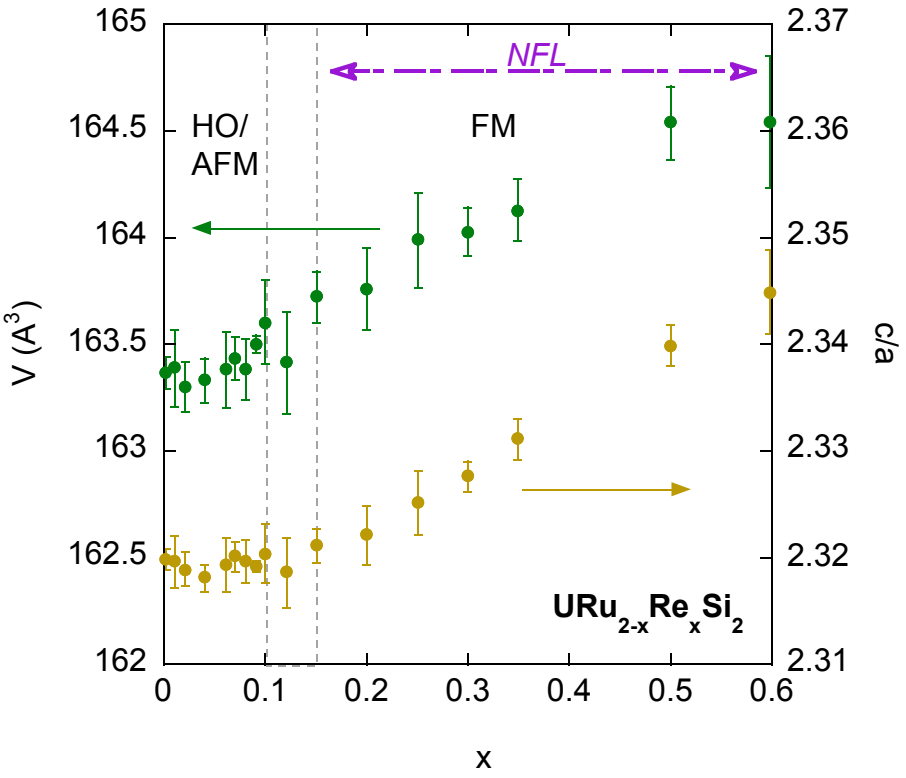

Figure III.3: Lattice volume and aspect ratio of $URu_{2-x}Re_xSi_2$. The electronic phase diagram is superimposed for reference.

IV

Electrical Resistivity

IV.A General Features

The in-plane electrical resistivity $\rho(T)$ of $URu_{2-x}Re_xSi_2$ is displayed for several values of x for $0 \leq x \leq 0.6$ in Fig. IV.1. The data for $x = 0$ agree well with published data [15], while data for $x > 0$ cannot be directly compared to those in Refs. [132, 143, 142] because those data lack an absolute resistivity scale, but the same general trends are seen. Note that the $x = 0$ and $x = 0.6$ data were scaled to match the room temperature values of the other data sets. Over a large number of samples, it seems that $\rho(300\ \mathrm{K}) \approx 350 - 400\ \mu\Omega$ cm, independent of x. The main characteristics of the $x = 0$ $\rho(T)$ data are the negative slope over $80 < T < 300$ K, the maximum at about 80 K, the anomaly associated with the HO transition at 17 K, and the SC drop at 1.4 K. The high-T resistivity is believed to reflect Kondo lattice physics, with a very high single-ion T_K [27] leading to the negative slope in $\rho(T)$, and a maximum at T_{coh} that indicates the onset of coherent Kondo scattering as T is lowered, which leads to the formation of a heavy quasiparticle band. As x increases, the HO anomaly is suppressed in T, as shown in Fig. IV.2, and can only be seen for $x \leq 0.1$. The $\rho(T)$ data below the coherence maximum for higher x are characterized by power-law T-dependence, as shown for $x = 0.3$ and $x = 0.6$ in Fig. IV.1. There is also an increase in the residual resistivity

$\rho(0\ \mathrm{K})$, leading to a decrease of the residual resistivity ratio RRR $= \frac{\rho(300\ \mathrm{K})}{\rho(0\ \mathrm{K})}$ as x increases. In addition, T_{coh} moves to higher T as x increases, and the high-T slope $\frac{\partial \rho}{\partial T}$ decreases, leading to a decrease in the maximum value of ρ. A similar increase in T_{coh} has been observed in pressure studies [82]. Naively, an increase in T_{coh} implies an increase in the energy scale of coherence, or a strengthening of the coherence mechanism, but instead it appears that the maximum in $\rho(T)$ may be broadening as x increases. Thus, the main effects of Re substitution on $\rho(T)$ seem to be simply the increase of disorder. As shown in Fig. IV.2, the HO anomaly similarly broadens with increasing x until it can no longer be defined.

To study any evolution with x of anisotropy in the electrical transport, $\rho(T)$ was measured with current J passed along both the a- and c-axes. Comparisons of the in- and out-of-plane data are shown in Figs. IV.3, IV.4, IV.5, IV.6, IV.7, and IV.8. Note that the data for $J||c$ in Fig. IV.3 appear to have a significant contribution from $J||a$, probably stemming from imprecise sample orientation. In particular, the high-T slope is much too high compared to published data [15], although the overall magnitude of $\rho(T)$ is in agreement. It is immediately evident that the HO transition is visible for both current directions and for $x = 0.02$ and $x = 0.04$, the minimum in the HO anomaly actually seems to be better defined along c. For $T > 100$ K, $\rho(T)$ for $J||c$ seems to be almost constant for all x, with the additional exception of $x = 0.25$, where alignment and measurement problems are evident. In addition, $\rho(T)$ for $J||c$ seems to be roughly a factor of 2 smaller than for $J||a$. This fact can be understood within the context of the appreciable structural anisotropy, which only increases with x, and the fact that c is the easy magnetic axis. The caveat to any statement about transport anisotropy in $URu_{2-x}Re_xSi_2$ is the large uncertainty in the absolute magnitude of the resistance, which stems mostly from uncertainty in the geometric factor due to the precise shape of the samples. Even in carefully prepared bar-shaped samples, the current path may be limited by cracks, which readily form perpendicular to the c-axis. An example of the kind of variation possible is exhibited in Fig. IV.5 and is probably

responsible for the fact that in Fig. IV.8, the data for $J||c$ have higher values than for $J||a$. In order to confirm this suspicion, several more samples at high x will be measured with $J||c$.

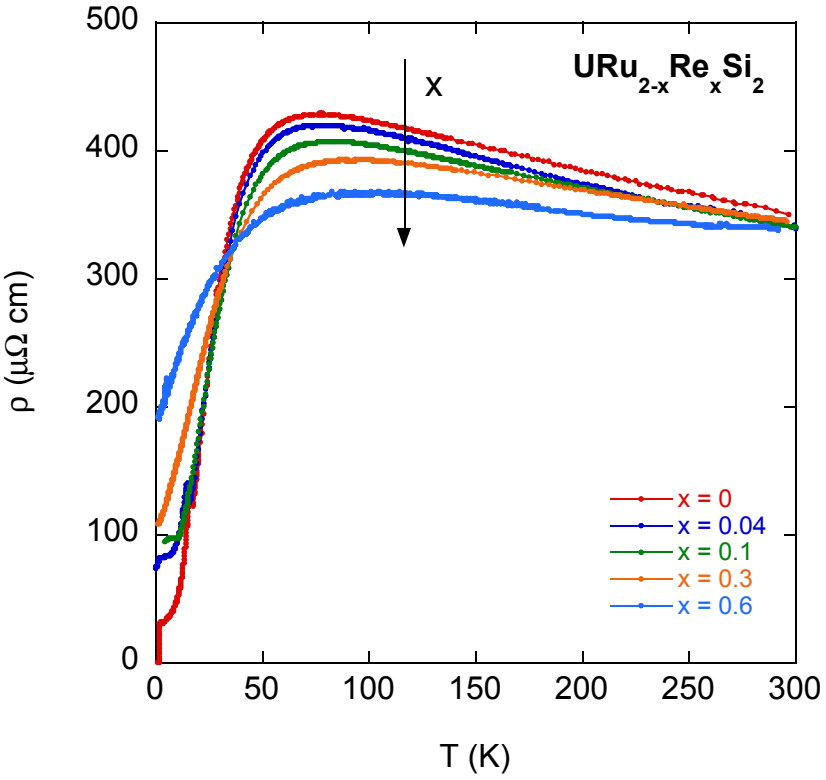

Figure IV.1: Comparison of in-plane resistivity for $0 \leq x \leq 0.6$.

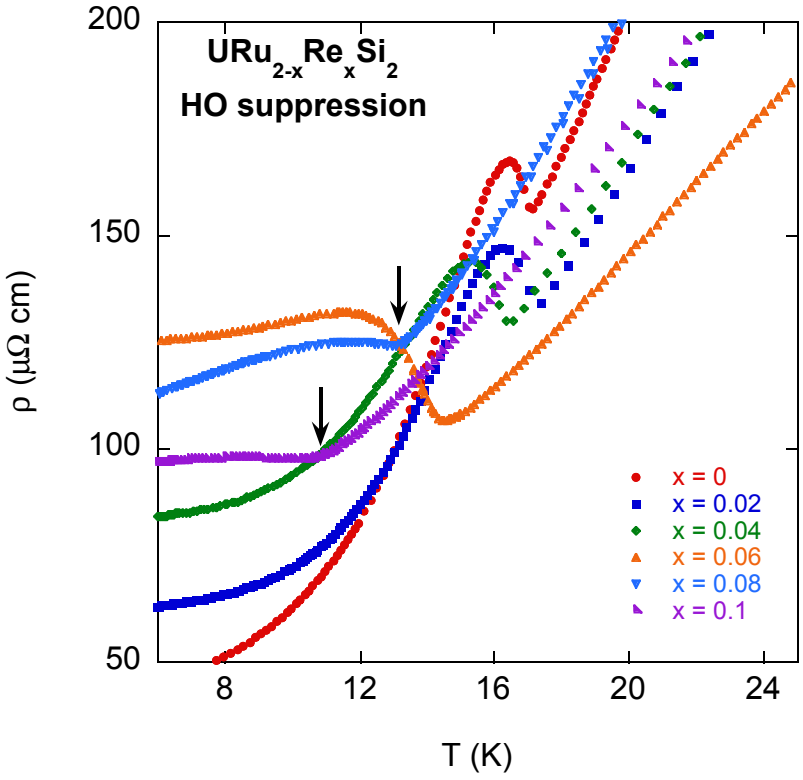

Figure IV.2: The HO transition in $\rho(T)$ for $x \leq 0.1$. The transition temperature T_0 is identified with the local minimum, marked by arrows for $x = 0.08$ and $x = 0.1$.

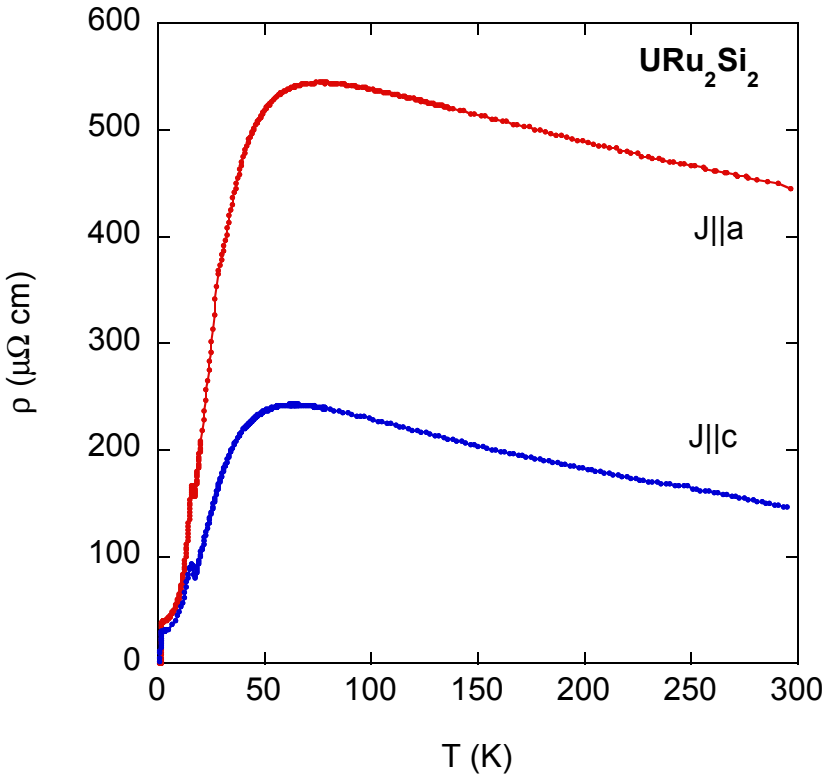

Figure IV.3: In- and out-of-plane resistivity for $x = 0$. The data for $J||c$ exhibit signs of misalignment (see text).

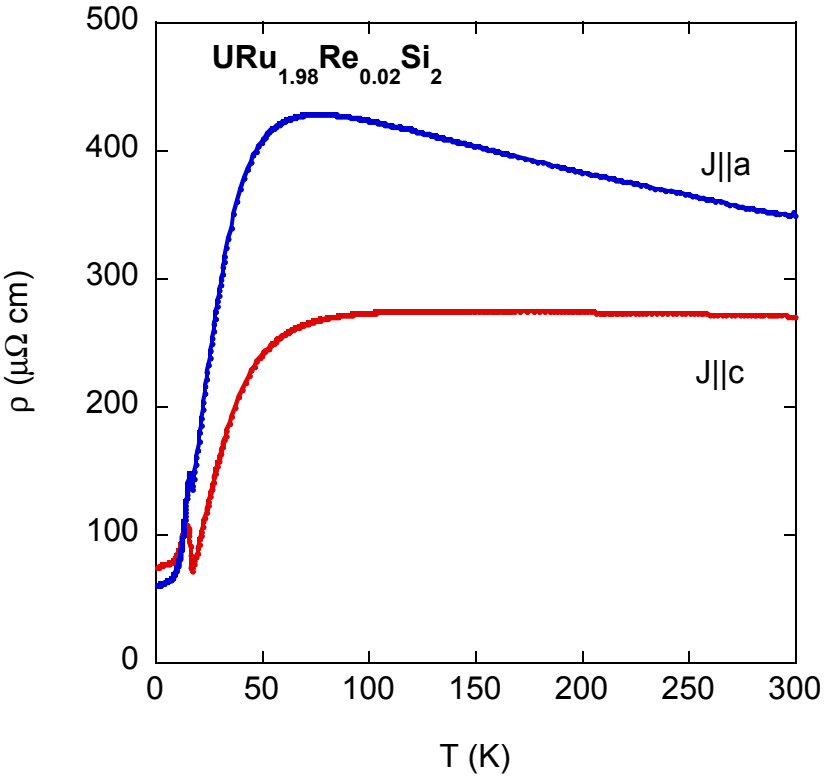

Figure IV.4: In- and out-of-plane resistivity for $x = 0.02$.

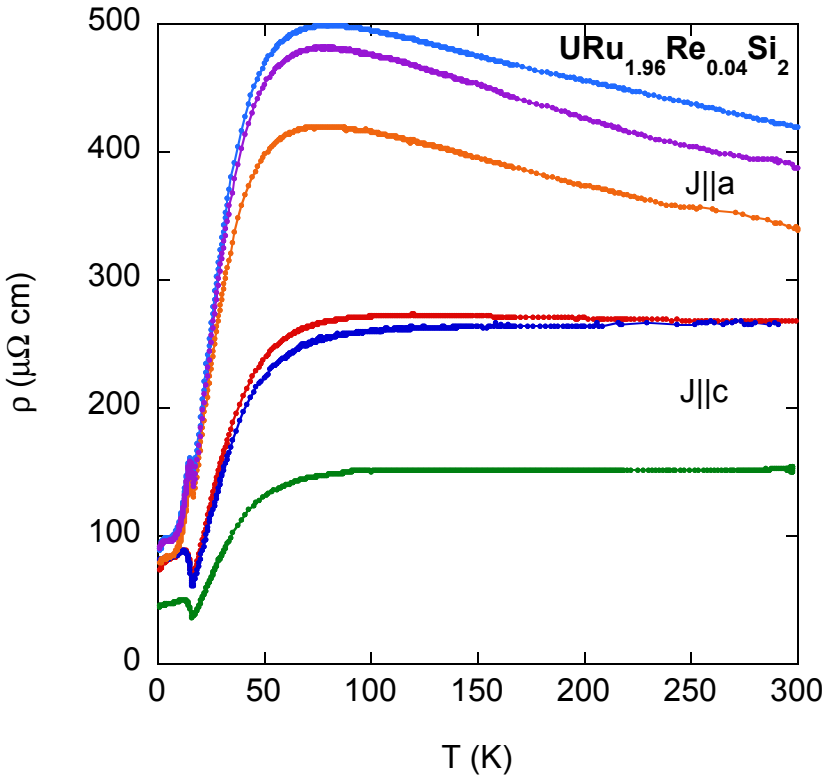

Figure IV.5: In- and out-of-plane resistivity for $x = 0.04$. Scatter in the absolute magnitude of $\rho(T)$ probably reflects a nonuniform current path, even in carefully cut samples.

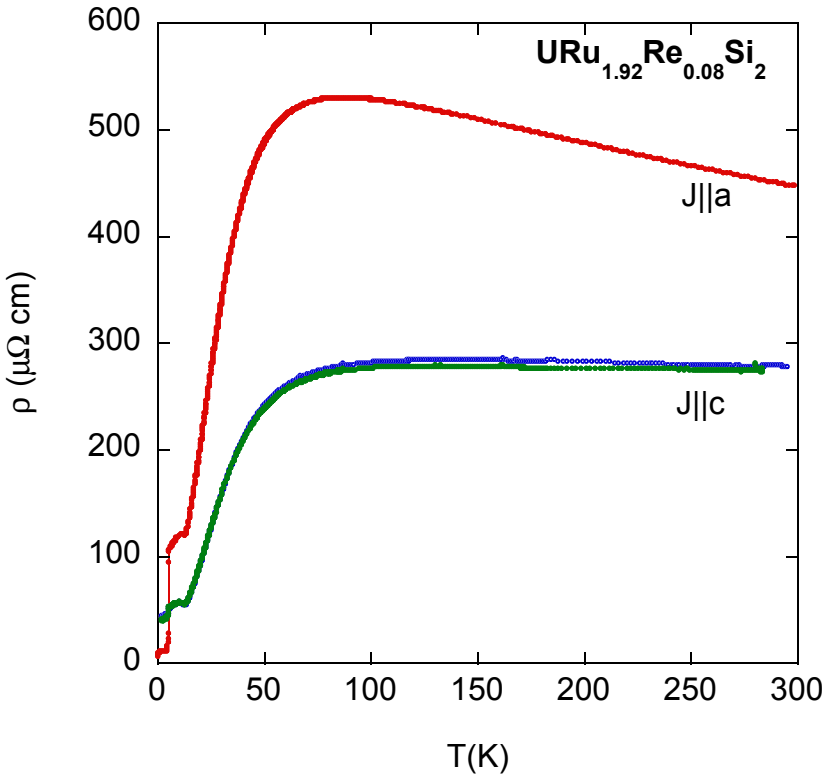

Figure IV.6: In- and out-of-plane resistivity for $x = 0.08$. The large drop in the data for $J||a$ is discussed in more detail in Chap. VII.

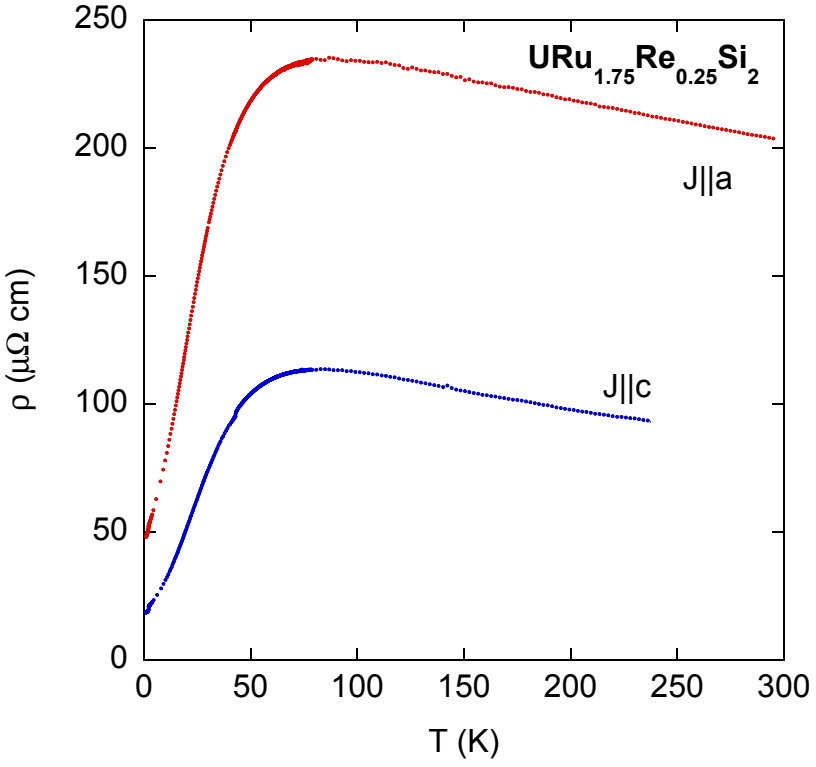

Figure IV.7: In- and out-of-plane resistivity for $x = 0.25$.

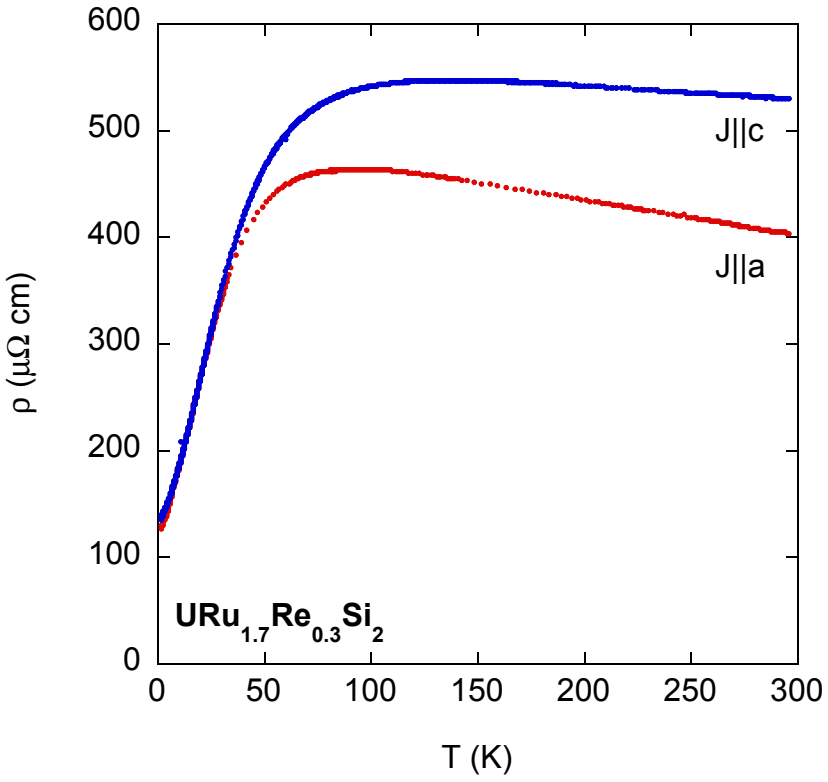

Figure IV.8: In- and out-of-plane resistivity for $x = 0.3$. The absolute magnitude of the data for $J||c$ is likely incorrect and may reflect the existence of cracks in the sample.

IV.B Energy Gaps and Power Laws

The low-T dependence of ρ was analyzed via fitting the data to two different functional forms in different ranges of x. Following Refs. [82] and [106], fits of the form

$$\rho = \rho_0 + aT^2 + b(\frac{T}{\Delta})(1 + 2(\frac{T}{\Delta}))e^{-\frac{\Delta}{T}} \tag{IV.1}$$

were performed on samples in the HO state. This function combines Fermi liquid scattering with scattering off of gapped AFM magnons. Here, $\rho_0 = \rho(0\text{ K})$ arises from static defects, a is the coefficient of the quasiparticle-quasiparticle scattering term, which is significant in a heavy fermion material, b is the coefficient of the magnon scattering term, and Δ is the gap size of the energy gap. Fits were performed on $\rho(T)$ data below the HO transition, as shown in Fig. IV.9. The range over which these fits could be performed as T_0 decreased with increasing x, and the broadening and flattening of the transition lead to some uncertainty whether fits for $x > 0.4$ are accurate. For all x, power-law fits of the form

$$\rho = \rho_0 + cT^n \tag{IV.2}$$

were performed. The power-law exponent n has a value of 2 if Fermi-liquid quasiparticle scattering is dominant, but may take different integer or half-integer values if scattering off of phonons or magnons is dominant. As a rule of thumb, a fit to Eqn. IV.2 is only robust if it is applicable over at least a decade in T. If such a fit produces non-integer $n < 2$, it might be considered as evidence of NFL behavior. For low x, fits of Eqn. IV.2, which yielded $n > 3$, were compared to fits of Eqn. IV.1 to the same T range, with Eqn. IV.1 always producing a better fit. Examples of successful power-law fits to $\rho(T)$ for higher x are shown in Figs. IV.10 and IV.11. In samples exhibiting a weak HO anomaly, the power-law fits could be performed in T ranges below and above the transition, although in some of these samples and those at higher x, the T range was limited by sharp drops in $\rho(T)$, shown in

Fig. IV.12. These features look like incomplete SC transitions, and will be discussed in Chapter VII. Fortunately, the magnitude of these features and the T at which they occurred were sample-dependent. For $x \geq 0.2$, fits of Eqn. IV.2 above and below the features yielded equivalent values of n, and there are some dramatic examples of fits over the entire uninterrupted T range, as in Fig. IV.11. A resistive phase diagram, generated by combining the values of Δ and n in their respective ranges of x, is shown in Fig. IV.13. Fits were performed to $\rho(T)$ along both a and c axes, although the values did not exhibit dramatic direction-dependence. Based on this phase diagram, the AFM gap seems to close at $x \approx 0.06$. As mentioned before, the gap value may be inaccurate, especially when compared to the analysis presented in Chapter V, although its x-dependence is consistent with the disappearance of HO. It is noteworthy that the power-law exponent $n < 2$ for all x and both J directions, confirming the earlier findings based on measurements of polycrystalline samples [142]. Outside of the HO phase, the value of n monotonically decreases with increasing x and even becomes sublinear for $x > 0.5$, which was not seen in Ref. [142]. This tendency is due to the broadening of the coherence peak as x increases. For $n > 1$, there must be an inflection point in $\rho(T$ where the curvature changes from negative to positive as T decreases. For $x \geq 0.5$, there is no longer an inflection point and the curvature remains negative to lowest T. Sublinear T-dependence is indeed unusual, but not unprecedented: it has been observed in the heavy fermion compounds $CeRh_{1-x}Co_xIn_5$ [152], $Ce_{1-x}Y_xCoIn_5$ [153], and $Sc_{1-x}U_xPd_3$ [154] ($\rho(T)$ diverges in the last case).

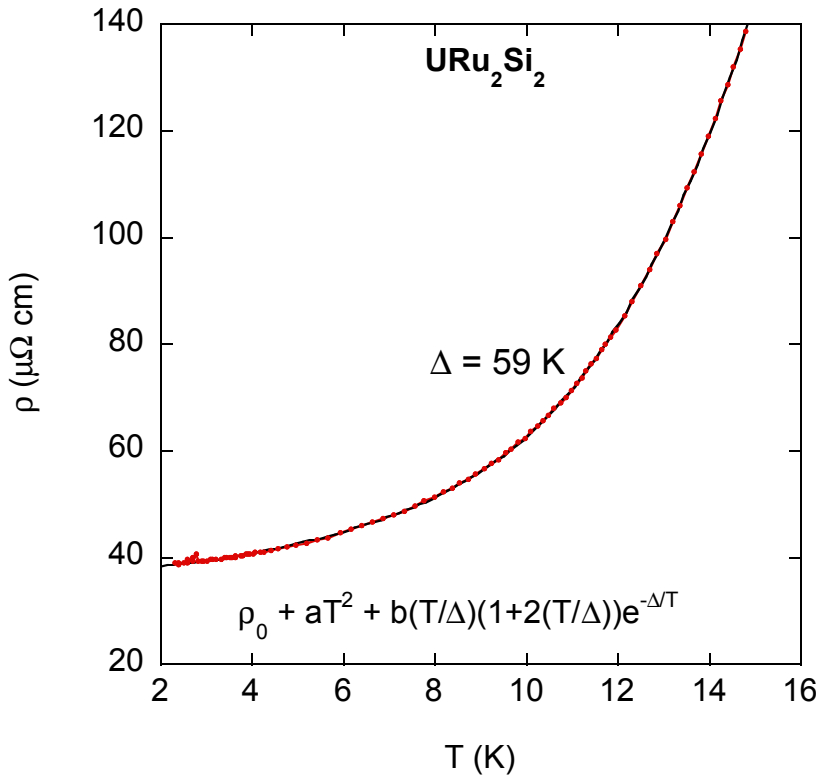

Figure IV.9: Example fit of $\rho(T)$ to gapped magnon scattering function. This specific form also includes a Fermi liquid scattering term.

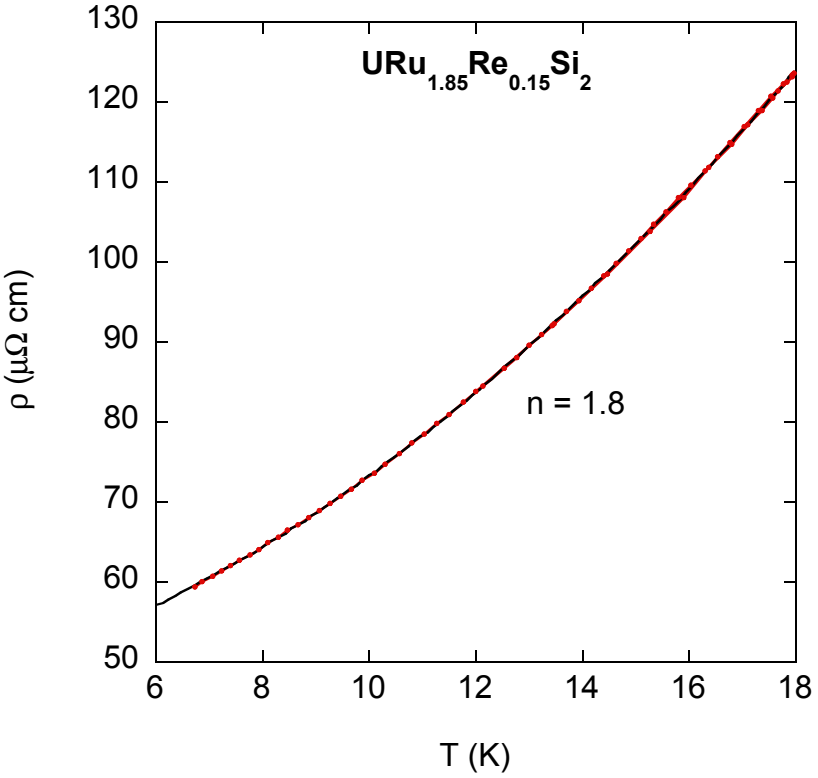

Figure IV.10: Power-law fit to $\rho(T)$ data for $x = 0.15$.

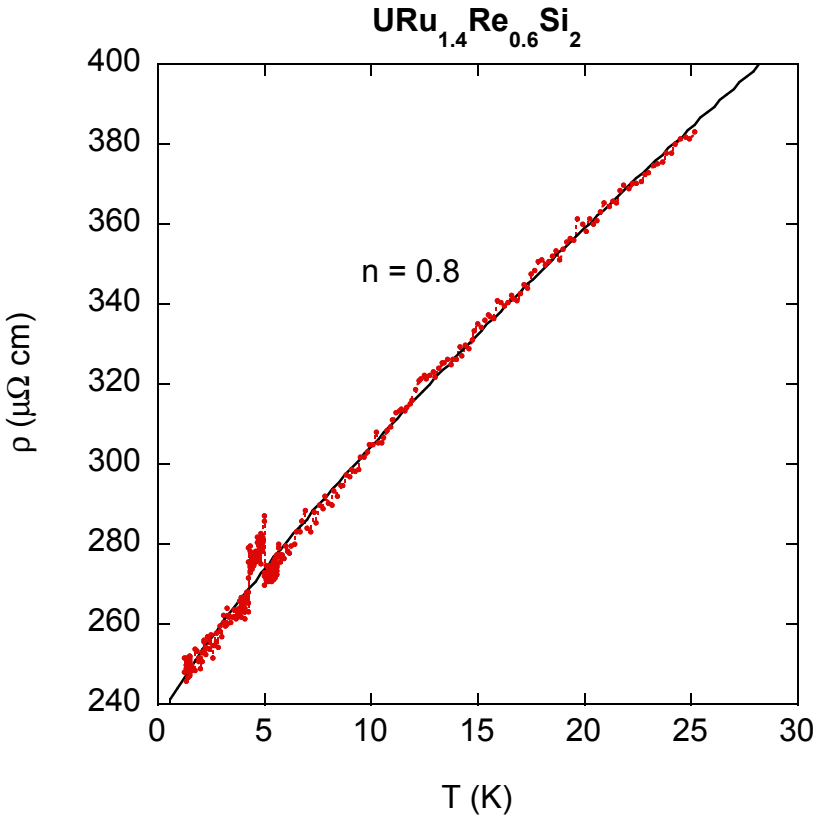

Figure IV.11: Power-law fit to $\rho(T)$ data for $x = 0.6$. The negative curvature persists over at least a decade in T.

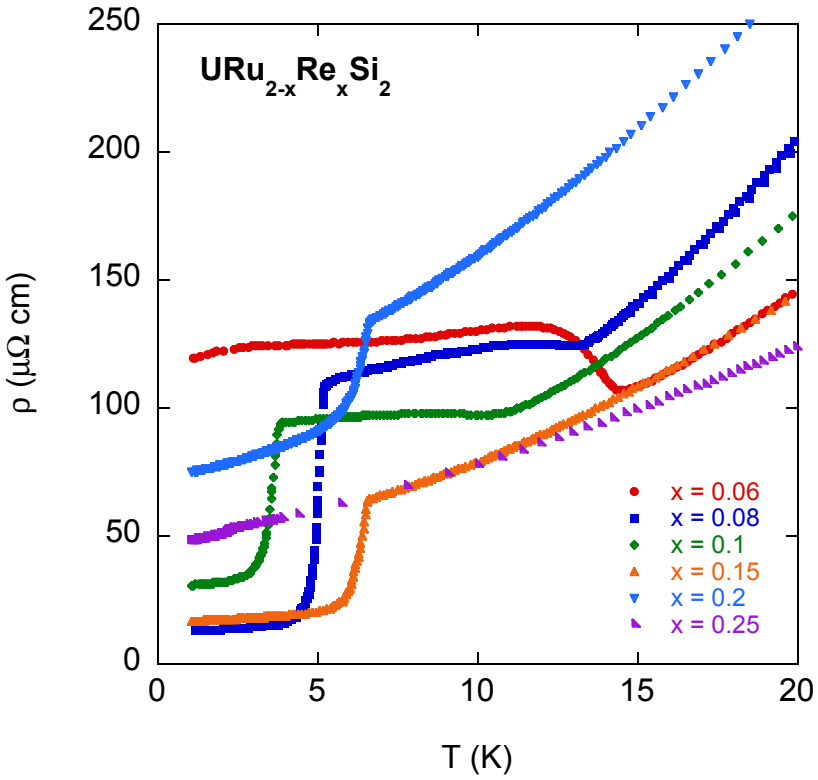

Figure IV.12: Examples of low-T drops in $\rho(T)$ data. These features make it impossible to perform reliable power-law fits to $\rho(T)$ over several decades in T. The nature of these features is discussed in more detail in Chapter VII.

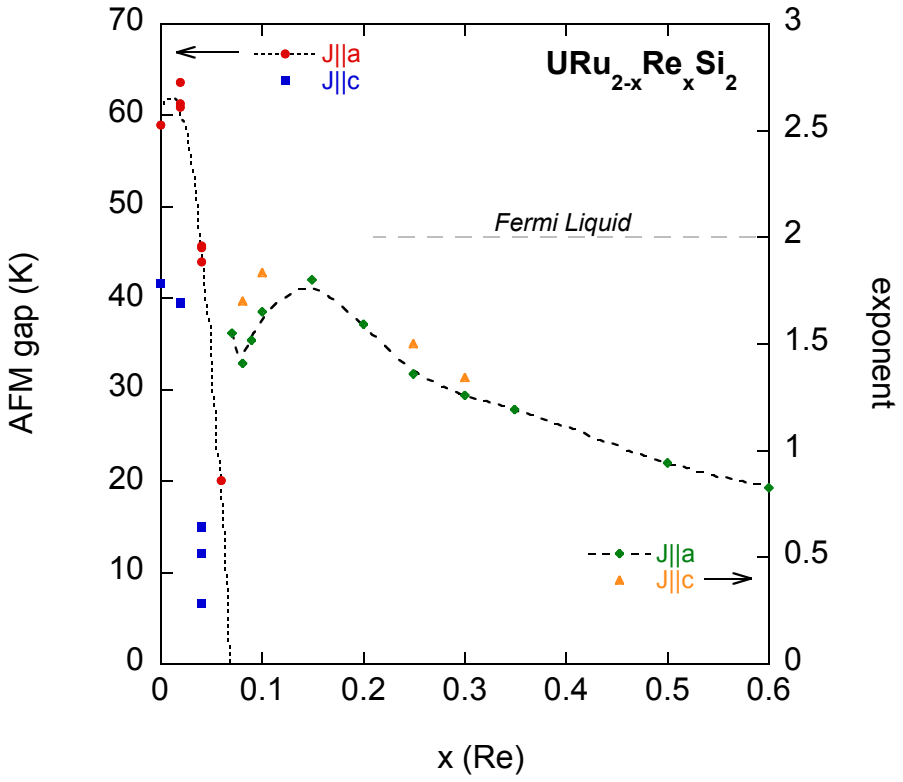

Figure IV.13: Phase diagram based upon electrical resistivity data. The HO phase is characterized by an AFM scattering gap, while the higher x exhibit power-law T-dependence, always with an exponent less than 2. Multiple points on the HO side reflect fits to data from different samples. Lines are guides to the eye.

V

Specific Heat

V.A General Features

The $C(T)/T$ data are shown in Fig. V.1. Because the entropy $S = \int dT\ C/T$, any residual S at 0 K is readily identifiable. At first glance, the most outstanding feature in C/T is the anomaly associated with the hidden order transition, which appears for $0 \leq x \leq 0.08$, as shown in Fig. V.2. Note that the anomaly associated with the SC transition at $x \approx 1.2$ K in $x = 0$, is not observed in any of the Re-substituted materials. Interestingly, for all values of x, an upturn at low T is evident. As shown in Fig. V.3, C/T at low temperatures increases with x, and between $x = 0.5$ and $x = 0.6$ a qualitative change in behavior occurs.

To isolate the electronic contribution to $C(T)$, it is necessary to subtract the estimated phonon contribution. At low T, $C(T)$ is typically modeled as

$$C = \gamma T + \beta T^3. \tag{V.1}$$

The term γ represents the electronic contribution, and is proportional to the electronic density of states at the Fermi surface, while β comes from the zero T limit of the Debye model for phonons. The Debye temperature θ_D is inversely proportional to $\beta^{-1/3}$, and $k_B\theta_D = \hbar\omega_D$, which gives the high frequency cutoff of the Debye model. With the phonon term subtracted, but not γ, the electronic contribution C_e/T is plotted in Fig. V.4. Compared to Fig. V.1, the HO transition is

much more pronounced and an increase at low T can be seen for all x, including the parent compound. The value of γ, estimated from C_e/T using the region of constant C_e/T in the range $15 < T < 25$ K, can then be used to estimate the effective electronic mass m^*. When appropriate, a lower-T estimate of γ was also made at $T < T_0$. Both θ_D and m^*/m_e, where m_e is the rest mass of a bare electron, are plotted in Fig. V.5. Note that because the values of m^*/m_e are estimated using extrapolations from data at rather high temperatures, they may ignore a possible low-T enhancement of γ that can arise from the presence of a narrow peak in $N(E_F)$. This scenario leads to an effective $\gamma(T)$, a situation that can also arise due to NFL behavior. The value of θ_D roughly agrees with published values [13]. That $\theta_D \approx 270$ K is further supported by the the full Debye C/T calculated from this value (Fig. V.6) as the peak at approximately 75 K is consistent with measured data [43]. As shown in Fig. V.5, the linear suppression of θ_D with x is observed, which has been used as a guide in the analysis of $C(T)$ for intermediate x, where it proves more difficult to uniquely determine a value of β. The reduction of θ_D with increasing x is expected as the heavier Re is substituted for Ru. Because the value of γ depends on the value of β, for the fits from $x = 0.25$ and $x = 0.3$, there is scatter in the value of m^*, which may reflect an inappropriate choice of β at these concentrations. However, if the value of β is adjusted to make the x-dependence more monotonic, the associated value of θ_D will substantially deviate, by about 20 K, from the plotted line, so that the monotonicity of $\theta_D(x)$ is considered the more reliable guide. At low x, there is a decrease in γ at $T < T_0$ associated with the HO transition, which has been attributed to the partial gapping of the Fermi surface by the HO transition [19]. These values of γ are also plotted in Fig. V.5, from which it is evident that the putative Fermi surface gap closes at about $x = 0.1$. Another relevant feature seen in Fig. V.4 is that for $T > 15$ K, a local maximum is evident in C_e/T, and the T at which it occurs decreases slightly with increasing x. It is tentatively associated with a deviation from T^2 of the phonon contribution to C/T, which occurs when the low-T limit is exceeded, or if the Debye model is in-

accurate. The Debye model invokes a frequency limit to the phonon spectrum and assumes a constant sound velocity for all modes. In a tetragonal pseudo-ternary intermetallic compound, both of these assumptions are questionable, even at low T. It should be noted that the values of β determined in the present study do not agree with those published previously for polycrystalline samples [132] and cannot be compared directly to those in Ref. [143], because of different fitting forms used to approximate the phonon contribution. This difference in analysis may also be the cause of disagreement between values of γ.

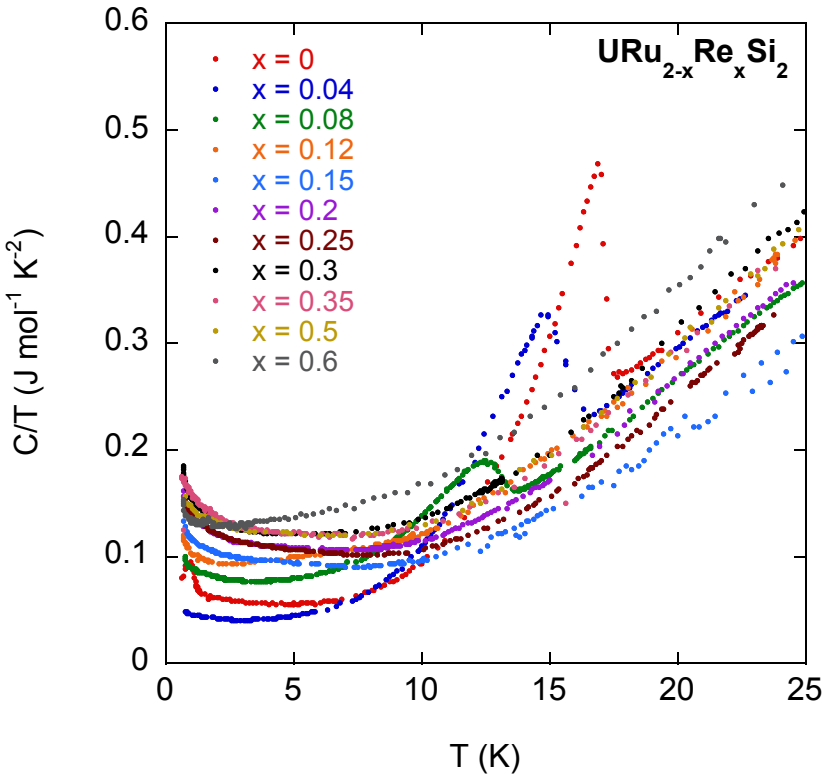

Figure V.1: The specific heat divided by temperature of $URu_{2-x}Re_xSi_2$ for all values of x.

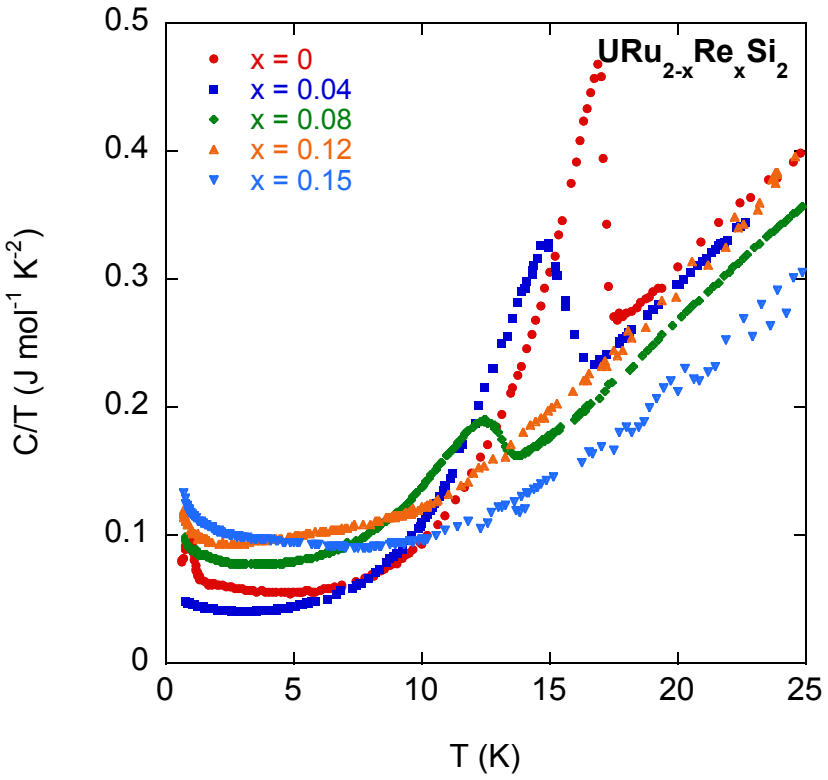

Figure V.2: The specific heat divided by temperature of $URu_{2-x}Re_xSi_2$ for $x \leq 0.15$.

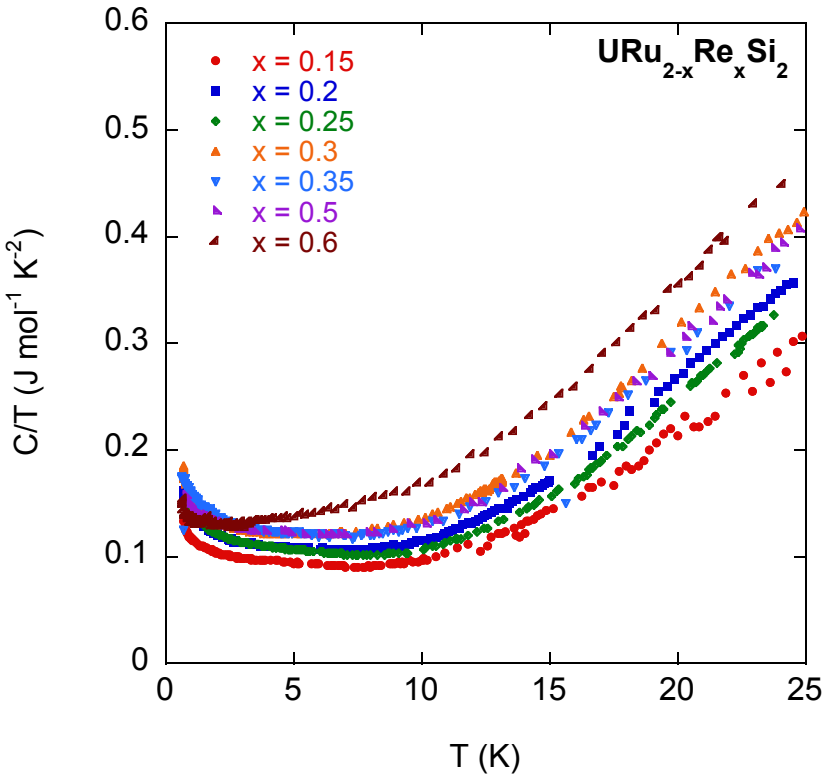

Figure V.3: The specific heat divided by temperature of $URu_{2-x}Re_xSi_2$ for $x \geq 0.15$.

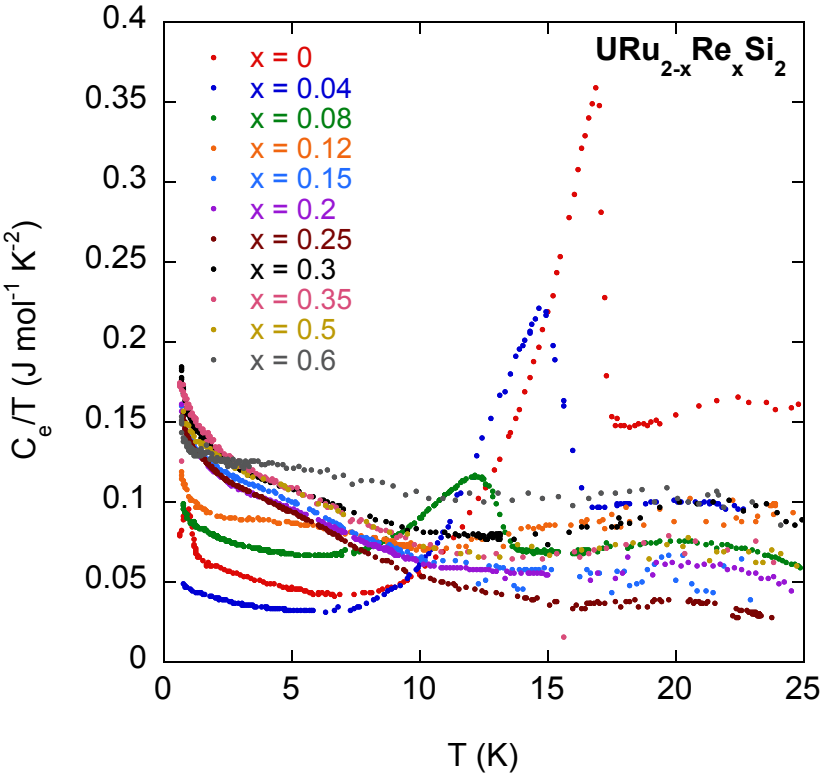

Figure V.4: The electronic specific heat divided by temperature of $URu_{2-x}Re_xSi_2$ for all x. These data were generated by subtracting the phonon contribution from the data in Fig. V.1.

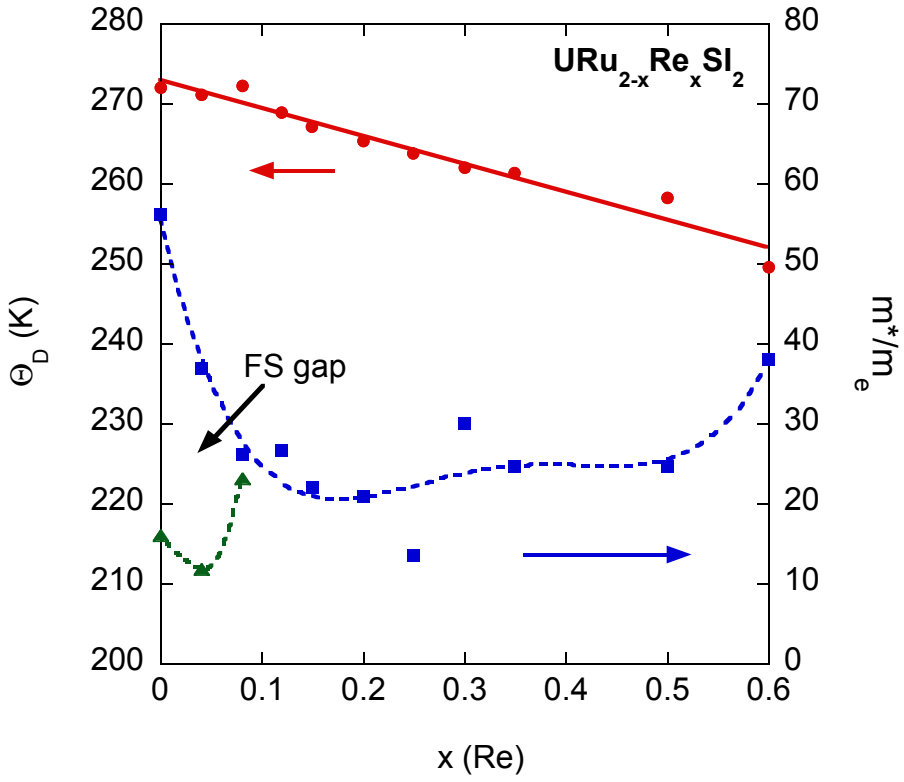

Figure V.5: The Debye temperature θ_D and electronic effective mass m^*/m_e for all x (see text). The Debye temperature linearly decreases with increasing x. For $x < 0.1$, the HO transition reduces the electronic specific heat, presumably by gapping part of the Fermi surface. Lines are guides to the eye.

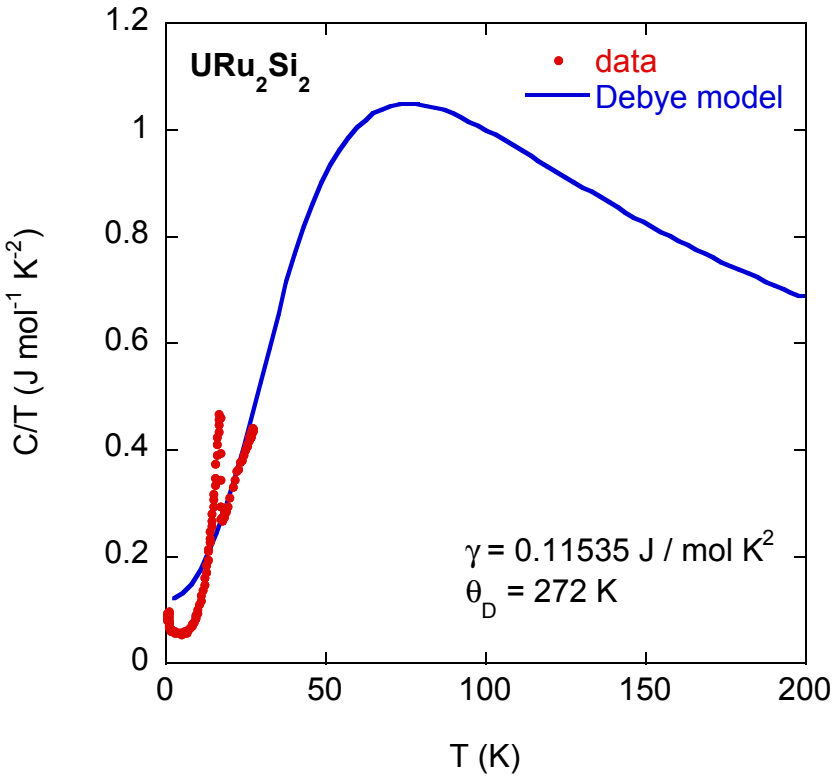

Figure V.6: Debye model $C(T)/T$ with $\theta_D = 272$ K. The peak at about 75 K is consistent with published data [43], supporting this choice for θ_D.

V.B Hidden Order

The evolution of the HO phase with x is best seen in the C/T data. In previous studies, the HO phase boundary was extrapolated to $T = 0$ K at $x = 0.15$ [142]. In $\rho(T)$ measurements, the significantly-broadened anomaly associated with the HO transition is still visible at $T \approx 10$ K in $x = 0.1$, but is no longer seen in $x = 0.15$. In the $C(T)$ data, the HO transition is no longer observed in $x = 0.12$, calling into question whether T_0 is smoothly suppressed to 0 K, and whether there is a HO QCP on the Re x-axis. However, T_0 does not represent the only energy scale associated with the HO phase, and is not necessarily directly proportional to the HO order parameter. Two other metrics of the HO transition are the jump in C at T_0, denoted as ΔC, and Δ_0, the 0 K value of the energy gap at the Fermi surface opened by the HO transition, which is determined by a fit of the form

$$C \propto e^{-\Delta_0/k_B T}. \tag{V.2}$$

The x-dependence of these parameters is shown in Fig. V.7. The x-dependence of T_0 extrapolates to linearly or with a weak power law to $x > 0.15$, even though the HO transition is not observed for $x \geq 0.12$. Similarly, Δ_0 also extrapolates linearly to values of x beyond those in which the HO transition is observed. In contrast, ΔC extrapolates linearly to $x = 0.1$, as might be expected, since $\Delta C \neq 0$ is necessary for there to be an observable anomaly in $C(T)$. Another parameter describing the HO transition is the reduction of γ due to the partial gapping of the Fermi surface, which was determined after subtraction of the logarithmic T-dependence described below. The construction is clearest in Fig. V.11, where the difference in C/T above and below the HO transition is most readily evident. In analogy with BCS theory, the dimensionless ratios $\frac{\Delta C}{\gamma T_0}$ and $\frac{\Delta_0}{k_B T_0}$ were determined (for reference, BCS weak-coupling yields ratios of 1.43 and 1.76, respectively [155]). These parameters are shown in Fig. V.8. In this plot, it is evident that $\Delta\gamma$ extrapolates linearly to 0 at $x \approx 0.1$. In addition, $\frac{\Delta C}{\gamma T_0}$ also extrapolates smoothly to 0 at $x \approx 0.1$, although $\frac{\Delta_0}{k_B T_0}$ extrapolates linearly to 0 at $x = 0.3$. These latter two extrapolations do not

offer much insight as they deviate from the BCS values by a large margin and are not constant. On the other hand, the fact that $\Delta\gamma$ and ΔC both extrapolate to 0 at $x \approx 0.1$ is consistent with the closing of a Fermi surface gap at $x = 0.1$, at which point there would be no change in the electronic contribution to the specific heat, and no entropy gain at T_0 once the gap is closed.

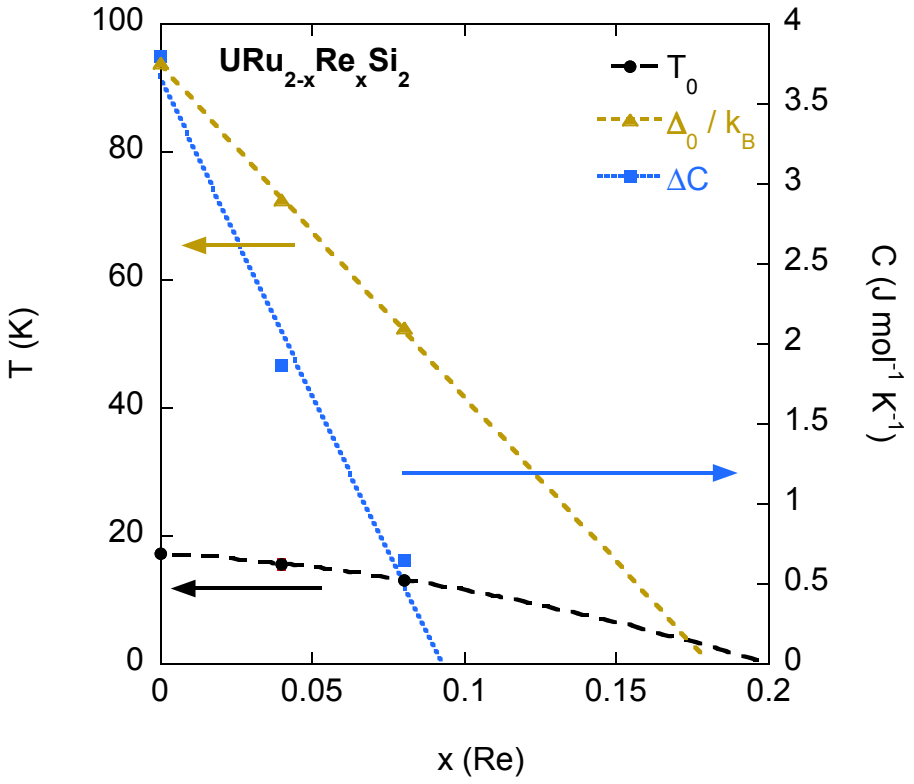

Figure V.7: Parameters associated with the HO transition: transition temperature T_0, Fermi surface gap Δ_0, and specific heat jump ΔC. The lines represent reasonable extrapolations.

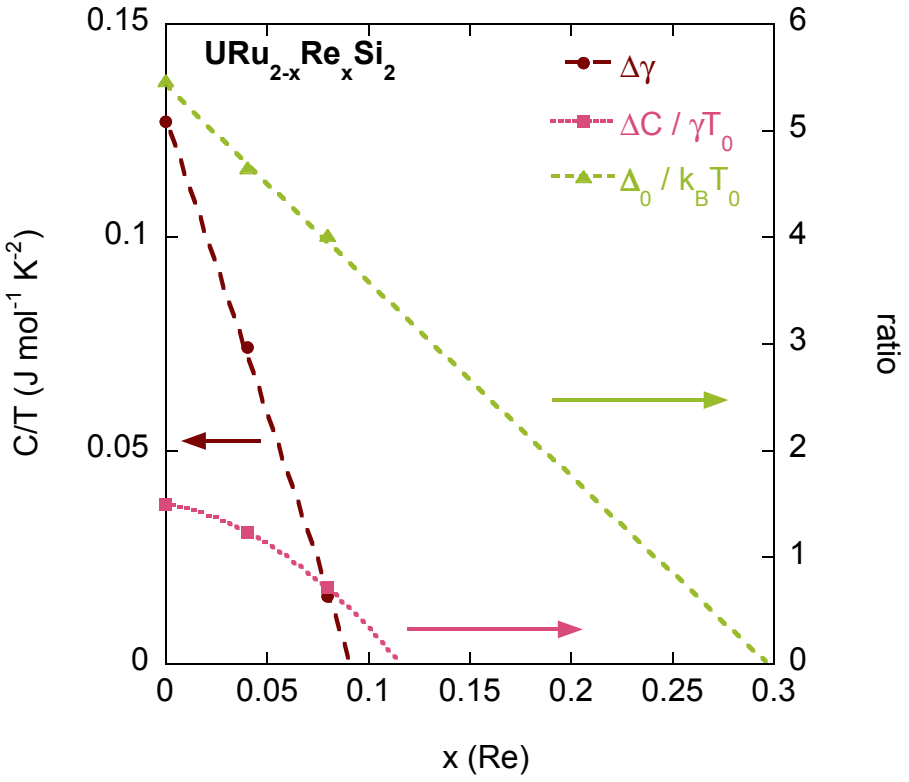

Figure V.8: Parameters associated with the HO transition: reduction in the electronic contribution $\Delta\gamma$, the ratio of the specific heat jump ΔC to γT_0, and the ratio of the Fermi surface gap Δ_0 to $k_B T_0$. The lines represent reasonable extrapolations.

V.C Logarithmic Temperature Dependence

The low-T upturn observed for all x seems to play an important role in $URu_{2-x}Re_xSi_2$. Divergence in C/T at low T is commonly associated with NFL behavior, within the context of which the data are fit to logarithmic or weak power-law functions of T. In $URu_{2-x}Re_xSi_2$, this type of analysis was used previously as a means to identify a quantum critical point [143, 142]. To characterize the low-T divergence in the present study, fits of the form $C_e/T = a - b \ln T$ were performed, generally over the range $1 < T < 8$ K. Example fits are shown in Fig. V.9, where it is demonstrated that the low-T log fits do not depend very sensitively on the Debye fit. The results of these fits are presented in Fig. V.10. The value of the constant peaks at $x = 0.4$, while the value of the logarithmic coefficient peaks at $x = 0.35$. This behavior agrees well with data presented by Bauer and coworkers [143, 142]. This fact is important, because if the logarithmic T-dependence is associated with a low-T increase in the electronic m^*, the maximum effective mass would be expected at the QCP.

The $C(T)$ data with both the Debye and logarithmic contributions subtracted is shown in Fig. V.11. In this view, two features are emphasized: the change in electronic contribution due to the HO transition, and the existence of a small, broad hump at $x = 0.5$. As shown in Fig. V.12, this hump persists over a large range of x, although it may actually be an artifact due to the assumption of logarithmic T- dependence. Over the limited range of T in question, a logarithmic dependence is indistinguishable from a weak sub-linear power law. Because the physical mechanism responsible for the upturn is not established, there is no strong theoretical motivation to choose one fitting form over the other. Although both forms can be considered reasonable, the logarithmic fits are used here because they involve one fewer free parameter. If the hump in C_{e-ln}/T is a real feature, then it may be tentatively ascribed to low-T spin fluctuations associated with the spin glassiness inferred in neutron scattering measurements [144]. It is

also reasonable to acknowledge that the feature may be due to an impurity phase. Despite uncertainties regarding its origin, the hump represents an energy scale that shows little x-dependence. In Fig. V.12, another persistent feature of C/T is clearly seen at low T: an even stronger divergence for $T < 1$ K. It is speculated that this may be the high-T tail of a nuclear Schottky anomaly, which might arise due to dipolar or quadrupolar splitting in a U, Ru, or Re atomic nucleus through hyperfine coupling, but the C/T data exhibit a T^{-4} dependence instead of T^{-3}, the expected leading term from a nuclear Schottky anomaly. Another possible explanation is that at intermediate x, Re inhomogeneity leads to the existence of low-x phase-separated portions of the sample, and the upturn is actually the high T onset of a SC transition, albeit one with a suppressed T_c. This possibility cannot be discounted outright, but there is no evidence from transport or magnetization measurements of a sizable SC transition at these temperatures. In several NFL materials, the logarithmic T-dependence of C/T has been observed to diverge even more strongly at lower T [9, 10, 11], suggesting that the stronger low-T divergence is a general feature of such systems.

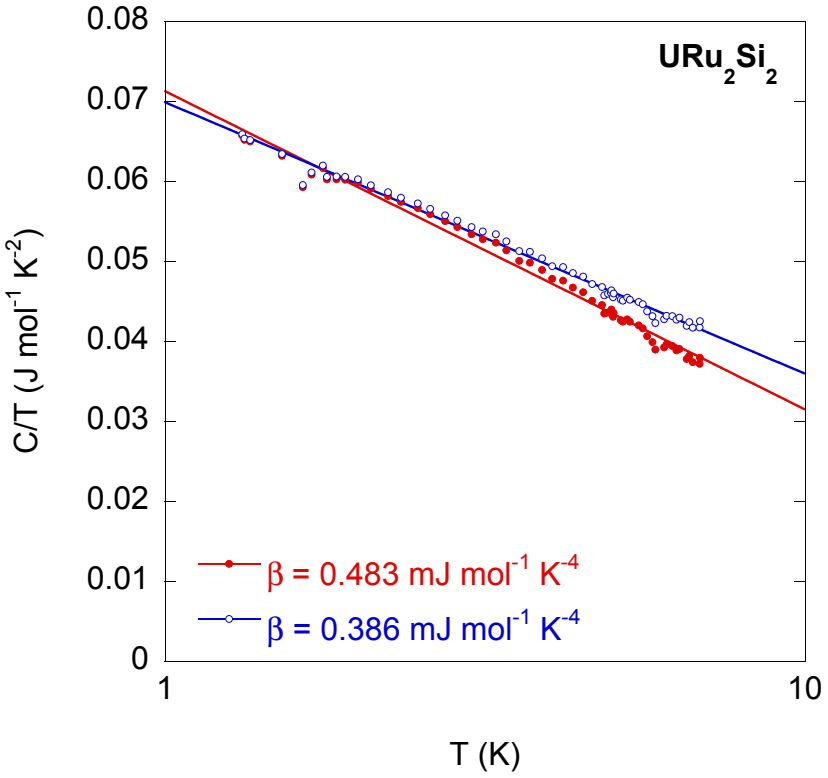

Figure V.9: Example logarithmic fits for URu_2Si_2. The two data sets are due to subtraction of different reasonable phonon contributions: $\beta = 0.483$ and 0.386 mJ mol^{-1} K^{-4} correspond to $\theta_D = 272$ and 293 K, respectively.

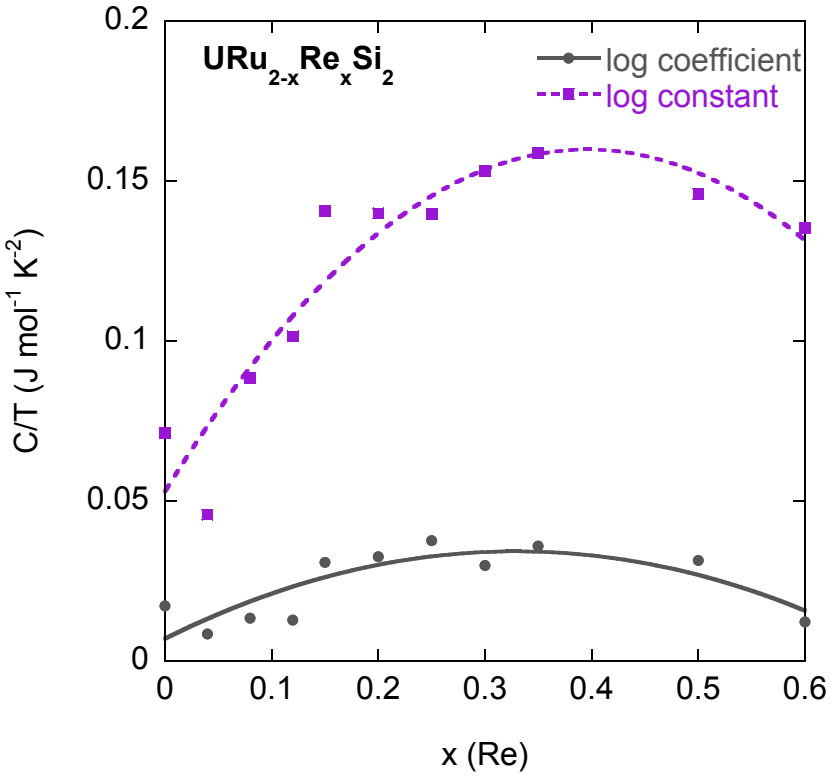

Figure V.10: Parameters from logarithmic fits to C/T of the form $a - b \ln T$. The value of the constant peaks at $x = 0.4$, while the value of the coefficient peaks at $x = 0.35$. Lines are guides to the eye.

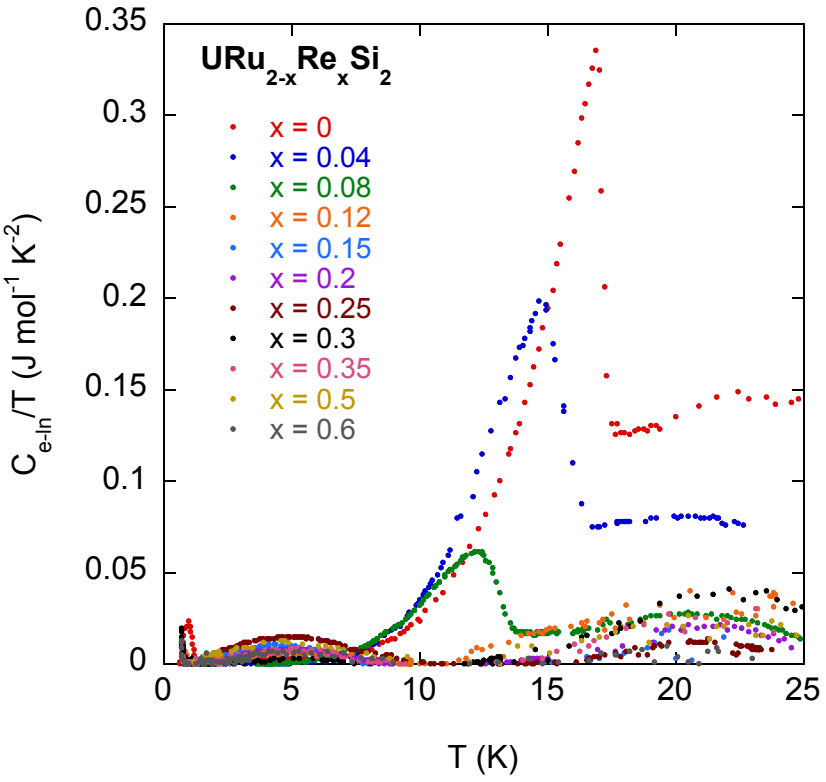

Figure V.11: The specific heat divided by temperature with both Debye and logarithmic contributions subtracted. This view dramatically emphasizes the decrease in electronic specific heat due to the HO transition and uncovers a persistent small hump at 5 K.

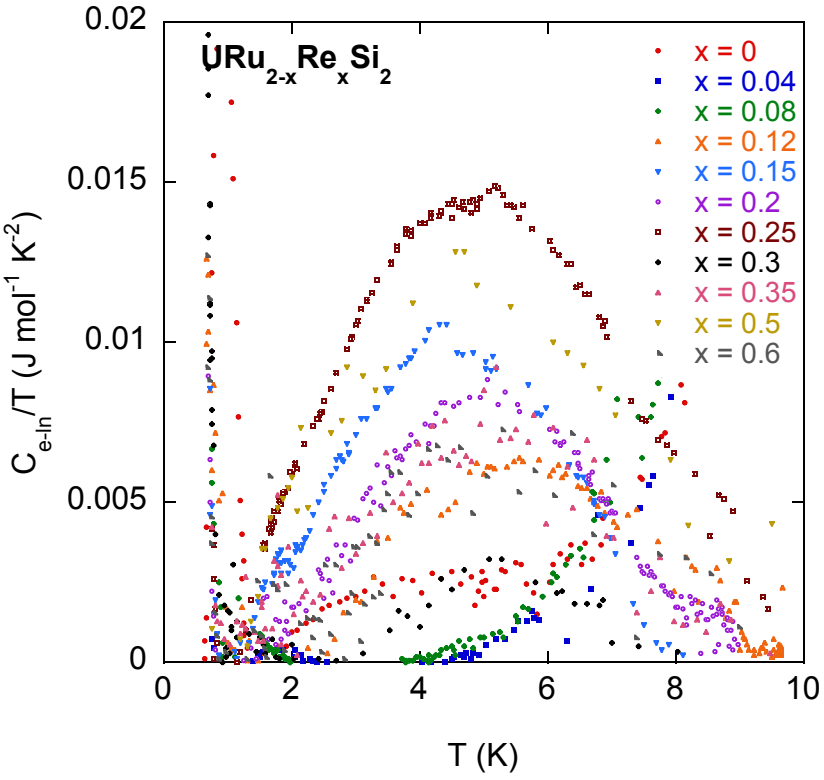

Figure V.12: The 5 K hump feature in the C/T data with Debye and logarithmic contributions subtracted. The feature persists over a large range of x.

VI

Magnetization

VI.A Magnetic Susceptibility

The magnetic susceptibility $\chi = \frac{\partial M}{\partial H}$ is calculated from measured low-field $M(T)/H$, which equals $\frac{\partial M}{\partial H}$ when $\chi(H)$ is constant. Plots of $\chi(T)$ with $H||[001]$ (c-axis) for all x are shown in Figs. VI.1 and VI.2. The data can be roughly divided into high-T and low-T regimes. The former is characterized by a hyperbolic T-dependence, which rolls over and exhibits a maximum that is believed to be associated with the onset of Kondo coherence; this behavior is largely independent of x. The low-T regime, on the other hand, exhibits dramatic x-dependence. At $x = 0$, the HO transition is visible at 17 K, while at lower T, χ diverges. The strength of this divergence and its origin are not clearly addressed in the literature, as it is often ignored entirely, although it is can be used to assess a sample's quality [99]. An approach usually taken with metallic systems is to treat a small low-T divergence as due to magnetic impurities and to subtract it from the data [156], although there is always uncertainty regarding whether the low-T signal really comes from impurities[157, 158]. In $URu_{2-x}Re_xSi_2$, the magnitude of this divergence clearly increases with x, as shown in Figs. VI.1 and VI.2, and it eventually engulfs the local maximum associated with coherence. Note that the low-T divergence in $x = 0.1$ exceeds that of $x = 0.15$, which may be due

to an extra magnetic impurity contribution. It is possible that such impurities exist in the bulk samples at levels lower than 5%, which is the approximate lower level of sensitivity of x-ray powder diffractometry. Alternatively, it may be due to an uncorrected contribution from free oxygen, a common contaminant in SQUID measurements that can undergo AFM order at T as high as 50 K [159, 160]. If the low-T divergence is simply due to magnetic impurity ions, then its growth with x would imply that Re substitution somehow adds isolated magnetic moments to the system, perhaps by inducing the underscreening of U local moments by the conduction band via the removal of electrons from the system. If this scenario were true, the size of the divergence should scale with impurity concentration. As seen in Fig. VI.3, this is clearly not the case: $\chi(2\text{ K})$ for $x = 0.6$ exceeds $\chi(2\text{ K})$ for $x = 0.08$ by 3 orders of magnitude instead of a simple factor of 10.

A feature evident in $\chi(T)$ is the magnetic irreversibility shown in Fig. VI.3. This behavior is exhibited by almost all samples, regardless of x. For $x > 0.2$, irreversibility due to magnetic ordering may be expected. One caveat is that the irreversibility temperature is always higher than the Curie temperature T_C of the material, calculated below in detail. This effect may be the result of spin fluctuations that persist to $T > T_C$, but the existence of spin fluctuations capable of generating magnetic irreversibility is more difficult to establish in lower x. Note that even in the absence of magnetic order, there is strong evidence for spin fluctuations in URu_2Si_2 persisting to 100 K [31, 43]. However, that T scale does not readily explain the low-T behavior, especially since magnetic irreversibility is not an accepted characteristic of URu_2Si_2. It has been previously shown that there exist higher-T magnetic phases extrinsic to the sample [94, 101]. In fact, the report of Amitsuka and coworkers states that low-H irreversibility is observed to some degree in all of their $U(Ru_{1-x}Rh_x)_2Si_2$ samples. Note that a potential contaminant in this system is UO_2, with $T_N \approx 31$ K [161, 162].

As shown in Fig. VI.4, there is marked magnetic anisotropy in $URu_{2-x}Re_xSi_2$. As mentioned previously, this behavior is consistent with a tetragonal crystal struc-

ture and magnetic easy axis parallel to the long c-axis. Fig. VI.5 shows the in-plane $\chi(T)$. Several features are important: a low-T divergence that increases in magnitude with x, and magnetic irreversibility with comparable T scales to the out-of-plane data, but no visible maximum in the vicinity of 50 K. In- and out-of-plane $\chi(T)$ data are compared directly across a wide range of x in Fig. VI.6. From this plot, it is evident that at $x = 0$, the low-T χ differs by about a factor of 4, but at $x = 0.5$, there is a difference of more than 2 orders of magnitude between in- and out-of-plane susceptibilities. This trend is related to the development of magnetic order at higher x and indicates a strengthening of the magnetic anisotropy - the magnetism becomes more Ising-like.

To quantify the behavior of the behavior of $\chi(T)$ for $H||[001]$, a standard Curie-Weiss (CW) analysis was performed at high T, while at low T, it was determined that an extra Pauli-type constant paramagnetic contribution was required to successfully describe $\chi(T)$ by a CW law. The general approach is shown for $x = 0.25$ in Figs. VI.7 and VI.8. Note that the coherence maximum separates the high- and low-T behavior. While the high-T behavior is well described by a CW law, which can be interpreted in a straightforward manner, the low-T data can be interpreted and fit in several ways, shown in Fig. VI.9. In addition to the Pauli-enhanced CW law, a simple power-law T-dependence, interpreted as due to NFL behavior [143], can be fit to the data, albeit poorly. The fit quality can be improved by adding a term similar to the CW temperature θ_{CW}. While some contact may be made with unconventional scaling exponents determine via neutron scattering [144], it is made difficult by the wide discrepancy between power-law exponents from these two fits. A further complication from these fits is that the coefficient cannot be interpreted in a straightforward manner like the Curie constant because its units involve a non-integer power of T. Between the two 3-parameter fits, the Pauli-enhanced CW law is thus used exclusively. The results of high-T CW fits for all x is shown in Fig. VI.10. Good fits to the data were generally obtained for $100 < T < 300$ K. The first thing to note is the constancy of the effective moment

μ_{eff}, which has a value slightly in excess of the free ion moment $\sim 3.6\mu_B$ of U^{3+} and U^{4+}. The values of θ_{CW} are large and negative for small x, becoming significantly less negative by only $x = 0.5$, but always remaining negative. The large negative values are commonly associated with strong AFM coupling between the paramagnetic spins, with $\theta_{CW} \sim T_N$. In the absence of true AFM order, it is noteworthy that the 100 K T scale corresponds instead to T_{coh}, and Kondo coupling between local and itinerant moments is indeed AFM in nature. It is unclear whether the change in value of θ_{CW} can be interpreted as a lowering of T_{coh}, because the local maximum in $\chi(T)$ disappears by these values of x, and in $\rho(T)$, T_{coh} is observed to actually increase with x. Results of fits to $\chi(T)$ at low T are shown in Fig. VI.11. The T range over which these fits were performed shifted from $T < 5$ K at low x to $30 < T < 50$ K at $x = 0.6$, well into the FM regime. The value of μ_{eff} is small, but gradually increases with x to a sizable value. In the absence of other data, at low x, the size of the moment would typically be associated with an impurity contribution, but by $x = 0.6$ the moment is large enough to be associated with a crystalline electric field-split ground state with a reduced moment. In the case of $URu_{2-x}Re_xSi_2$, this trend may be due to the aforementioned reduction in Kondo screening resulting from Re substitution and the removal of electrons from the conduction band. The trend in θ_{CW} is more straightforward to interpret. At low x, in the absence of magnetic order, its value is negligible, whereas it increases due to the onset of FM order. At higher x, the magnitude of θ_{CW} is indeed tens of K, although these values do not correspond directly to the values of T_C determined in the next section.

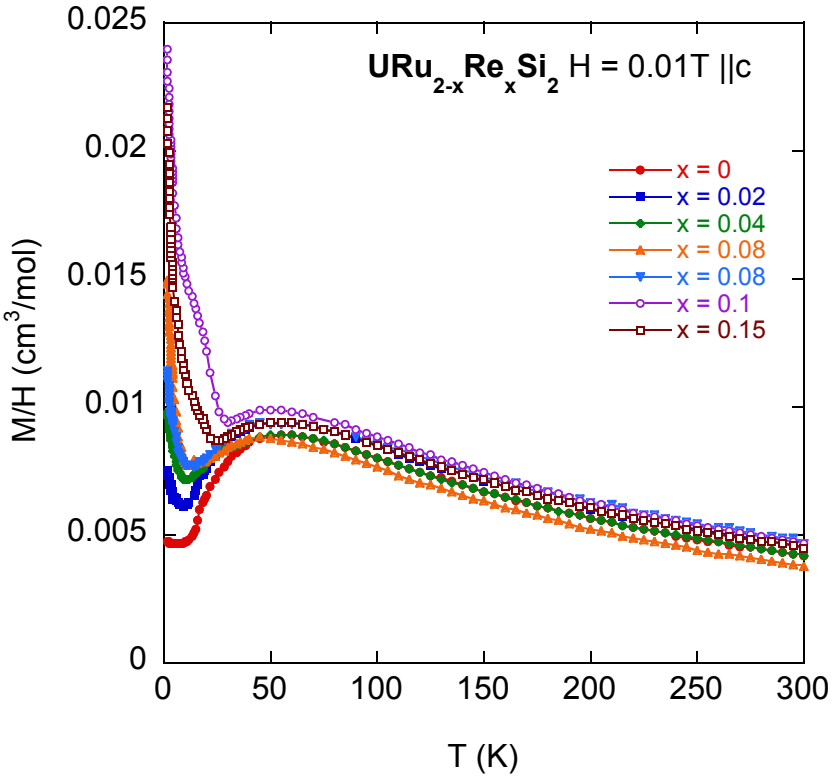

Figure VI.1: Magnetic susceptibility for low x.

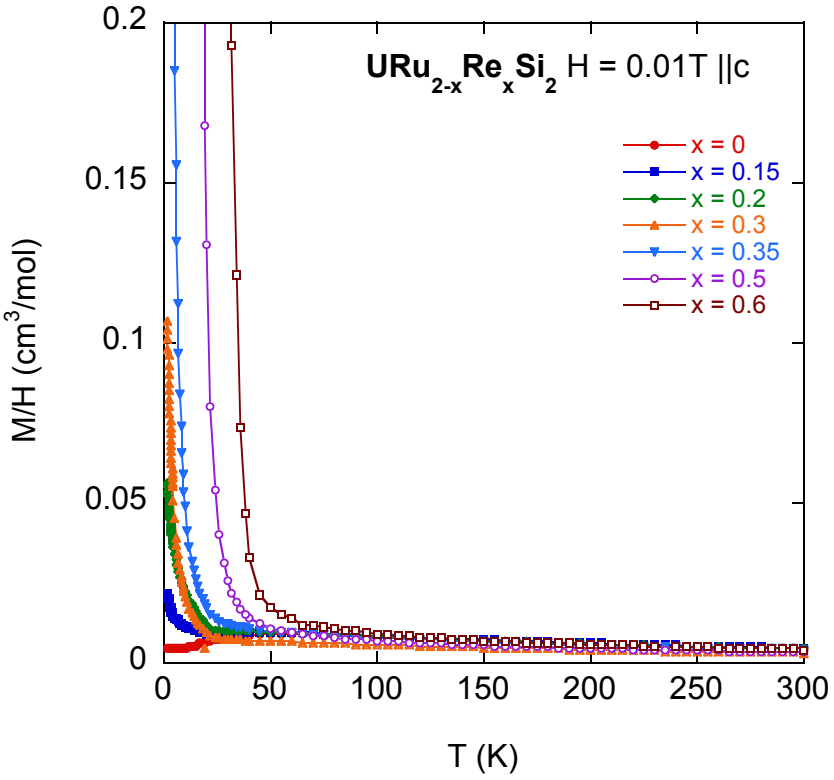

Figure VI.2: Magnetic susceptibility for high x.

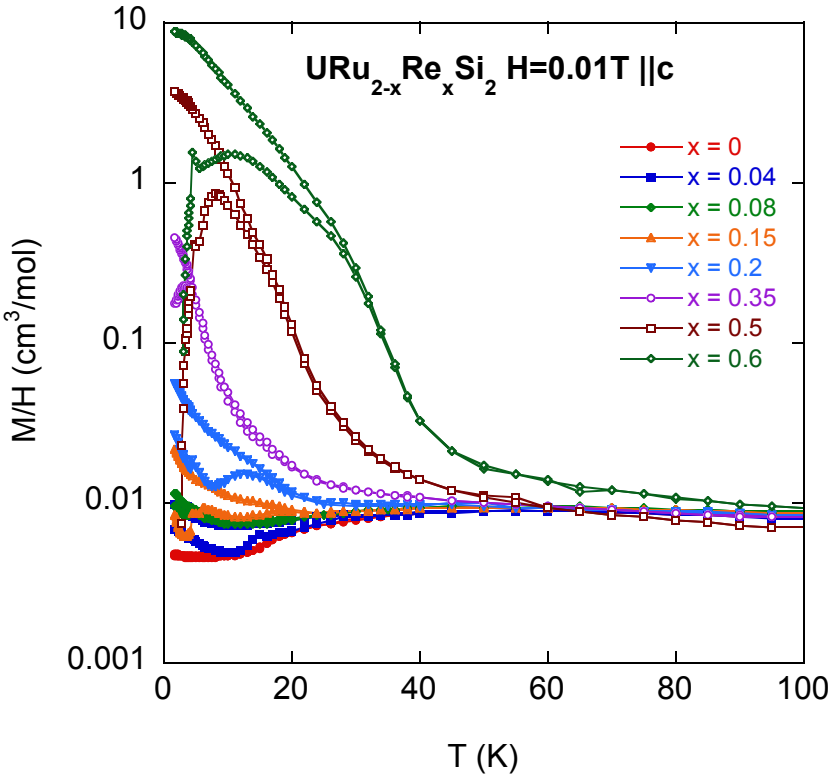

Figure VI.3: Irreversibility in magnetic susceptibility.

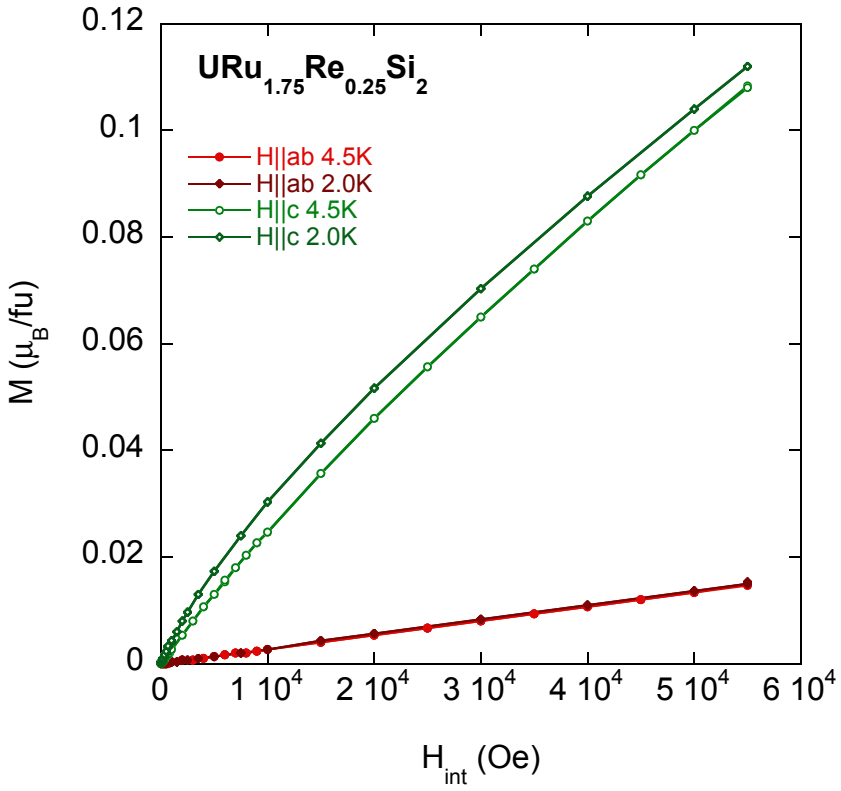

Figure VI.4: Low-T M(H) direction dependence for $x = 0.25$.

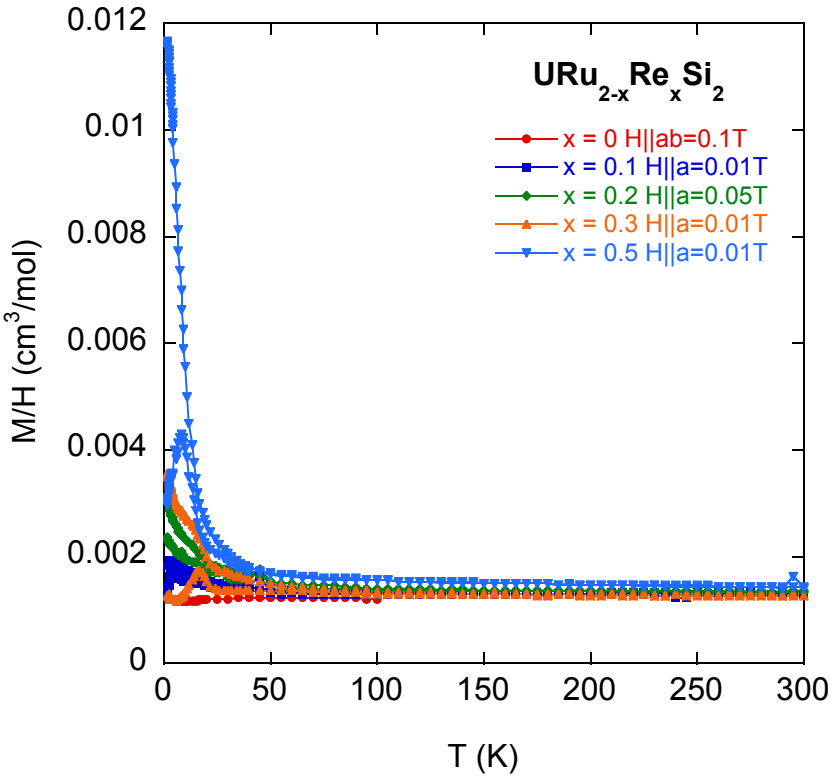

Figure VI.5: In-plane magnetic susceptibility. Irreversibility is clearly observed in this direction as well.

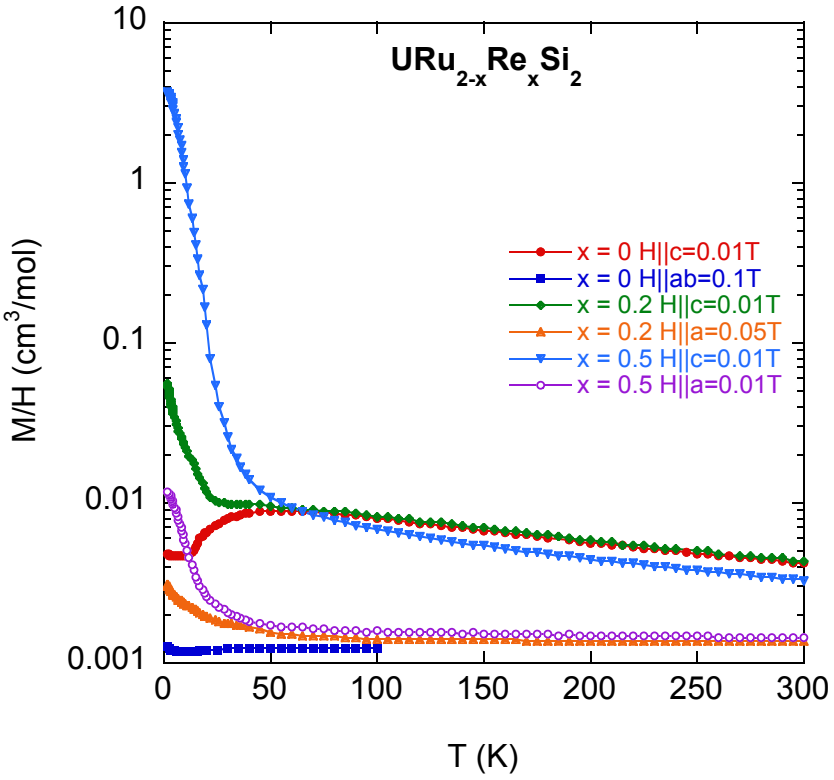

Figure VI.6: Comparison of in- and out-of-plane magnetic susceptibility.

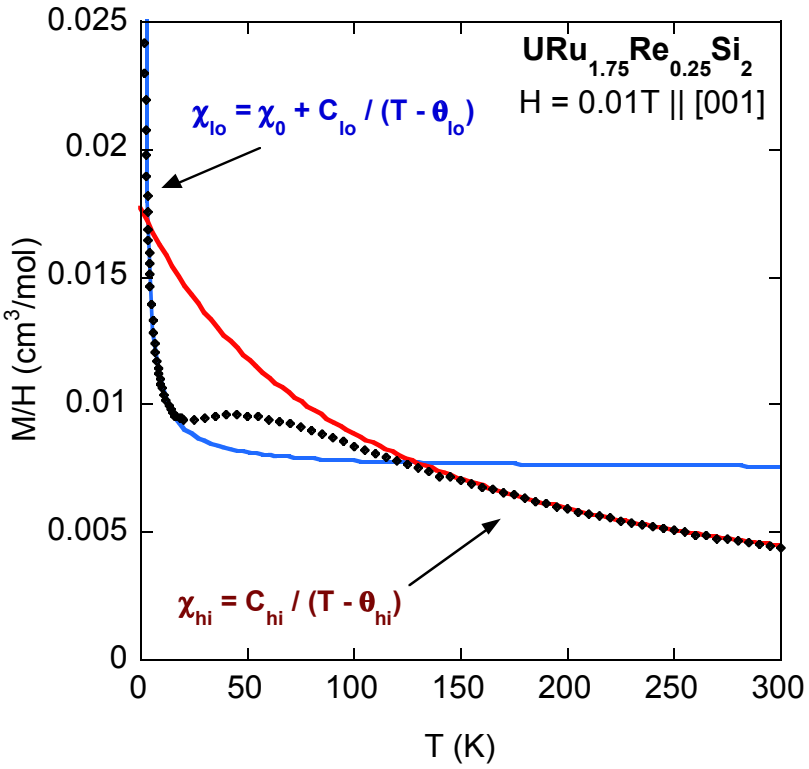

Figure VI.7: Example of Curie-Weiss fits to $\chi(T)$ for $x = 0.25$.

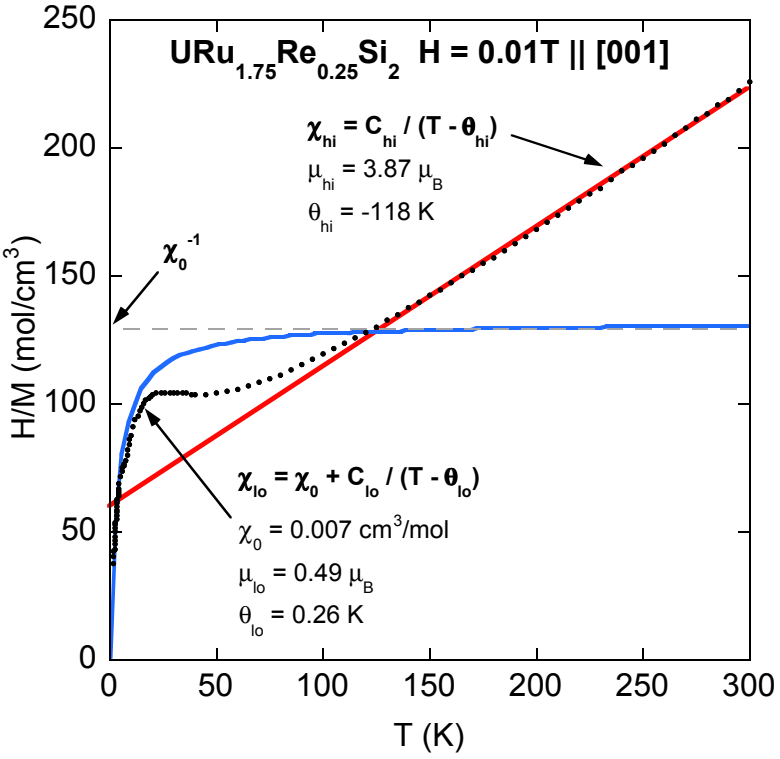

Figure VI.8: Example of Curie-Weiss fits to $\chi^{-1}(T)$ for $x = 0.25$.

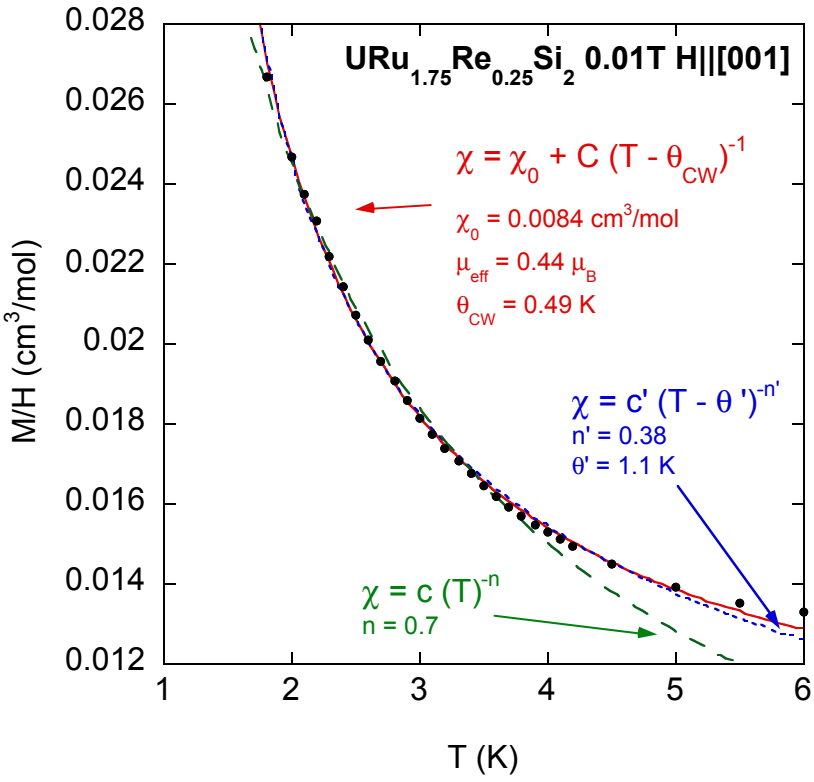

Figure VI.9: Comparison of low T fits to $\chi(T)$ for $x = 0.25$.

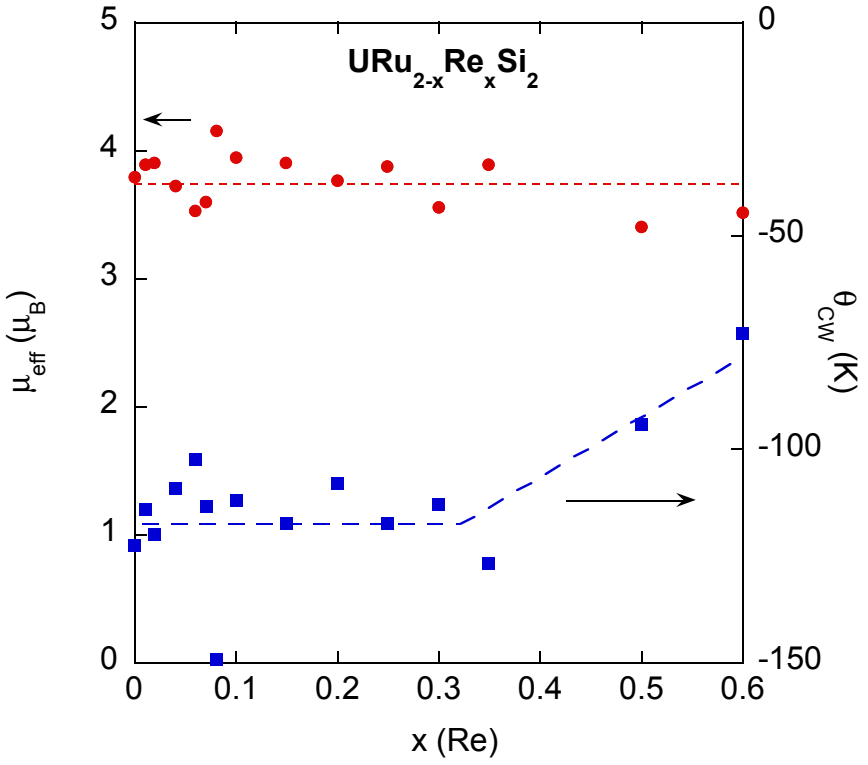

Figure VI.10: Parameters from high T Curie-Weiss fits.

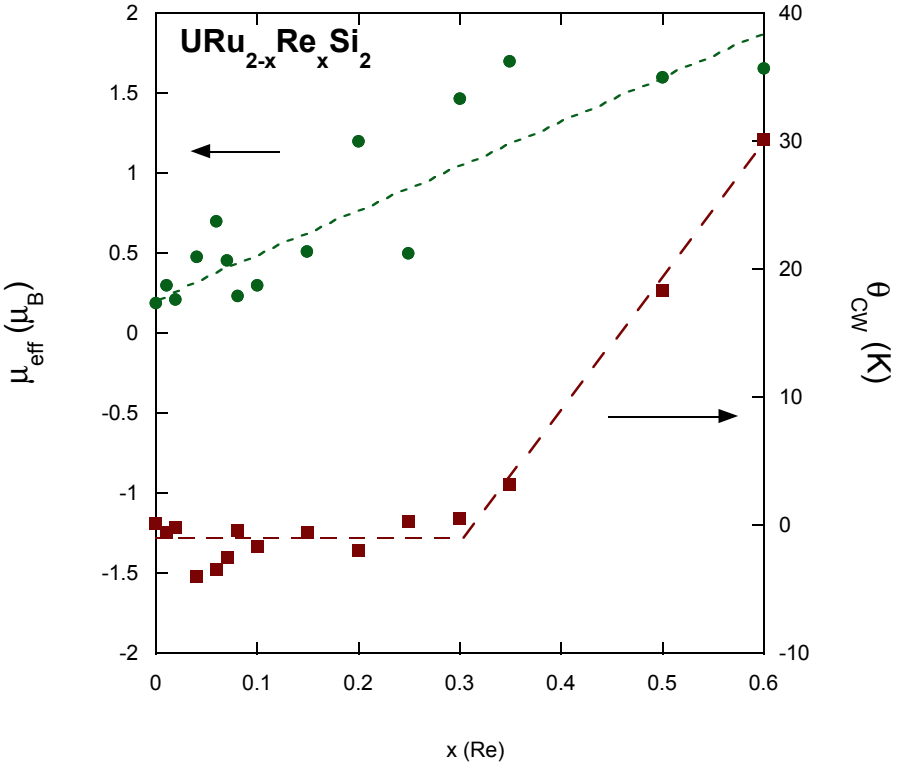

Figure VI.11: Parameters from low T Curie-Weiss fits. The T range over which the fits are performed changes at higher x.

VI.B Scaled Arrott Analysis

A large challenge in the characterization of the FM phase is the determination of the ordering temperature T_C at each x, in the absence of anomalies in $\rho(T)$ and $C(T)$. This is especially important in terms of identifying the value of x at which the FM phase boundary extrapolates to 0 K, which may be a QCP. Through a large number of $M(H)$ measurements for the various x, shown in Figs. VI.12, VI.13, VI.14, VI.15, VI.16, VI.17, and VI.18, it was found that a scaled Arrott analysis, based on the Arrott-Noakes equation of state [163], was appropriate. From $M(H)$ data, it is clear that the magnetization exhibits hysteresis at low T. The ordered moment is small compared to the paramagnetic μ_{eff} and $M(H)$ does not saturate at high H, indicative of itinerant FM.

A conventional Arrott analysis, which works for mean-field FM systems, fails when applied to $URu_{2-x}Re_xSi_2$. Using the scaled Arrott analysis, the proper choice of critical exponents linearizes $M(H)$ isotherms in the critical region via a plot of $|M|^{1/\beta}$ vs $|H/M|^{1/\gamma}$, allowing a self-consistent determination of T_C and the ordered moment M_0. To identify the scaling exponents β and γ, an approximate T_C is first determined along with the scaling exponent δ, from a plot of $\frac{\partial \ln H}{\partial \ln M}$ vs H, as shown in Figs. VI.19, VI.20, VI.21, VI.22, and VI.23. The three exponents are typically defined for reduced magnetization m, field h and temperature $t = \frac{(T-T_C)}{T_C}$ by

$$m \sim t^{\beta} \qquad (t < 0), \tag{VI.1}$$

$$m \sim h^{1/\delta} \qquad (t = 0), \tag{VI.2}$$

and

$$\frac{\partial m}{\partial h} = \chi \sim t^{-\gamma} \qquad (t > 0), \tag{VI.3}$$

and are related by

$$\delta - 1 = \gamma/\beta. \tag{VI.4}$$

In the plots of $\frac{\partial \ln H}{\partial \ln M}$ vs H, δ and T_C are estimated by finding the isotherm with a zero slope over the widest range of H, because $m \sim h^{1/\delta}$ strictly only at $t = 0$. In

general, this analysis is only meaningful over an intermediate range of H, because of the possible presence of magnetic domains and unsaturated magnetic impurities at low H, along with the effects of terms of higher order in M at higher H. In practice, the plots of $\frac{\partial \ln H}{\partial \ln M}$ vs H are used to identify the range of H over which $\frac{\partial \ln H}{\partial \ln M}$ is constant, and the analysis is limited to that range of H. Plotting scaled field $H/|t|^{\delta\beta}$ vs scaled magnetization $|M|/|t|^{\beta}$, Figs. VI.24 and VI.25, collapses the $M(H)$ data within the critical T range onto two curves, corresponding to $T > T_C$ and $T < T_C$. This collapse onto two scaling curves is the first criterion used to experimentally determine the proper exponents and T_C. The second criterion is to have the $M(H)$ isotherms transformed into parallel lines evenly spaced in T in a plot of $|M|^{1/\beta}$ vs $|H/M|^{1/\gamma}$, as shown in Figs. VI.26, VI.27, VI.28, VI.29, and VI.30. The linear T-dependence is more clearly seen in plots of the $M^{1/\beta}$ intercepts vs T, shown in Fig. VI.31, in which a linear fit yields a value of T_C that must be consistent with the value determined from the scaling analysis. The $M^{1/\beta}$ intercept of the linear fit, raised to the β power, is an estimate of M_0 at 0 K. These values are all fractions of μ_B. The other set of intercepts, $|H/M|^{1/\gamma}$ vs T, shown in Figs. VI.32, VI.33, VI.34, VI.35, and VI.36, yield an estimate of the initial susceptibility. Because the inverse initial susceptibility is linear in T, it is possible to relate the slope to μ_{eff}, although its real meaning is questionable because of the noninteger exponent on H/M. Interestingly, these values also show a monotonic increase with x. Although the value of the initial susceptibility is only valid in the critical region, it is instructive to compare a plot of its values to measured data, as shown in Figs. VI.37, VI.38, VI.39, VI.40, and VI.41. For $x = 0.5$, there appears to be decent agreement between the data and the initial susceptibility, although for lower x, the agreement is not as satisfactory.

A summary of this analysis is presented in Figs. VI.42 and VI.43. The error bars reflect a range of reasonable values within which the scaled Arrott analysis works. It is particularly interesting that T_C, M_0, γ and $\delta - 1$ all extrapolate to 0 at $x \approx 0.15$ - this remarkable convergence strongly indicates the existence

of a FM instability there. The critical exponents determined via this analysis are extremely peculiar, as they deviate substantially from mean-field values ($\beta = 0.5$, $\gamma = 1$, $\delta = 3$) and those describing conventional FM systems, where $\beta < 0.5$ and $\delta > 3$ [164, 165]. It is interesting that $\beta = 0.8$ is independent of x and significantly larger than the values it normally exhibits in 3-dimensional systems. Recall that $m \sim t^{\beta}$, so β describes how the ordered moment grows as T is lowered below T_C. Values of β closer to 1 imply a slower saturation than found in a mean field magnet. As $\chi \sim t^{-\gamma}$, values of $\gamma \neq 1$ imply deviation from CW behavior, which is uncommon in theoretical treatments, even those involving quantum criticality. There are a limited number of examples of experimentally determined magnetic scaling exponents with $\gamma < 1$ in both nominally stoichiometric [166, 167] and chemically substituted materials [168, 169], however $\gamma \to 0$ appears to be unprecedented. As the value of γ decreases, $\chi(T)$ diverges more weakly, eventually becoming constant when $\gamma = 0$. A T-independent χ characterizes the paramagnetic response of itinerant electrons at low T, so this trend of γ may necessitate an itinerant origin of the FM order. Finally, because $m \sim h^{1/\delta}$ describes the slope of $M(H)$ at T_C, δ extrapolating to 1 also results in conventional low-H, low-T paramagnetic behavior. Because β and γ must be positive, δ cannot be less than 1.

Despite their unprecedented nature, the determined values of these critical exponents do not appear to be physically unreasonable. One caveat is that these exponents describe low-H behavior, but are extracted from an analysis at rather high values of H, and may not reflect the detailed low-H magnetic response of the actual system. In fact, similar behavior is suggested to exist in the high-H phase diagram of URu_2Si_2, where the existence of a QCP seems insensitive to the existence of other ordered phases [122]. The seeming robustness of the critical point, where the actual low-energy details of a system, even impurities or defects, are irrelevant to the emergence of order, has been dubbed a "quantum protectorate" by Laughlin and Pines [170, 171]. On the other hand, it is possible that disorder is required for the existence of non-mean field FM quantum criticality

[172], and so should not be so simply dismissed.

A reasonable criticism of the preceding analysis is that the FM contribution to $M(H)$ may not have been isolated properly. For instance, in a weakly magnetic system, it is possible that a strong paramagnetic contribution to $M(H)$ exists in addition to the FM response. Generally, a two-component system such as this might exist in a system with small FM ordering local moments weakly coupled to an unpolarized conduction band, where a sufficiently heavy paramagnetic band could contribute a magnetic response of the same magnitude as the weak FM response. This scenario is a bit unrealistic, because a heavy band would be expected to arise from strong hybridization between local and itinerant moments, and in $URu_{2-x}Re_xSi_2$, U ions contribute the dominant magnetic moments, so even if the FM moments are localized, they are not decoupled from the conduction band. Regardless, a form of the same argument might still hold for a spatially inhomogeneous distribution of paramagnetic and FM moments. In principle, the subtraction of a non-saturating susceptibility from a FM M(H) would increase the exponent δ ($m \sim h^{1/\delta}$) by increasing the curvature in $M(H)$. However, attempts to subtract a significant paramagnetic contribution from the $M(H)$ data failed. In particular, it was impossible to even estimate δ, rendering the scaling analysis meaningless. Thus, it is not possible to recover more conventional magnetic exponents. This result is consistent with claims that magnetic disorder or heterogeneity leads to the invalidation of mean-field Arrott analysis [173, 174]. Fortunately, although the results of the analysis are unusual, they do yield a self-consistent description.

A significant challenge remains in the interpretation of these critical exponents, as there appears to be no compatible theory currently available (some believe that 3D FM QCP's cannot exist [175]). As discussed in Ref. [142], the closest descriptions are due to models of disordered quantum critical itinerant ferromagnets, particularly the works of Belitz, Kirkpatrick, and coworkers [172, 176, 177], which predict that $\delta = 1.5$, $\beta = 2$, and $\gamma = 1$. To my knowledge, no models exist describing $\gamma \to 0$, so it is possible that the present work may offer new insight into

the nature of the FM quantum critical point.

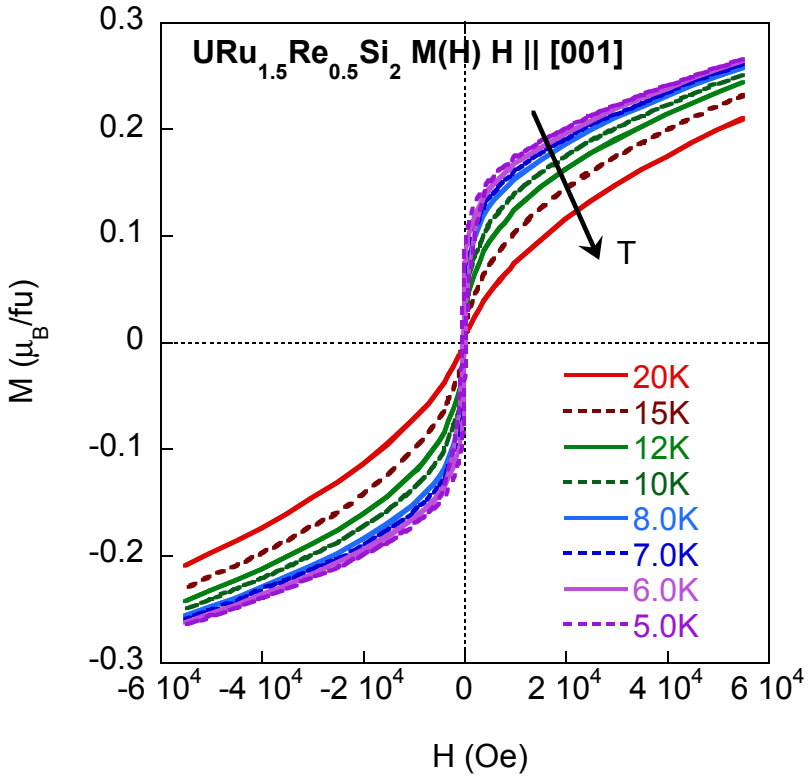

Figure VI.12: Magnetization versus field for $x = 0.5$.

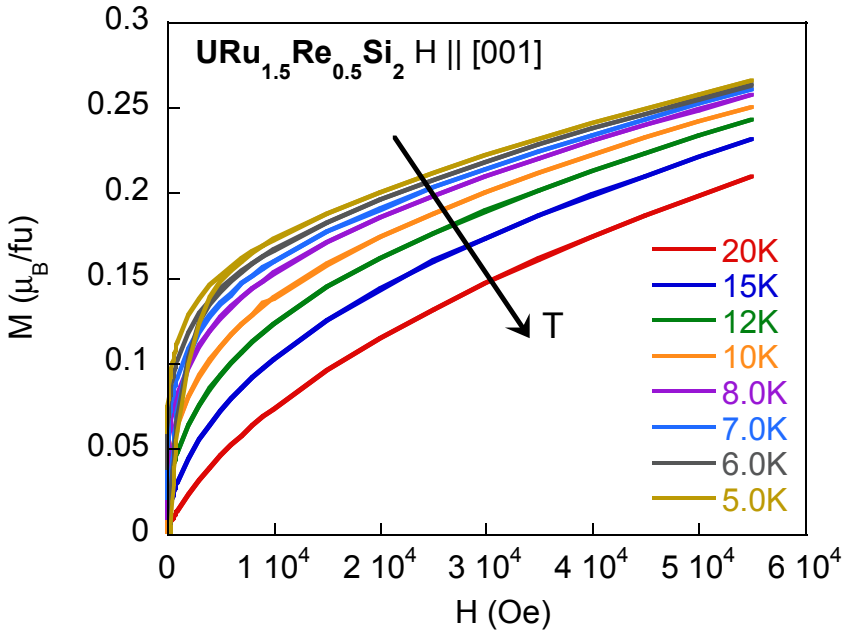

Figure VI.13: Magnetization versus field for $x = 0.5$ first quadrant.

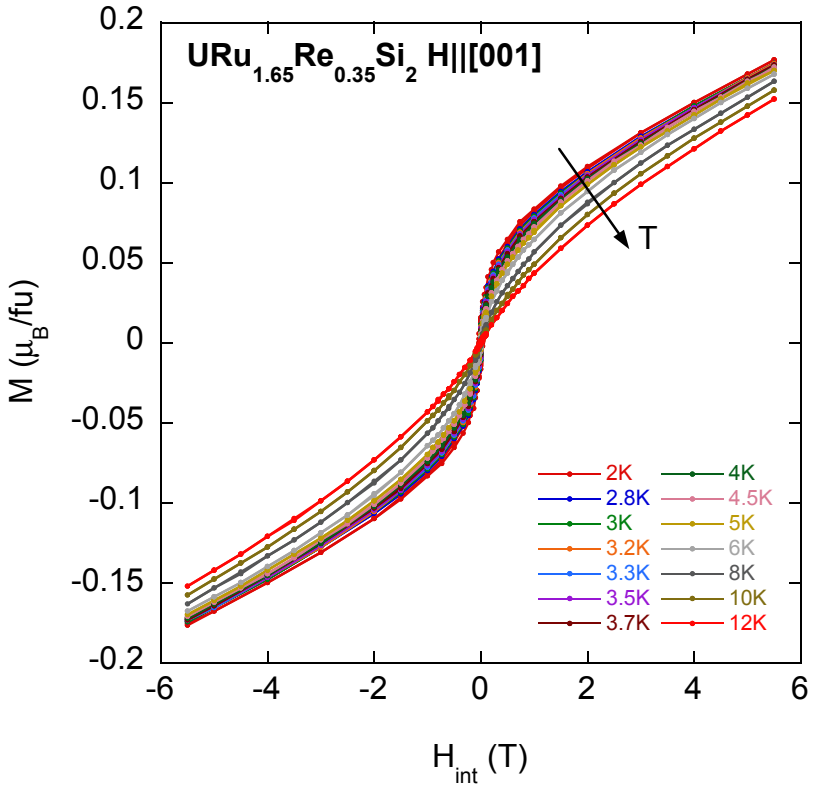

Figure VI.14: Magnetization versus field for $x = 0.35$.

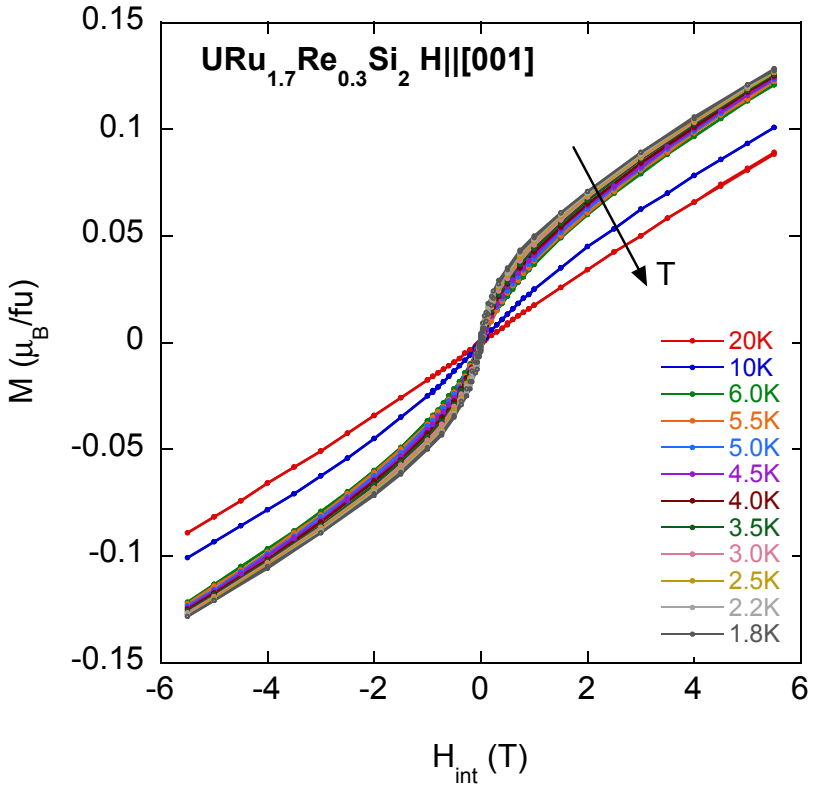

Figure VI.15: Magnetization versus field for $x = 0.3$.

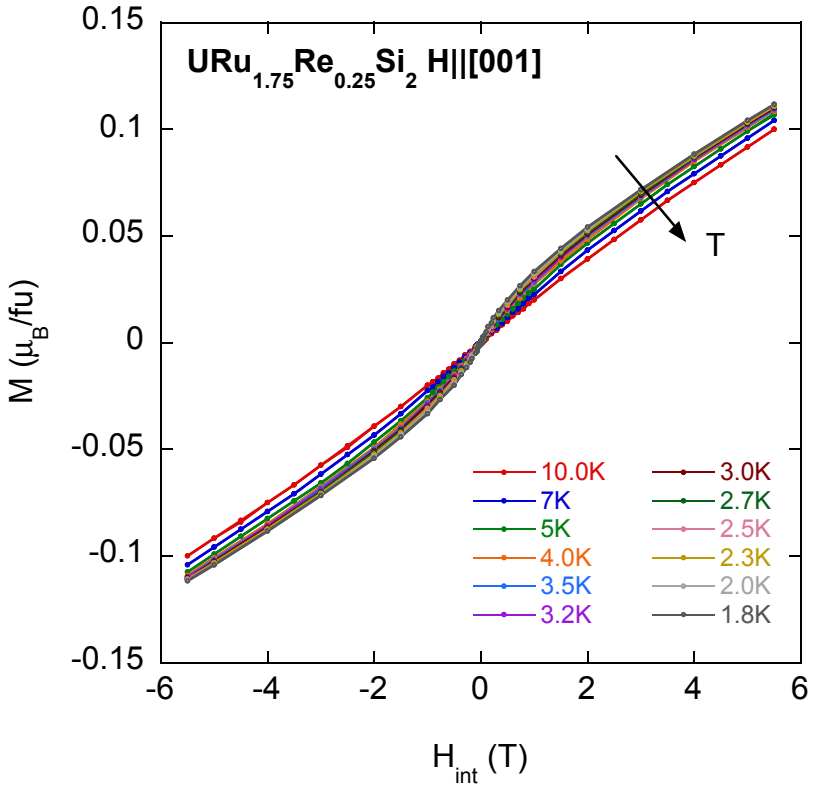

Figure VI.16: Magnetization versus field for $x = 0.25$.

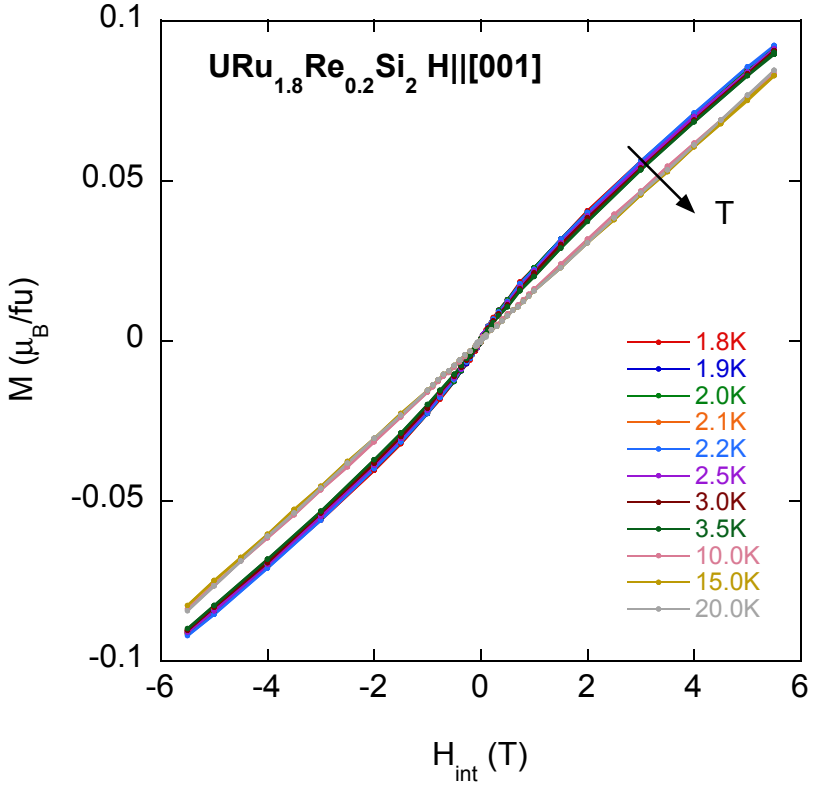

Figure VI.17: Magnetization versus field for $x = 0.2$.

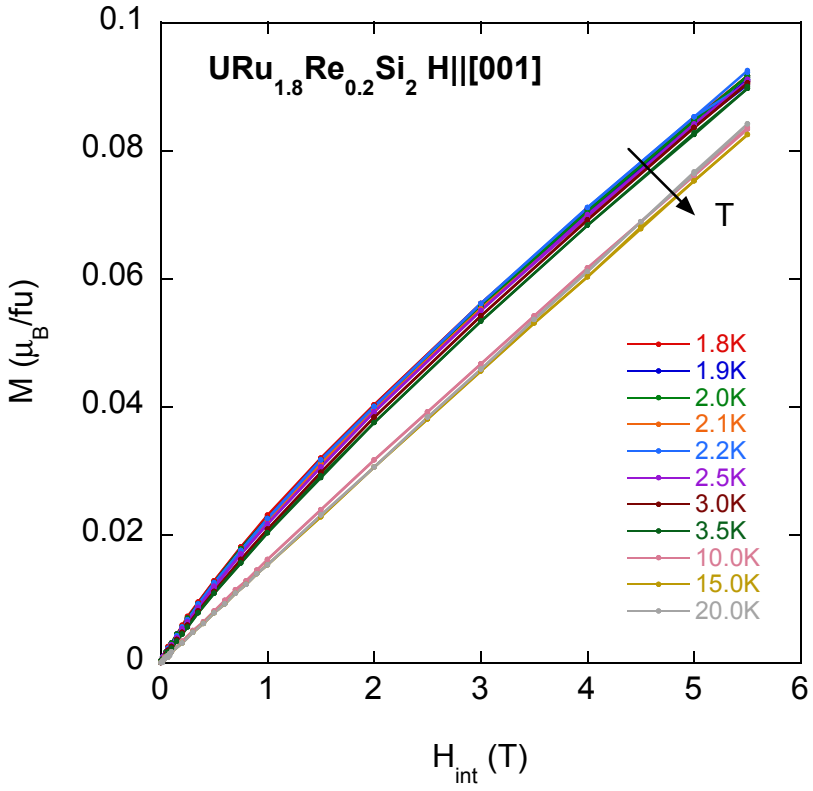

Figure VI.18: Magnetization versus field for $x = 0.2$ first quadrant.

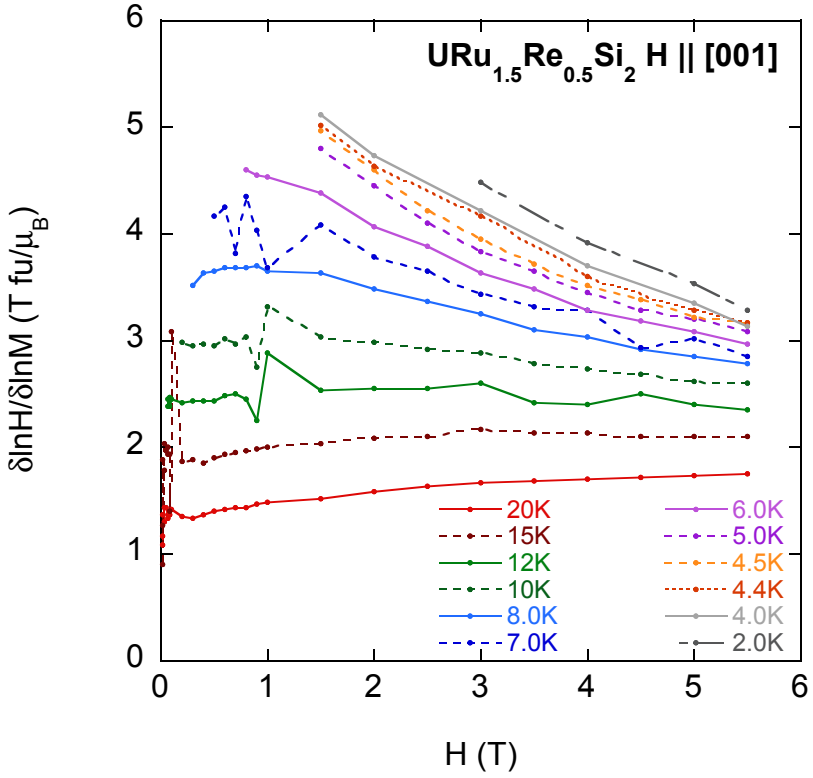

Figure VI.19: Determination of magnetic exponent δ for $x = 0.5$.

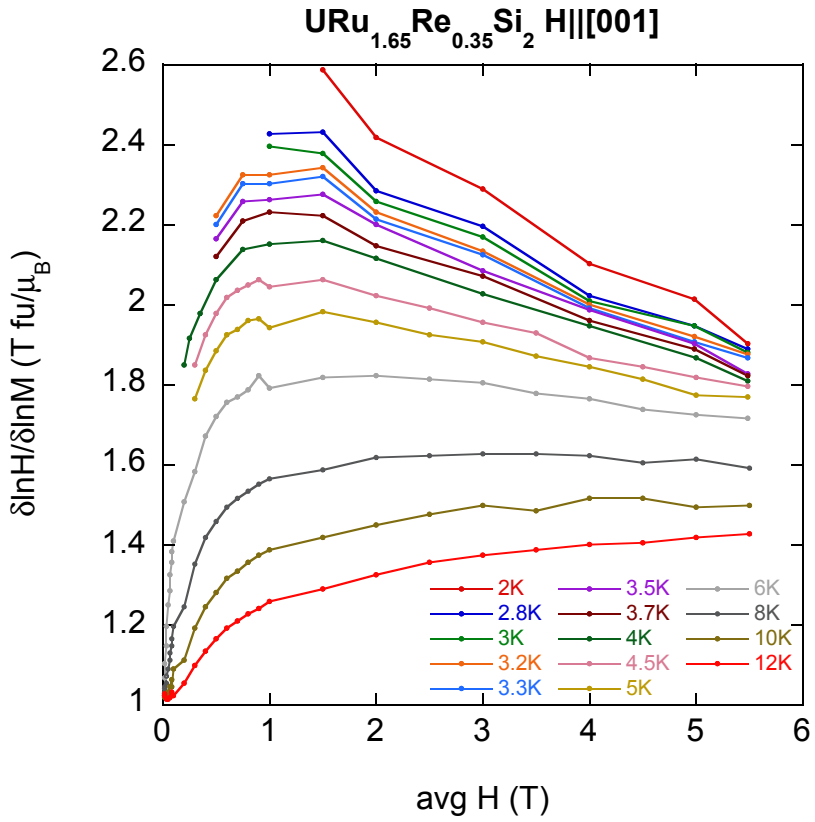

Figure VI.20: Determination of magnetic exponent δ for $x = 0.35$.

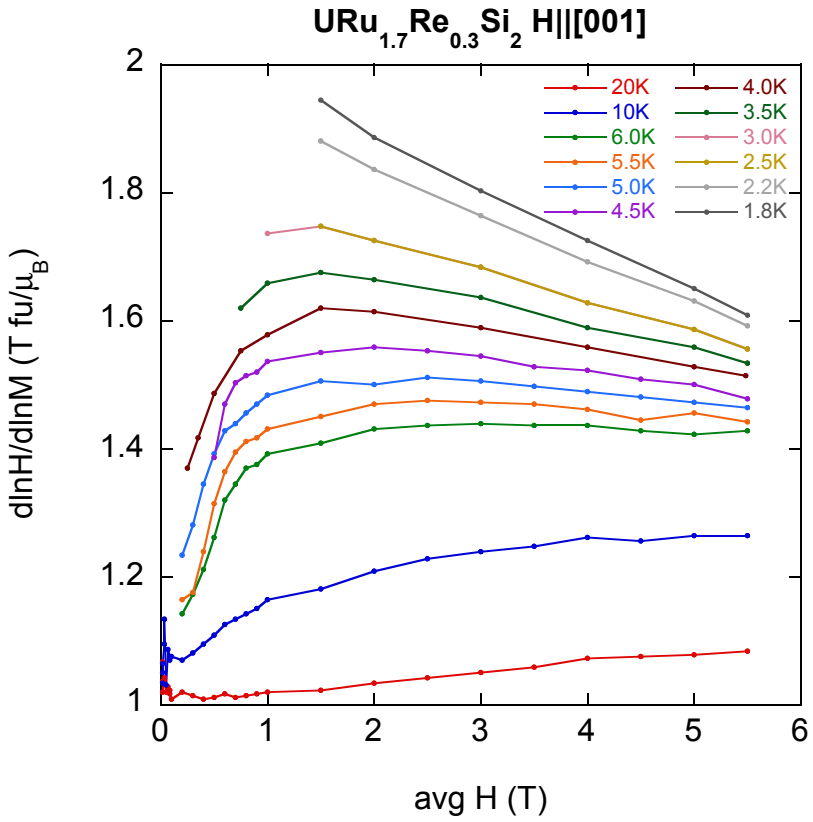

Figure VI.21: Determination of magnetic exponent δ for $x = 0.3$.

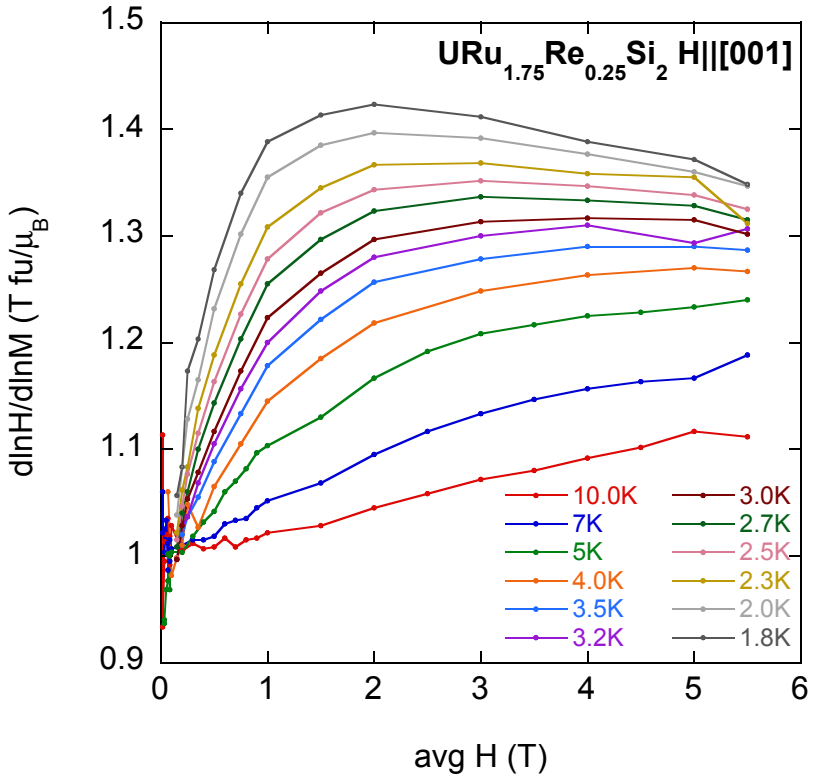

Figure VI.22: Determination of magnetic exponent δ for $x = 0.25$.

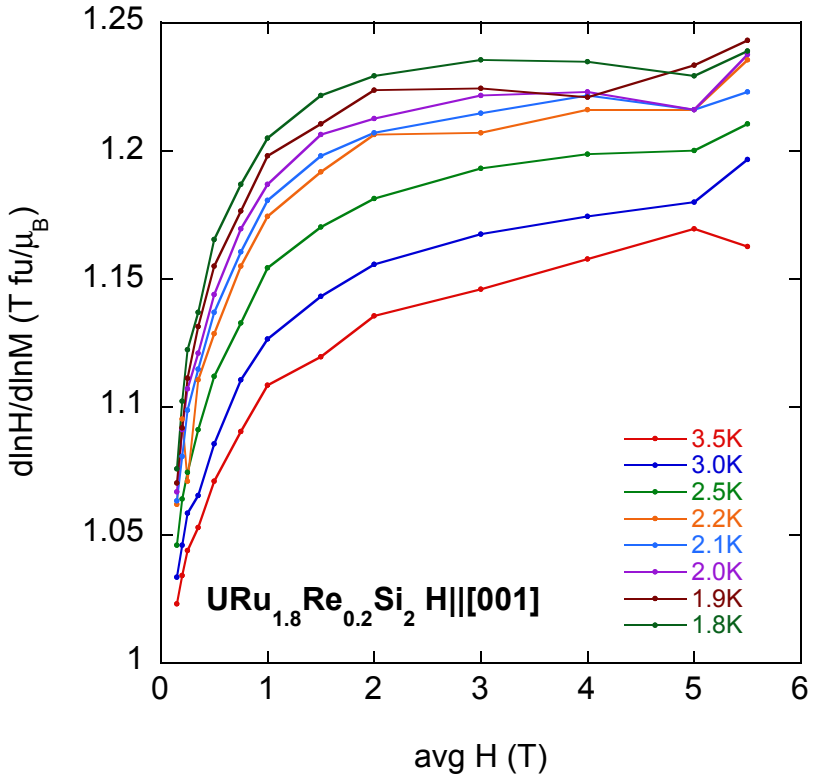

Figure VI.23: Determination of magnetic exponent δ for $x = 0.2$.

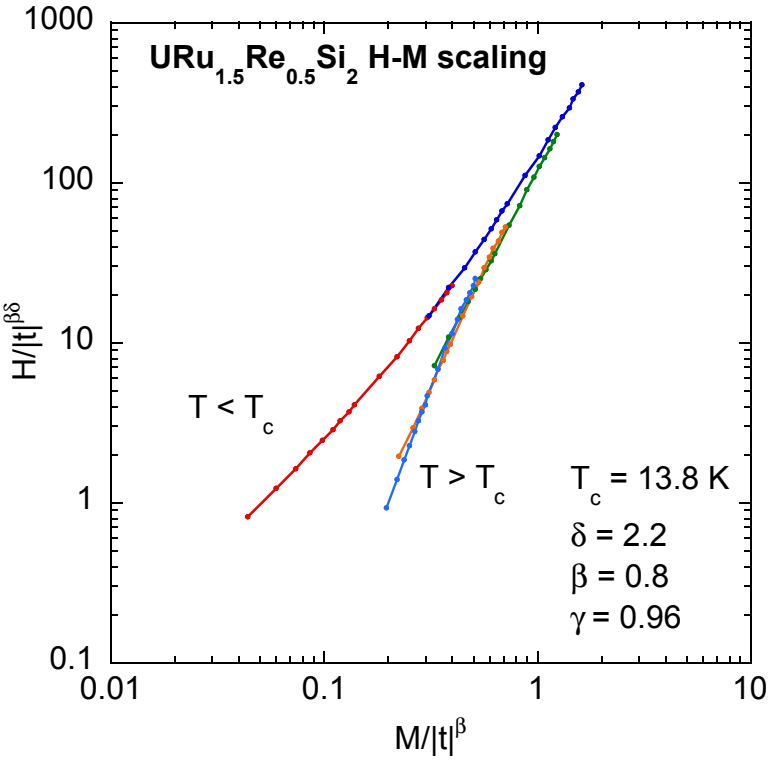

Figure VI.24: Arrott-Noakes magnetic scaling for $x = 0.5$.

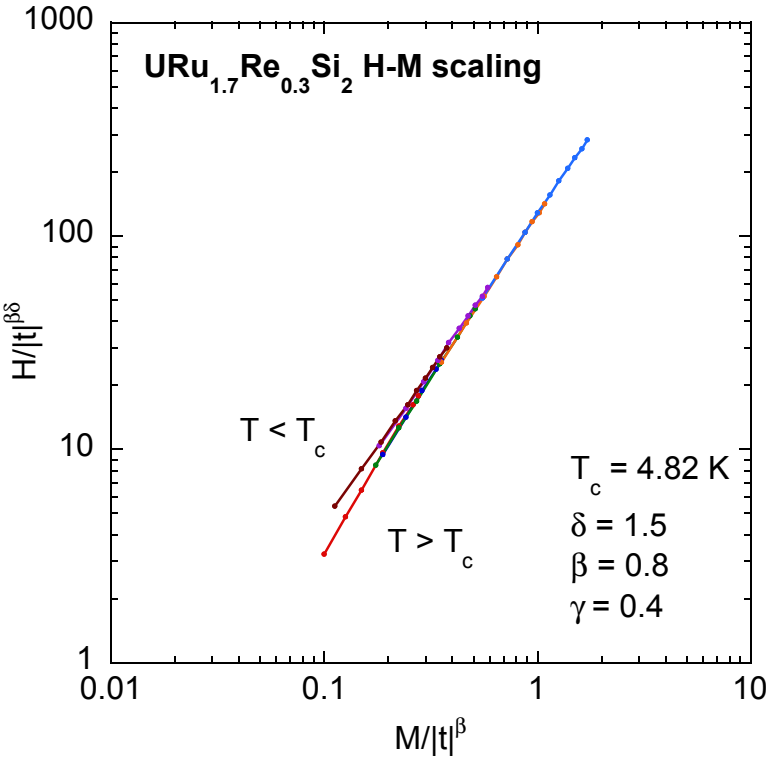

Figure VI.25: Arrott-Noakes magnetic scaling for $x = 0.3$.

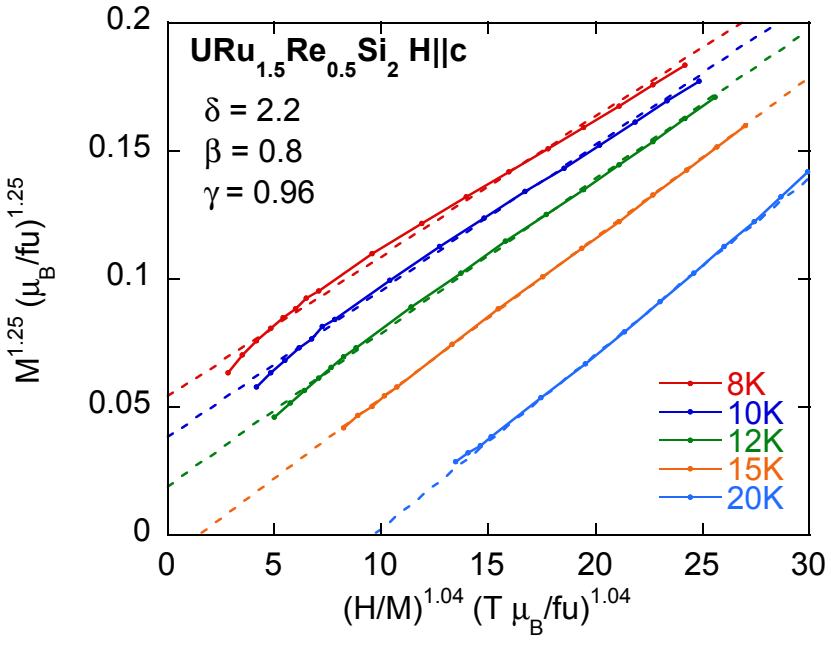

Figure VI.26: Scaled Arrott plot for $x = 0.5$.

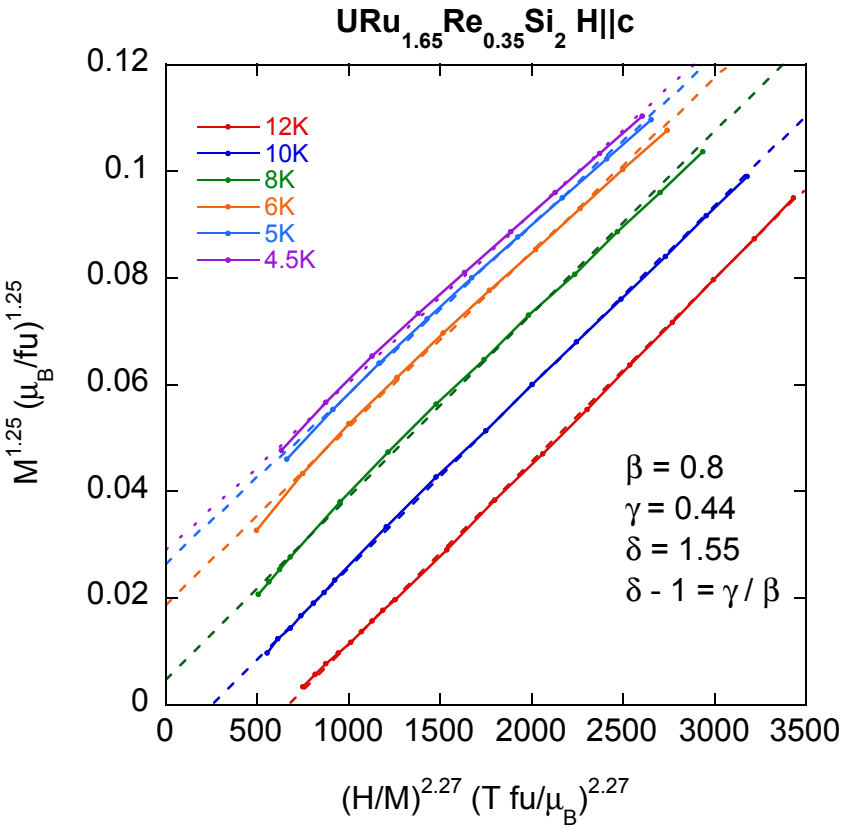

Figure VI.27: Scaled Arrott plot for $x = 0.35$.

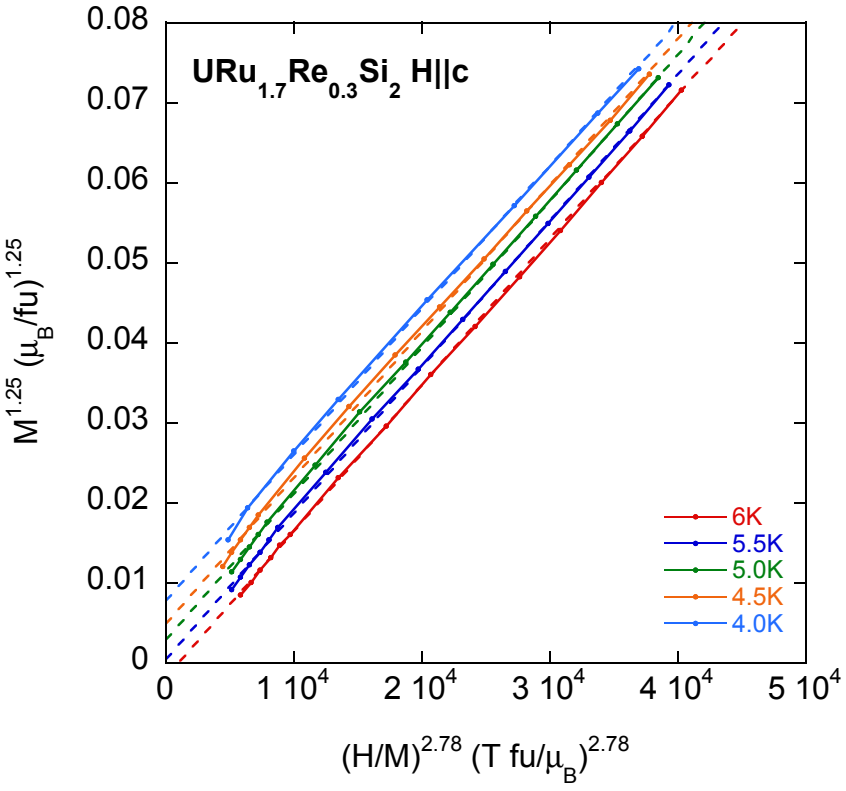

Figure VI.28: Scaled Arrott plot for $x = 0.3$.

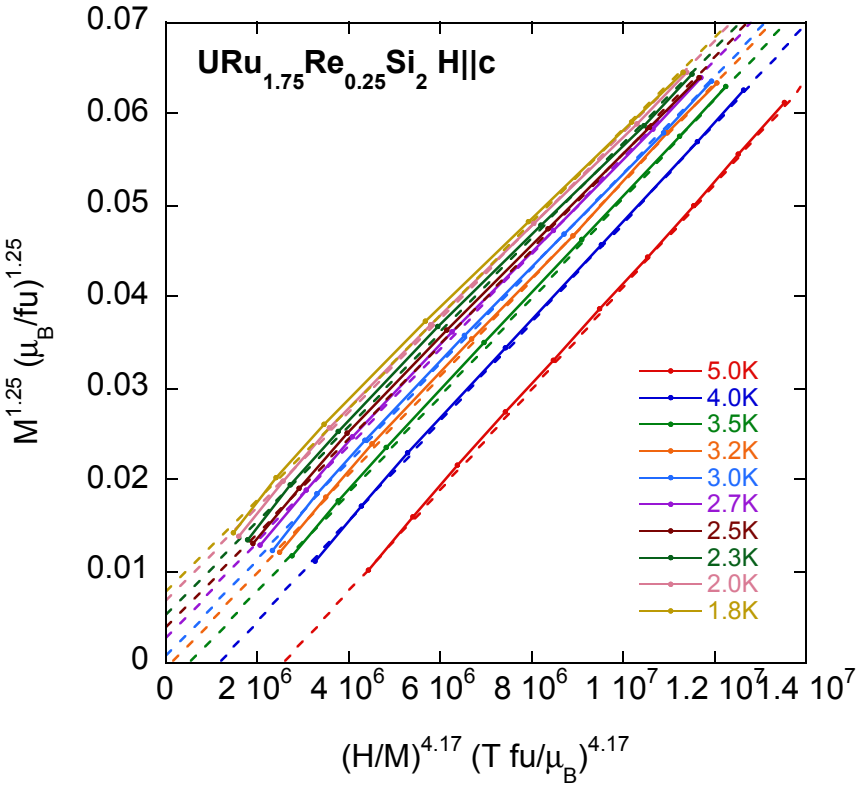

Figure VI.29: Scaled Arrott plot for $x = 0.25$.

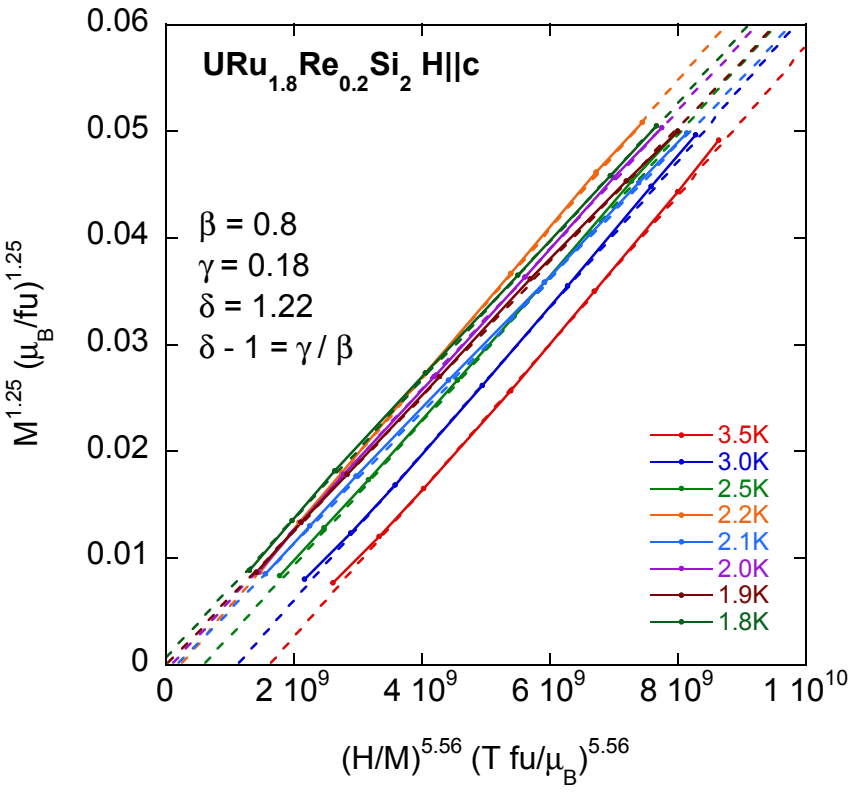

Figure VI.30: Scaled Arrott plot for $x = 0.2$.

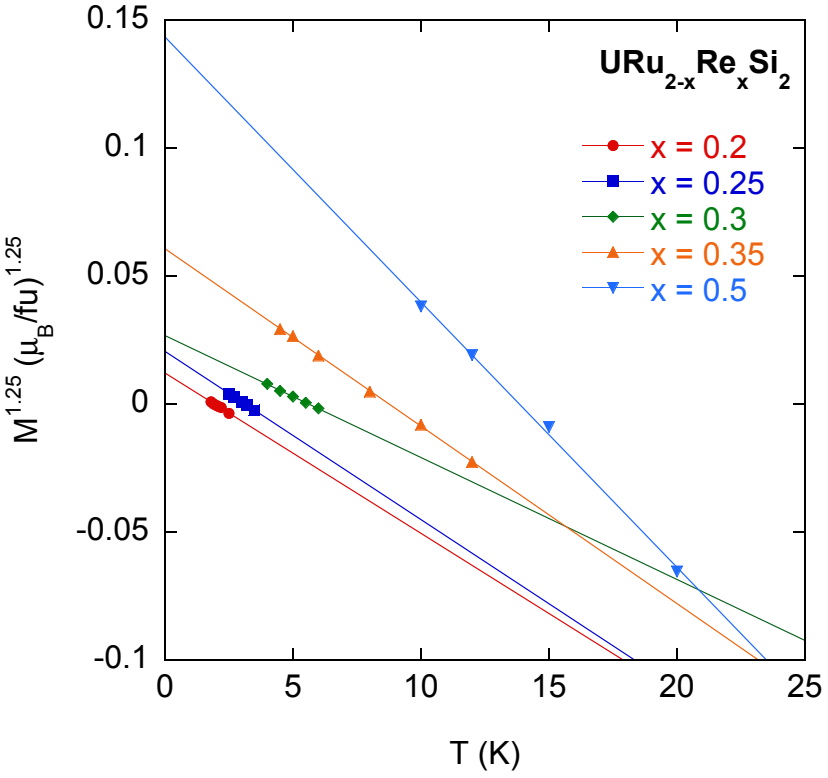

Figure VI.31: Determination of spontaneous moment for $x = 0.25 - 0.5$.

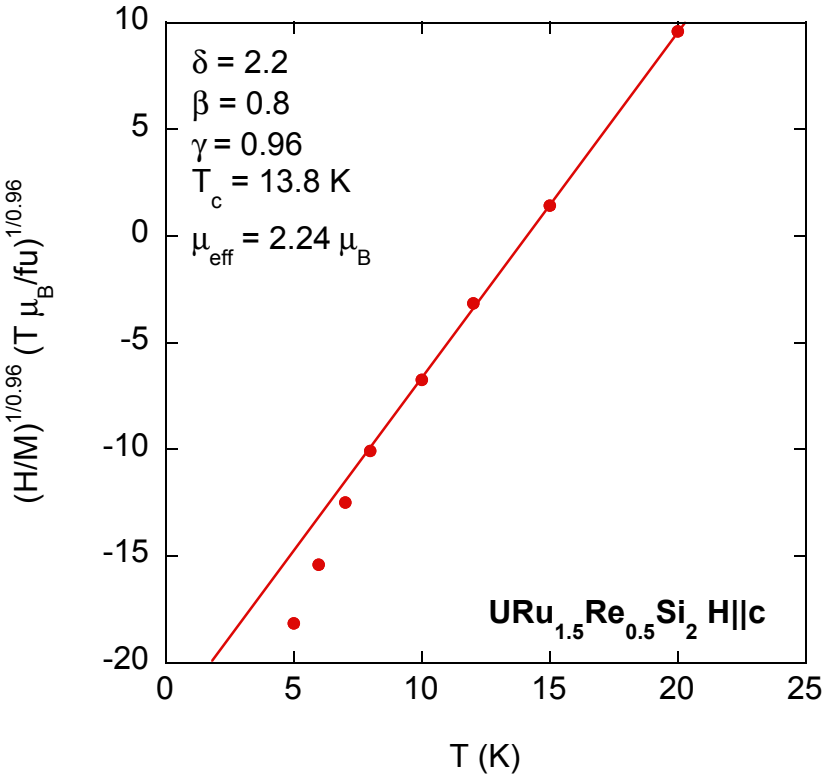

Figure VI.32: Determination of initial susceptibility for $x = 0.5$.

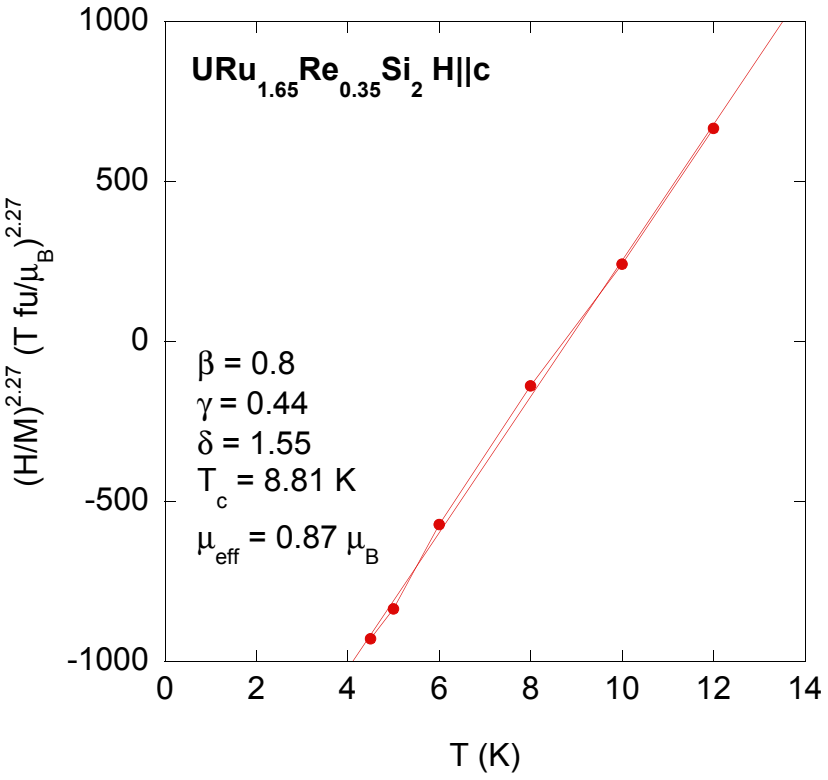

Figure VI.33: Determination of initial susceptibility for $x = 0.35$.

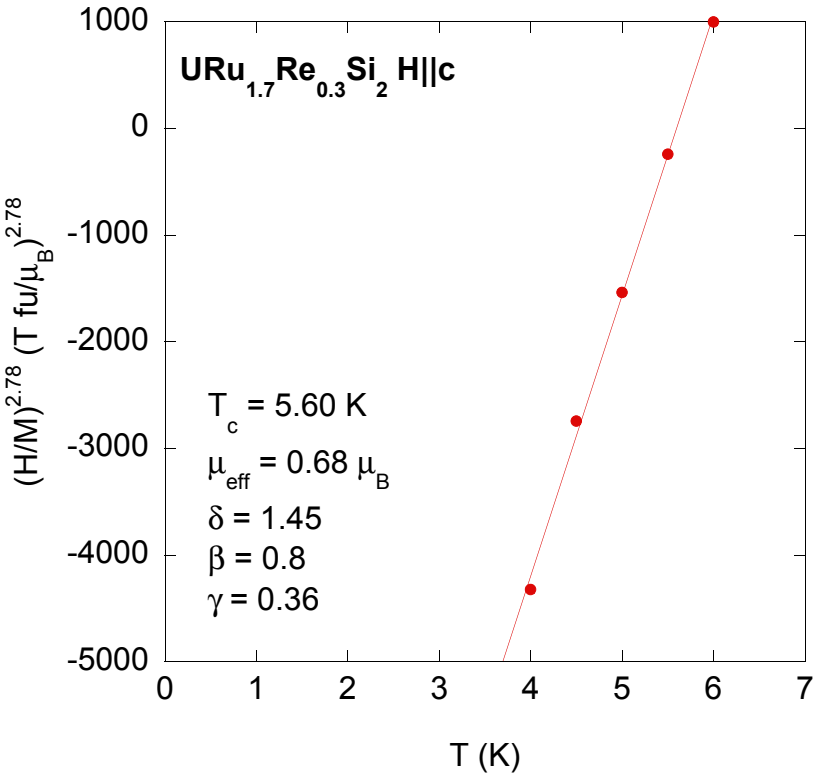

Figure VI.34: Determination of initial susceptibility for $x = 0.3$.

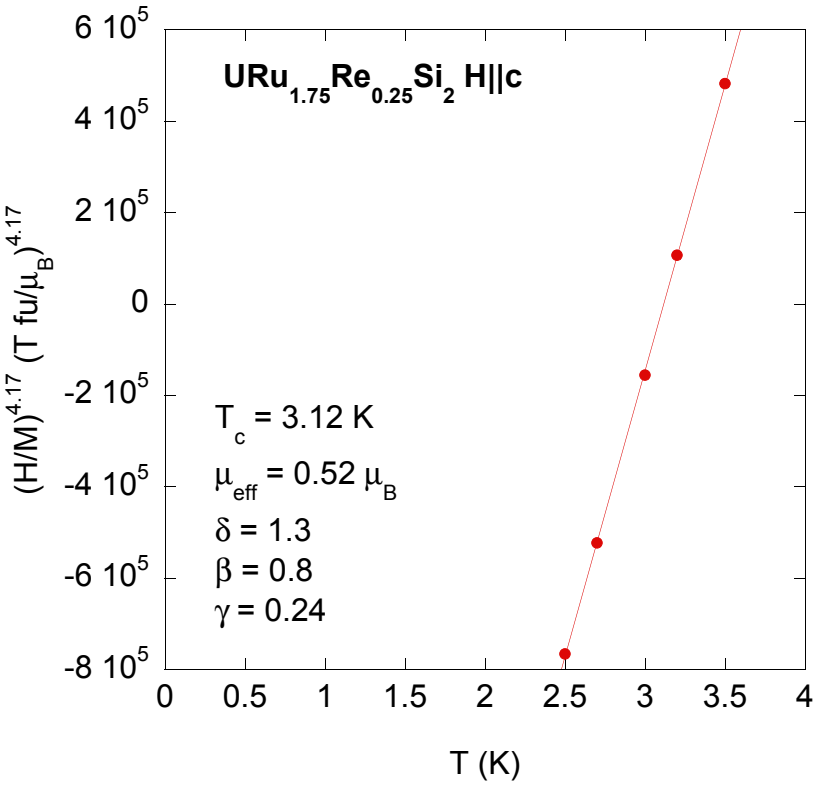

Figure VI.35: Determination of initial susceptibility for $x = 0.25$.

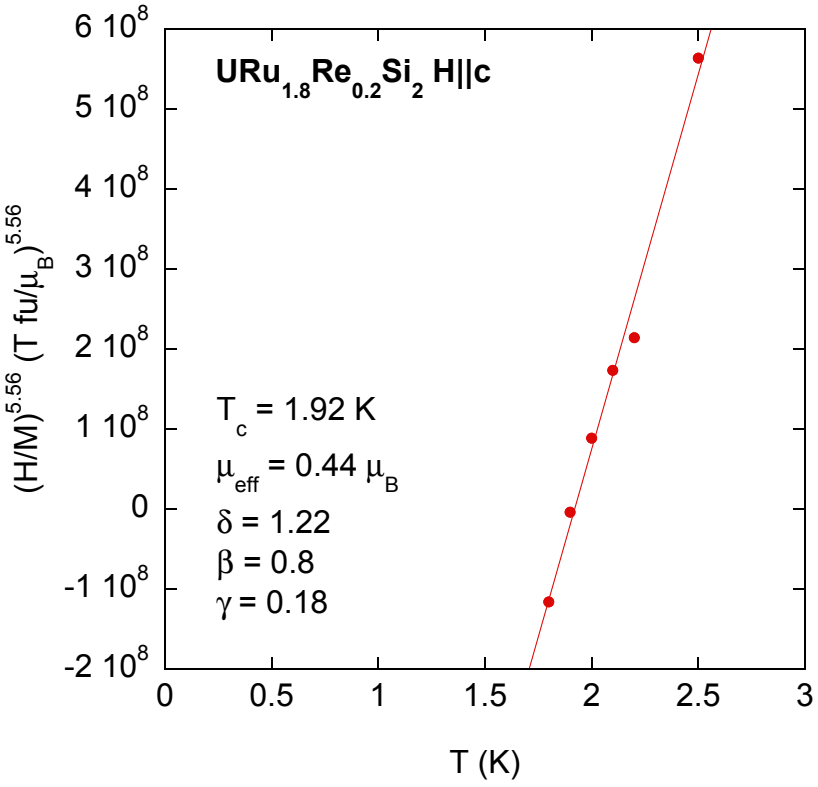

Figure VI.36: Determination of initial susceptibility for $x = 0.2$.

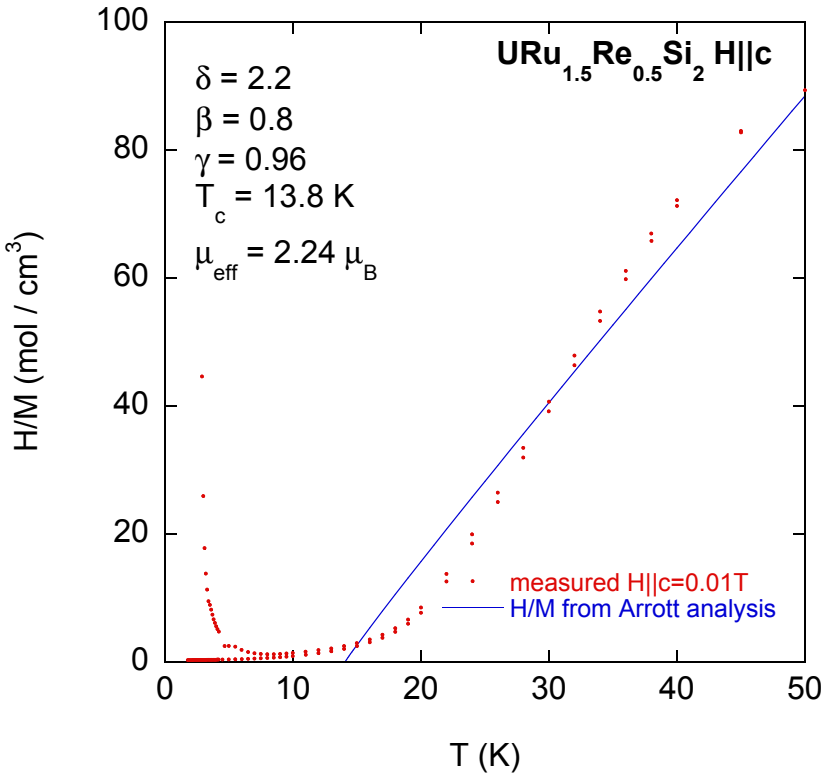

Figure VI.37: Comparison of initial susceptibility for $x = 0.5$.

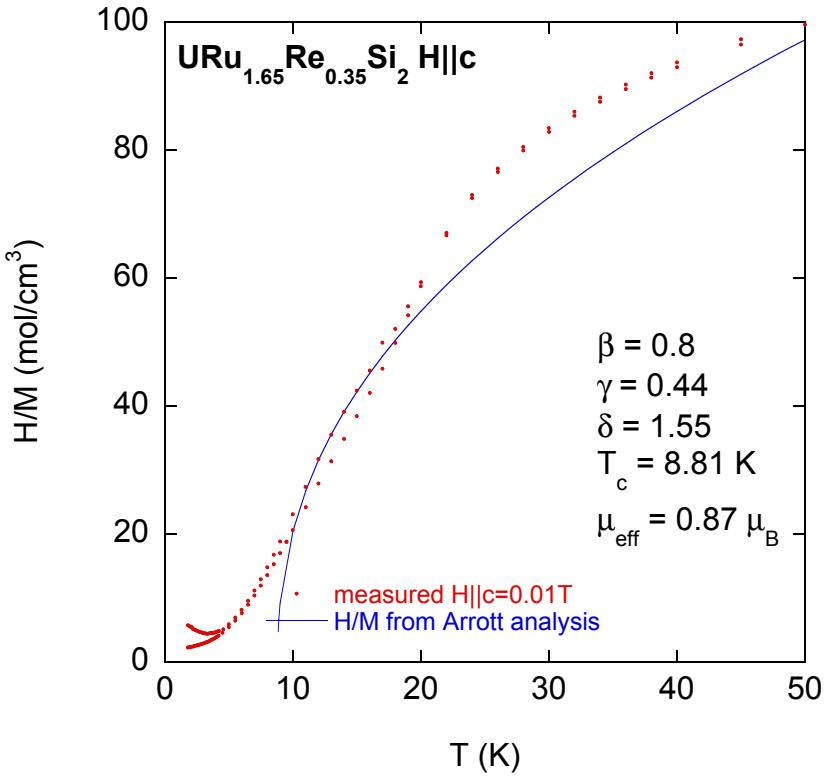

Figure VI.38: Comparison of initial susceptibility for $x = 0.35$.

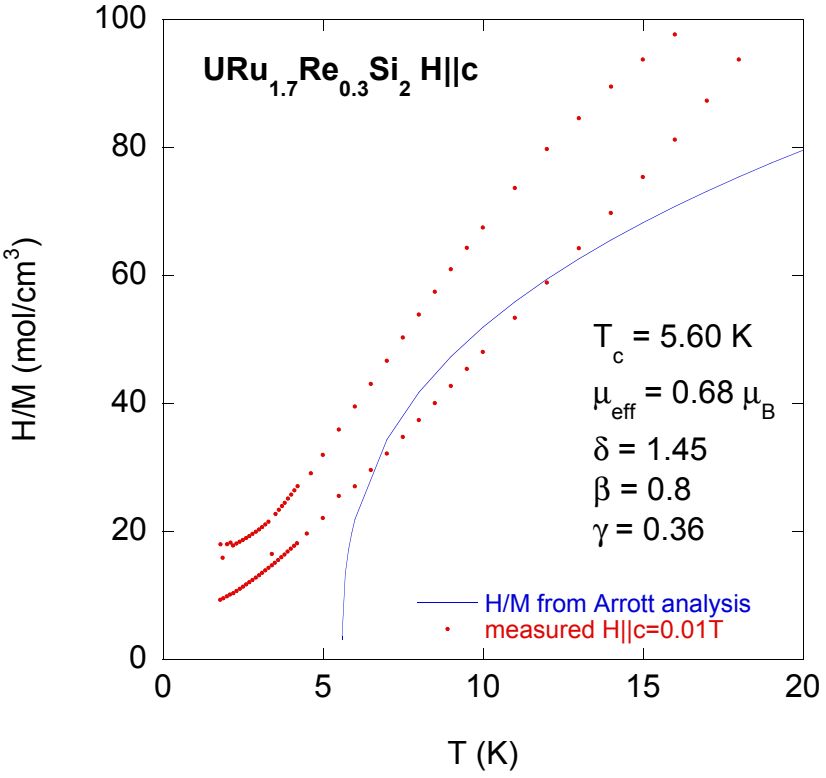

Figure VI.39: Comparison of initial susceptibility for $x = 0.3$.

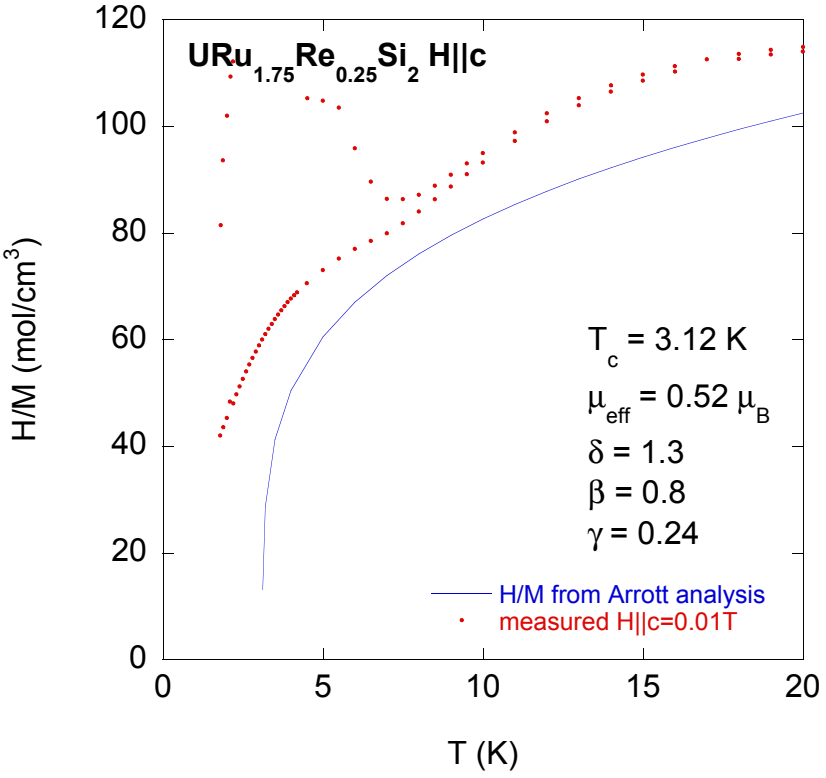

Figure VI.40: Comparison of initial susceptibility for $x = 0.25$.

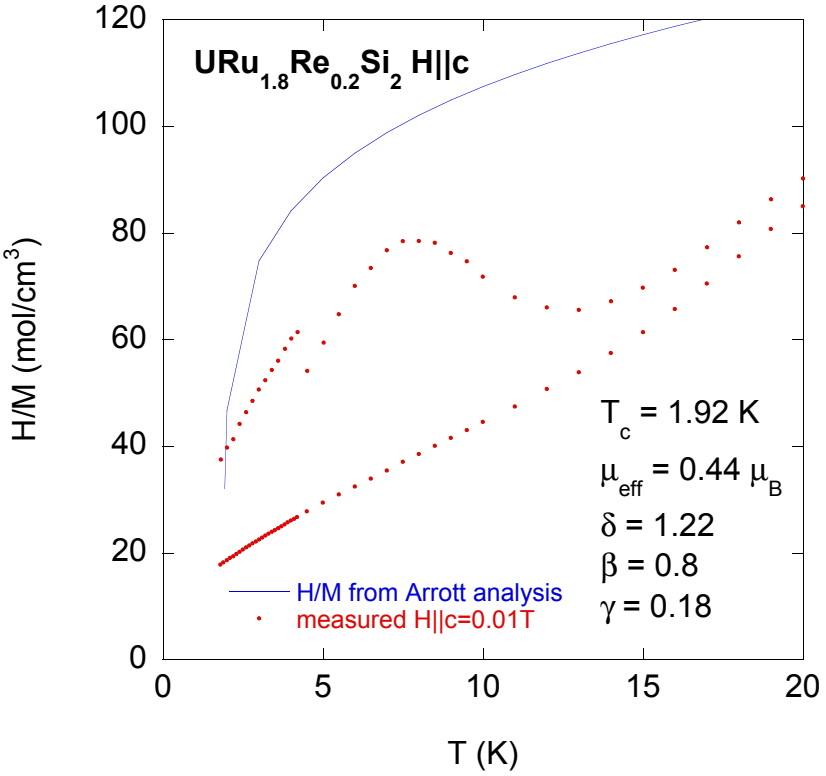

Figure VI.41: Comparison of initial susceptibility for $x = 0.2$.

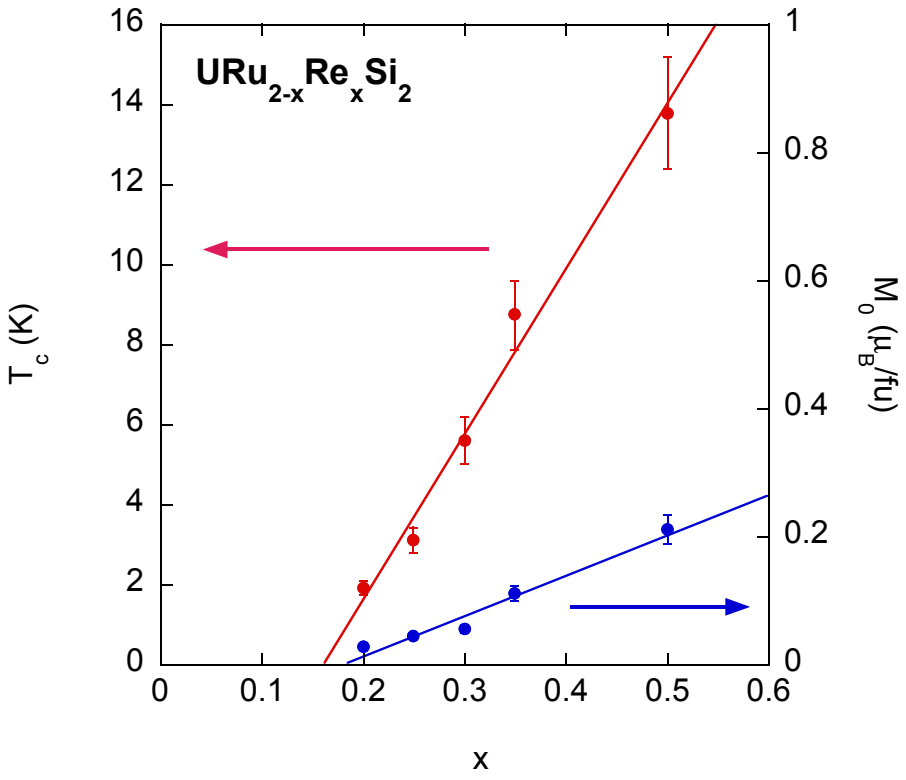

Figure VI.42: Composition dependence of T_C and M_0.

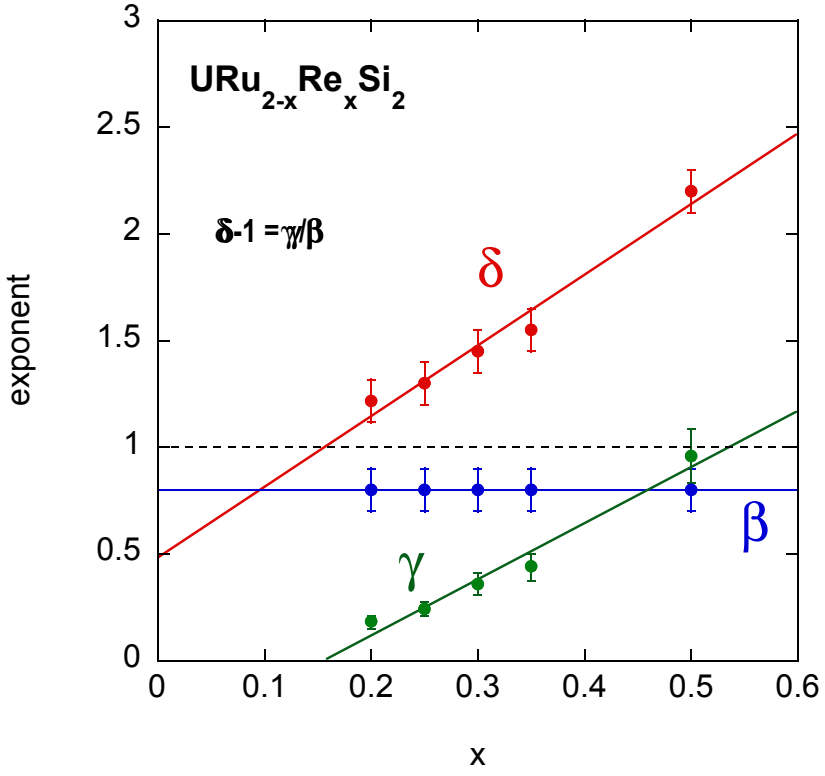

Figure VI.43: Composition dependence of magnetic scaling exponents.

VII

Discussion

VII.A Impurity Phases

The substitution of Re into $URu_{2-x}Re_xSi_2$ has been a challenging metallurgical problem since the earliest days when it was realized that the $ThCr_2Si_2$ only exists for $x \leq 1$ [132]. Most recently, it was noted that impurity peaks that could be identified with Re appeared in x-ray powder diffraction patterns and that impurity superconductivity with $T_c \approx 2.2$ K appeared in some samples [143]. As part of the same work, electron microprobe measurements confirmed the Re concentration to within 7% of the nominal concentration in a range of x [142]. As discussed in Chapter II, much effort was taken to ensure the homogeneous distribution of Re into URu_2Si_2 during sample preparation. No impurity peaks due to Re are seen in powder x-ray diffraction patterns. The bulk properties of the single crystals measured in this study are similar to the published properties of polycrystalline samples [132, 134, 143, 142], which indicates their similar chemical composition. Nevertheless, the superconducting transitions observed in $\rho(T)$ (Fig. IV.12) have not been seen before. These transitions do not occur for low x, but they become dramatically apparent at $x = 0.07$ and persist to $x = 0.2$. The transition temperatures vary from $2.5 - 7$ K and vary from sample to sample, as do the magnitudes of the resistive drops, although a complete transition has never been observed. It

should be noted that for $x = 0.04$ and as high as $x = 0.5$, very slight drops are also observed in $\rho(T)$, but these occur at $T < 3$ K. Evidence in favor of the superconducting nature of the transition is presented in Fig. VII.1, where it is shown that at constant T, the resistive drop is suppressed by the application of a high enough current. The strongest signatures of this superconductivity appear to occur at the same concentrations where HO disappears and FM appears, which, considering the growing number of examples of superconductivity near magnetic quantum critical points ($CeIn_3$ [178], UGe_2 [179], Fe [180]), were a very appealing prospect for the $URu_{2-x}Re_xSi_2$ system. The resistive upper critical field curves for $x = 0.08$, 0.15, and $x = 0.2$, shown in Figs. VII.2, VII.3, and VII.4, are remarkably large. The 90%, 50%, and 10% lines represent the values of $\rho(T)$ relative to the normal state value, minus the residual value due to the incomplete transition. These curves demonstrate that this superconductivity is most likely not due to pure URu_2Si_2, which exhibits $T = 0$ K upper critical fields of ~ 3 T and ~ 12 T for $H||c$ and $H||a$, respectively.

Aside from making it difficult to perform fits to $\rho(T)$ over the largest possible ranges of T, signatures of the superconductivity also affected $\chi(T)$, which was usually measured at 0.01 T. An example of this, measured for several different values of H, is shown in Fig. VII.5. The drops in $\chi(T)$, in units of volume susceptibility (technically unitless) are smaller than 1% of the value $\frac{1}{4\pi}$ expected of bulk superconductors. Further evidence that the signature is magnetically weak comes from virgin zero-field-cooled $M(H)$ measurements at low T, as shown in Fig. VII.6. Isolating the superconducting signal was difficult; for reference, the measured $M(5.5\text{ T}) = 475$ emu/mol. Nonetheless, χ determined from the initial slope of $M(H)$ below the lower critical field also yields a value less than 1% of $\frac{1}{4\pi}$.

To summarize these findings, drops in $\rho(T)$ are incomplete, estimates from $\chi(T)$ yield small volume fractions, and no anomalies are observed in $C(T)$. These all seem to indicate some form of filamentary superconductivity. Given the cleavage habit and known proclivity of $URu_{2-x}Re_xSi_2$ for stacking faults, it

may be that inter-platelet regions in the bulk samples serve as sites of preferential segregation for an impurity superconducting phase. Regardless of its structure, the composition of this phase is unknown. Three of four elements that make up $URu_{2-x}Re_xSi_2$ are superconductors: Ru ($T_c = 0.5$ K), Re ($T_c = 1.8$ K), and U ($T_c \ll 1$ K) that cannot account for $T_c \sim 7$ K. Of all the binary alloys, Ru-Re has the highest $T_c = 2.2$ K, at about 20% Ru [148]. However, if possible contamination by another element is considered, then an apparent match is found. The Re-W system, with 12% W, exhibits $T_c > 7$ K [148] and several Re-W compounds have $T_c > 5$ K [181]. This distribution of transition temperatures reflects well that observed in this study. Elemental W itself exhibits a low $T_c = 0.012$ K, but it only takes 35% Re in W to enhance it to $T_c > 6$ K [181].

The source of W contamination is probably the tri-arc furnace, as both the pulling rod and electrodes are made of 2% thoriated tungsten, and it could be introduced via direct contact with the pulling rod or via sputtering off of the electrode tips. With crystal growth times on the order of 1 hour or longer, the single crystals were exposed to W for much longer times than their polycrystalline counterparts. This scenario does not necessarily imply that all Czochralski growth in arc furnaces yields contaminated crystals, because it is possible that $URu_{2-x}Re_xSi_2$ has an unusually high W solubility, perhaps because of its Re content.

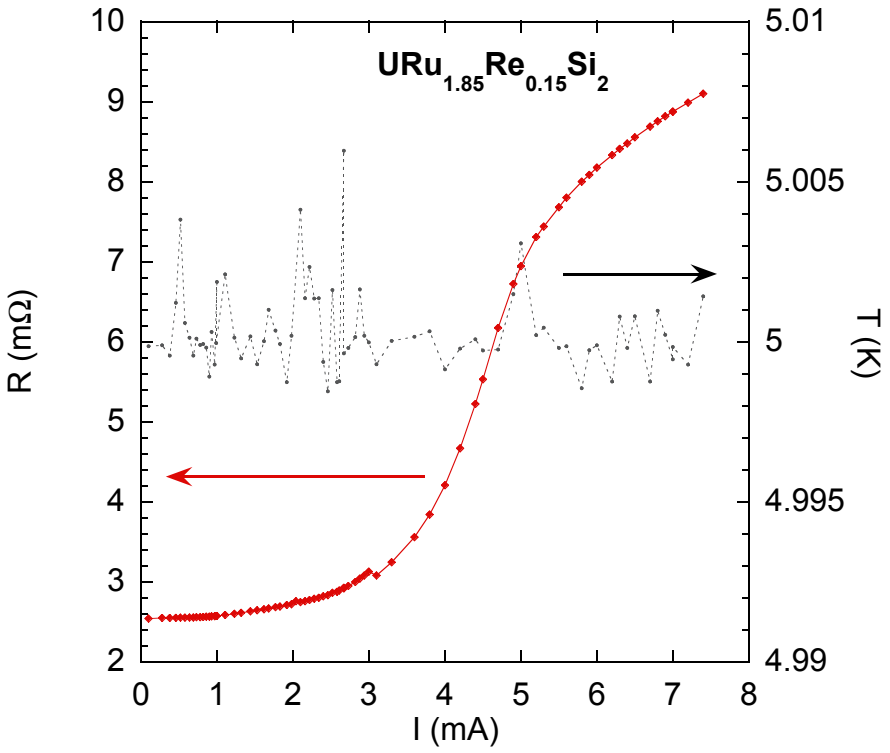

Figure VII.1: Superconducting critical current for $x = 0.15$. Note that the return to the normal state is not due to sample heating.

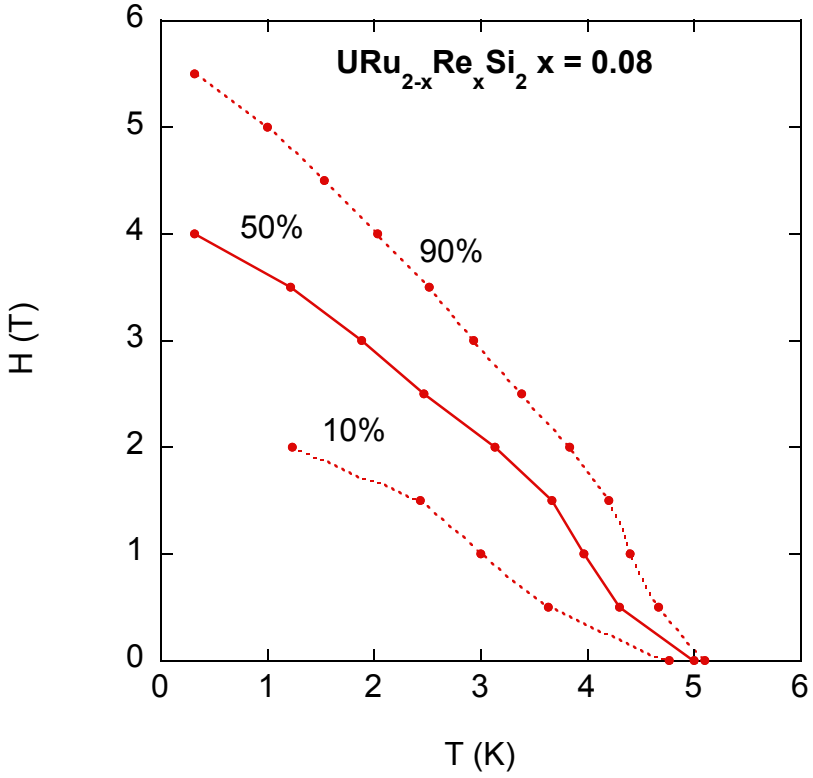

Figure VII.2: Superconducting upper critical field for $x = 0.08$.

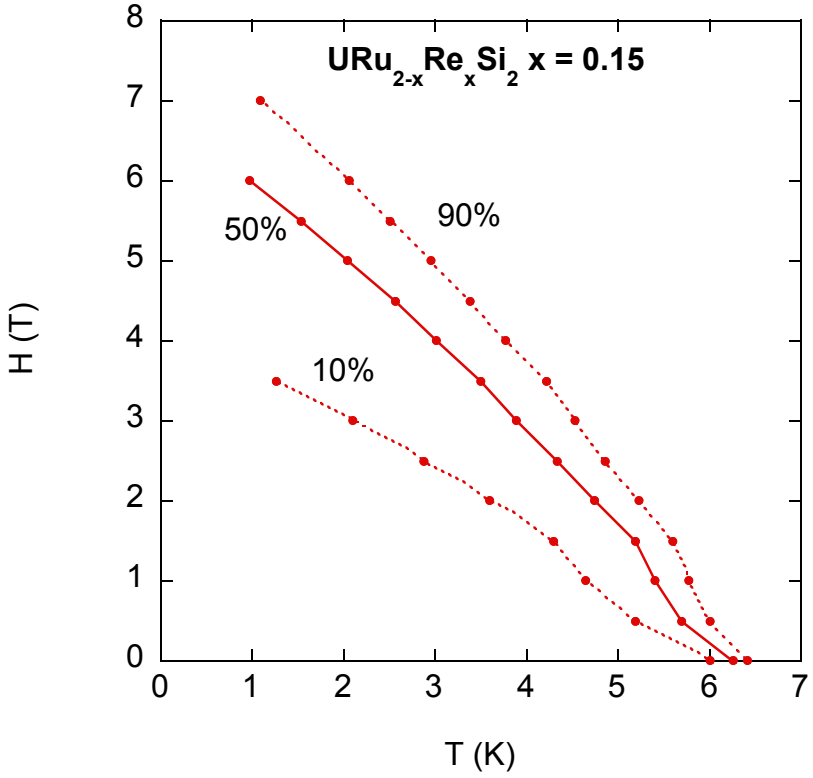

Figure VII.3: Superconducting upper critical field for $x = 0.15$.

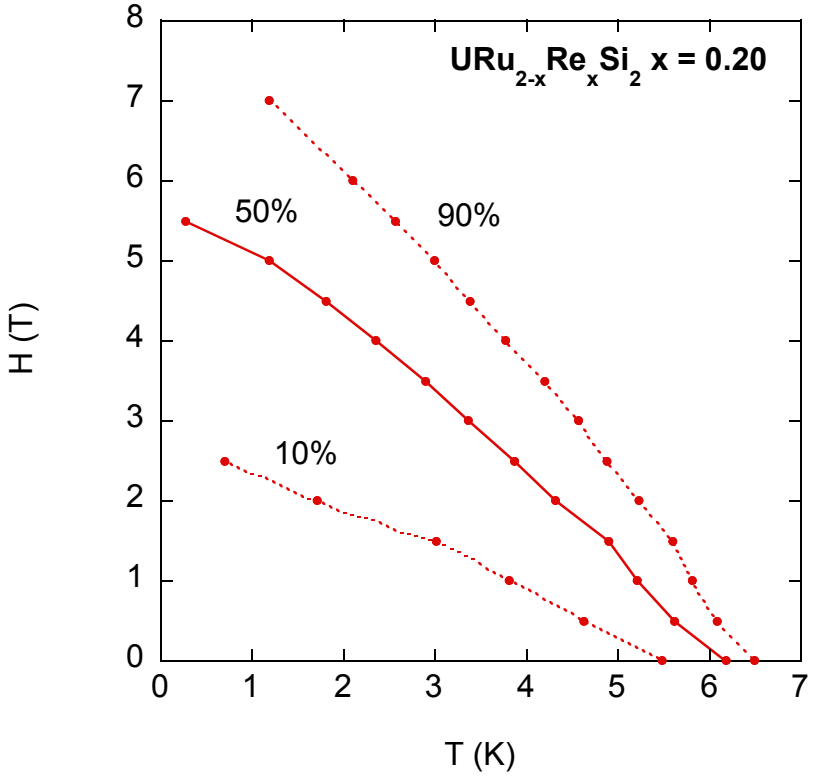

Figure VII.4: Superconducting upper critical field for $x = 0.25$.

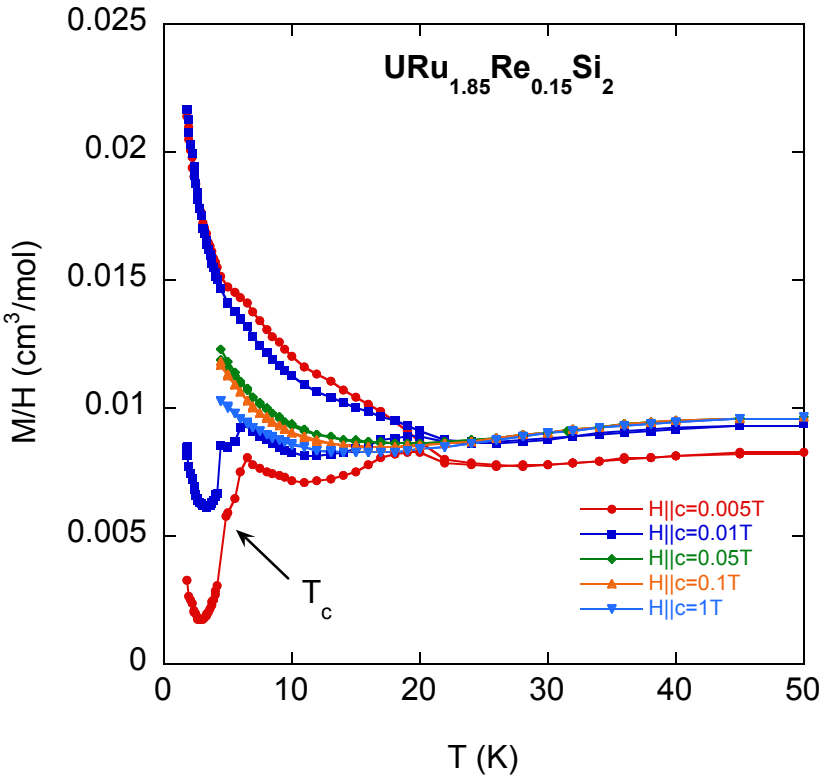

Figure VII.5: $\chi(T)$ exhibiting SC transition for $x = 0.15$. The step at T_c is less than 1% of $\frac{1}{4\pi}$ in the appropriate units.

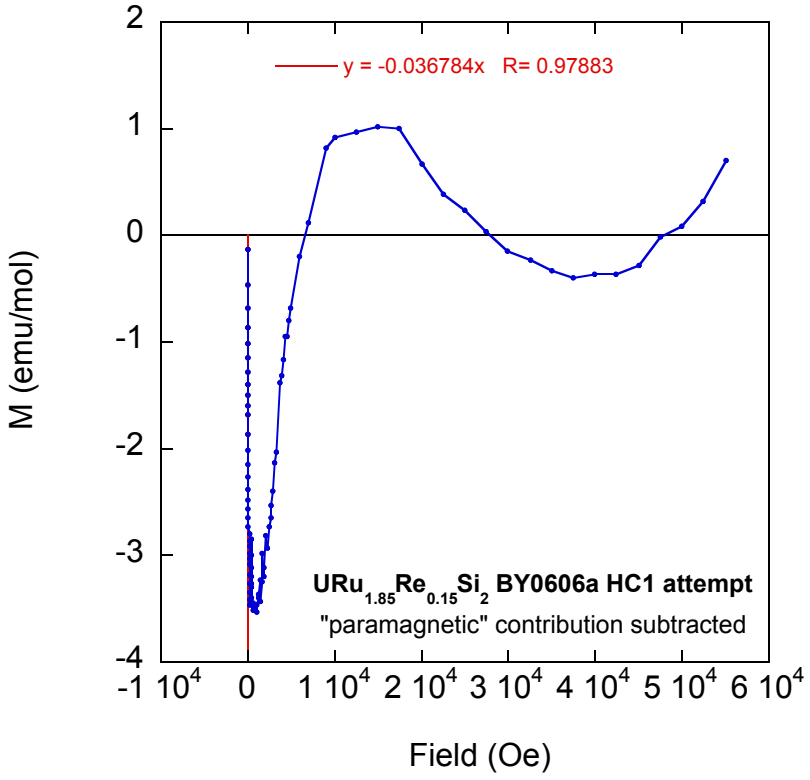

Figure VII.6: Diamagnetism in $M(H)$ for $x = 0.15$ at 2 K. The initial slope is less than 1% of $\frac{1}{4\pi}$.

VII.B Phase Diagram

A consistent picture of the physical properties of $URu_{2-x}Re_xSi_2$ has emerged from measurements of the single crystal samples in this study. One of the most important general features of the phase diagram is its separation into high- and low-T regimes. The high-T regime, characterized by impurity Kondo screening and the onset of Kondo coherence at ~ 100 K, remains relatively unchanged despite appreciable Re substitution by $x = 0.6$. In $\rho(T)$ and $\chi(T)$, the data are qualitatively constant in this data range, although broadening is observed in $\rho(T)$.

The constancy of the high-T single-ion Kondo and coherence energy scales implies that the heavy fermion state is very robust, which is born out by the appreciable values of γ calculated from $C(T)$ data for all x. It is worth noting that applying the Kadowaki-Woods ratio to values of the coefficient of the T^2 term in Eqn. IV.1 yields values of γ ranging from $0.05 - 0.15$ J mol^{-1} K^{-2}, and a similar range of values for γ is obtained by assuming a Wilson-Sommerfeld ratio of 1 and performing a calculation based on the value of χ_0 determined from fits of a Pauli-enhanced CW law, as described in Fig. VI.7. These calculated values compare well with those shown in Fig. V.5, but, despite their consistency, they should only be regarded as order-of-magnitude estimates. Because the heavy fermion state persists over the entire range of x, the Doniach phase diagram cannot be used to explain the low-T properties of the system, even at $x = 0$. That is, the single-ion Kondo T scale is very high and there is no crossover to an RKKY-dominated regime where light-electron magnetic order dominates. That the heavy fermion state is independent of HO has been suggested in high-H measurements of $U(Ru_{1-x}Rh_x)_2Si_2$, where a QCP persists despite the suppression of HO [122].

The combined $T - x$ phase diagram, based on $\rho(T)$, $M(H,T)$, and $C(T)$ measurements, is shown in Fig. VII.7. The roughly defined coherence regime persists for all x and appears to broaden in T as x increases. The ordered phases in the low-T portion of the phase diagram can be considered as arising from the

renormalized heavy quasiparticle bands, as was suggested almost twenty years ago by Dalichaouch and coworkers, who performed their substitution studies in an attempt to tune the Fermi energy through a sharp density of states in URu_2Si_2 [132]. The substitution of Re removes electrons from the system, but for $x > 0.1$, the crystal lattice starts to also stretch along the c-direction. Thus it may be considered that Fermi-level tuning plays a dominant role in the evolution and suppression of the HO phase, but at higher x, changes in the structure of the Fermi surface are probably dominated by the effects of the lattice stretching. The increase of disorder due to Re substitution also seems to play an important role, in that features, such as the coherence maximum and HO transition, broaden with increasing x. That Re substitution increases disorder but does not change energy scales has also been observed in pressure measurements of the HO state for $x < 0.1$, where a critical pressure of 15 kbar is maintained despite a suppression of T_0 with increasing x [106], and similar broadening may be observed in $\rho(H)$ and $M(H)$ measurements in high field [126] .

The effects of the posited Fermi-level tuning on the ordered phases at low x is dramatic, starting with the disappearance of SC. It is possible that the introduction of disorder through chemical substitution is solely responsible for pair-breaking, but at that Re concentration, no other properties seem dramatically affected, that is, unless one considers the small increase in T_0 (Fig. VII.7) and the $\rho(T)$ AFM gap (Fig. IV.13). The antagonistic behavior between the HO and SC states under hydrostatic pressure and uniaxial stress is well established [82, 86, 87, 106, 107] and has been described in terms of two ordered phases competing for the same portion of Fermi surface [82, 106, 107]. It is possible that substitution of less than 1% Re actually enhances the HO phase at the expense of the SC phase. Note that the opposite effect, enhancement of the SC phase at the expense of the HO phase, was seen in the case of Rh and Ir substitution in polycrystalline samples [133]. For $x > 0.02$, T_0 is suppressed, which may be due to the effects of electron removal, disorder, or perhaps the onset of crystal lattice stretching. Based on

Fig. V.7, T_0 and Δ_0 are large at $x = 0.08$, and HO is no longer observed at $x = 0.12$. Measurements of $\rho(T)$ extend the phase boundary to $x = 0.1$ (Fig. VII.7). A similar sharp fall-off is observed with Rh substitution [138]. It might be suggested that the discontinuity in T_0 is indicative of a first order transition, but based on Fig. V.7, the specific heat jump ΔC does extrapolate to 0 at $x = 0.1$, suggesting that there is no large release of S upon leaving the HO phase as x is increased. The only other parameter that seems to extrapolate to 0 at $x = 0.1$ is $\Delta\gamma$, as shown in Fig. V.8. Both $\Delta\gamma$ and Δ_0 are expected to describe a Fermi surface gap, the former as a measure of the fraction gapped, the latter as a measure of the gap size in energy. Contrary to convention, in $URu_{2-x}Re_xSi_2$, Δ_0 and T_0 may not be proportional to the HO parameter. If the HO parameter is proportional to $\Delta\gamma$, then there is a second-order phase transition and quantum critical point at $x = 0.1$. If it is not, then the HO phase terminates abruptly, which might be attributed to the disorder induced by Re substitution. Similarly, the coincidence of the disappearance of HO and the stretching of the crystal lattice may not be accidental, and the change in the Fermi surface induced by the lattice stretching may be what destroys HO. Several measurements are planned to confirm this description: measurement of $\rho(T)$ on $x = 0.12$ to confirm the absence of HO, and measurements of $C(T)$ on $x = 0.02$ and $x = 0.1$ to confirm the x-dependence of Δ_0.

The x-dependence of the properties of the FM phase was discussed at length in Chapter VI. The FM order seems to be itinerant in nature, as it is not marked by anomalies in $C(T)$ and $\rho(T)$, and features a very small M_0 relative to μ_{eff}. Relative to prior studies, the FM instability on the x-axis has been established at the lower value of $x \approx 0.15$, potentially tying the linear x-dependence of T_C to the linear x-dependence of the lattice anisotropy c/a. The appearance of AFM order has already been linked to c/a via hydrostatic pressure and uniaxial stress studies on URu_2Si_2 [93, 98]. In the case of Re substitution, the c-axis lengthens, which may stabilize FM order instead of AFM order.

Alternatively, removal of electrons might lead to a gradual underscreen-

ing of the U moments, which can be arbitrarily underscreened (thus arbitrarily small) and couple to each other via the RKKY interaction carried by the heavy renormalized conduction electrons. The monotonic x-dependence of the power-law exponent n could be associated with this effect. The bulk properties of an FM ordered phase of small underscreened local moments could mimic those of itinerant FM, in that the small size of the moment would lead to small entropy change and thus not appear in $C(T)$ and perhaps cause minimal change to $\rho(T)$ as well.

A lingering question involves the relationship between the $T - x$ phase diagram and the NFL behavior in the system, as quantified in Fig. VII.8. In Ref. [142], the maximal logarithmic divergence in C/T was correlated with the FM QCP. In the present study, the QCP has been identified at lower x, while the NFL phase diagram remains relatively unchanged. The results of the scaled Arrott analysis strongly support the existence of a FM QCP, in that the order parameter M_0 and the ordering temperature T_C are both continuously suppressed to 0. The additional suppression of γ and $\delta - 1$ is equally compelling. Thus the existence of a QCP is not in question, which immediately suggests that logarithmic T-dependence of C/T and power-law T-dependence of ρ are not clearly related to quantum criticality. Arguments against using the logarithmic T-dependence of C/T as a metric for NFL behavior in this system are that it is observed over the entire range of x, and that C/T actually more strongly diverges at lower T. Likewise, no certain explanation exists for the x dependence of the power-law exponent n, which seems to decrease monotonically, becoming more NFL-like deeper into the FM phase. Particularly at high x, where $n < 1$, it seems possible that ρ at low T is dominated by an exceptionally broadened coherence peak. In contrast, at $x = 0.15$, the coherence feature is well defined, and at lower T more conventional power-law T-dependence is recovered. For values of x in between, it appears that $\rho(T)$ can be considered a convolution of the two extremes. A cursory inspection of Fig. IV.1 gives the impression that increasing x serves to 'smear' $\rho(T)$ out in T. Preliminary photoemission studies currently being carried out may help

resolve this issue.

The results of this study accentuate the findings of the previous study of Bauer and coworkers: the $URu_{2-x}Re_xSi_2$ system is very unusual. The anomalous $\rho(T)$ and $C(T)$ observed in polycrystalline samples have been confirmed in nominally cleaner single crystals. A scaling analysis of $M(H,T)$ has revealed some very unusual critical exponents, which do not seem to make good contact with currently available theories of ferromagnetic quantum criticality. In addition, traditional hallmarks of NFL behavior do not seem to show the x-dependence they would be expected to have were they associated with quantum criticality, instead they seem to be associated with other phenomena. It is possible that the expected effects of quantum criticality in $\rho(T)$ and $C(T)$ are lost because of competing contributions from other effects in the system. It is safe to say that the search for quantum criticality in $URu_{2-x}Re_xSi_2$ has been successful, although it seems to have have left us in unfamiliar territory.

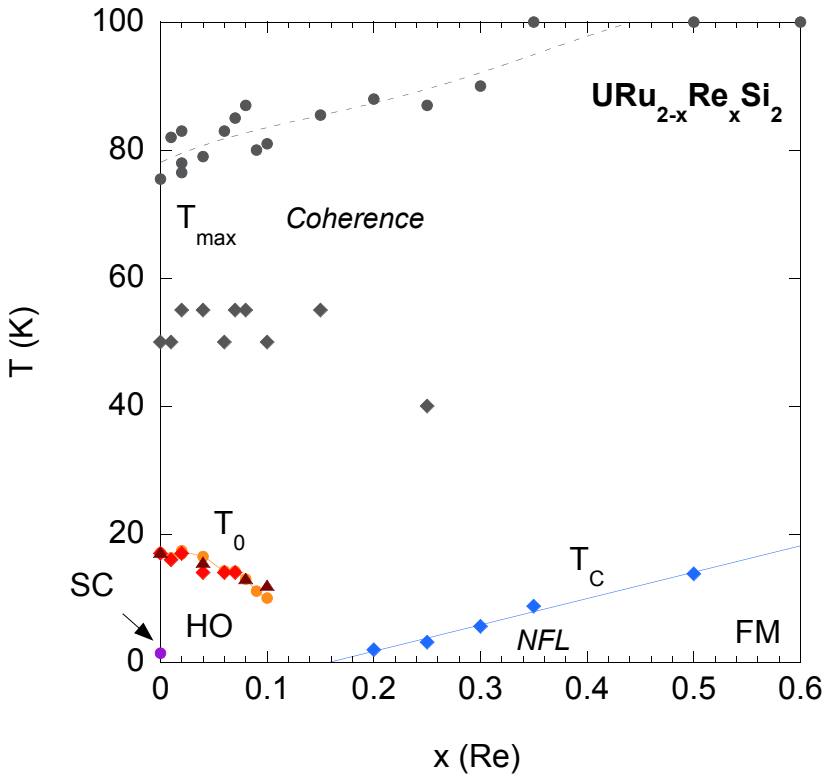

Figure VII.7: $T - x$ phase diagram. Circles are based on $\rho(T)$, diamonds on $M(H,T)$, and triangles on $C(T)$ data.

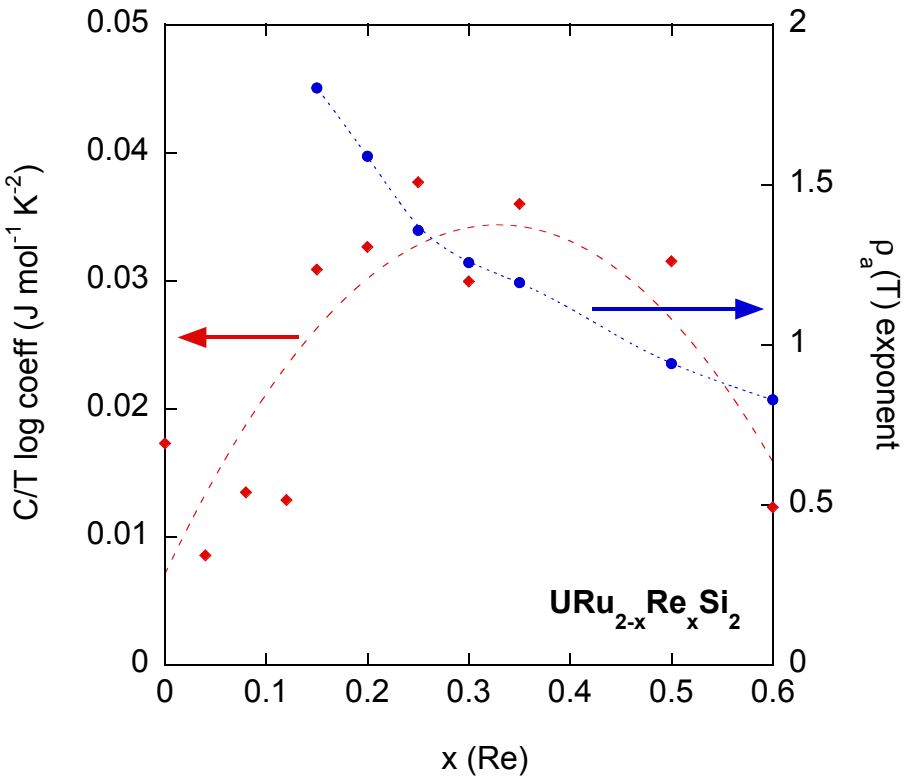

Figure VII.8: NFL phase diagram.These two parameters are considered conventional indicators of NFL behavior.

Bibliography

[1] S. Doniach, Physica B **91**, 231 (1977).

[2] S. Süllow, M. C. Aronson, B. D. Rainford, and P. Haen, Phys. Rev. Lett. **82**, 2964 (1999).

[3] G. R. Stewart, Rev. Mod. Phys. **56**, 755 (1984).

[4] K. Kadowaki and S. B. Woods, Solid State Comm. **58**, 507 (1986).

[5] D. L. Cox, Phys. Rev. Lett. **59**, 1240 (1987).

[6] O. O. Bernal, D. E. MacLaughlin, A. Amato, R. Feyerherm, F. N. Gygax, A. Schenck, R. H. Heffner and L. P. Le, G. J. Nieuwenhuys, B. Andraka, H. v. Löhneysen, O. Stockert, and H. R. Ott, Phys. Rev. B **54**, 13000 (1996).

[7] A. H. Castro Neto, G. Castilla, and B. A. Jones, Phys. Rev. Lett. **81**, 3531 (1998).

[8] M. C. Aronson, R. Osborn, R. A. Robinson, J. W. Lynn, R. Chau, C. L. Seaman, and M. B. Maple, Phys. Rev. Lett. **75**, 725 (1995).

[9] M. B. Maple, C. L. Seaman, D. A. Gajewski, Y. Dalichaouch, V. B. Barbetta, M. C. de Andrade, H. A. Mook, H.G. Lukefahr, O.O. Bernal, and D. E. MacLaughlin, J. Low Temp. Phys. **95**, 225 (1994).

[10] M. B. Maple, M. C. de Andrade, J. Herrmann, Y. Dalichaouch, D. A. Gajewski, C. L. Seaman, R. Chau, R. Movshovieh, M. C. Aronson, and R. Osborn, J. Low Temp. Phys. **99**, 223 (1995).

[11] G. R. Stewart, Rev. Mod. Phys. **73**, 797 (2001).

[12] W. Schlabitz, J. Baumann, J. Diesing, W. Krause, G. Neumann, C. D. Bredl, U. Ahlheim, H. M. Mayer, U. Rauchschwalbe, Poster presented at the Fourth International Conference on Valence Fluctuations ICVF, Cologne 1984 (unpublished).

[13] W. Schlabitz, J. Baumann, B. Pollit, U. Rauchschwalbe, H. M. Mayer, U. Ahlheim, and C. D. Bredl, Z. Phys. B **62**, 171 (1986).

[14] T. T. M. Palstra, A. A. Menovsky, J. van den Berg, A. J. Dirkmaat, P. H. Kes, G. J. Nieuwenhuys, and J. A. Mydosh, Phys. Rev. Lett. **55**, 2727 (1985).

[15] T. T. M. Palstra, A. A. Menovsky, and J. A. Mydosh, Phys. Rev. B **33**, 6527 (1986).

[16] G. Grüner, Rev. Mod. Phys. **60**, 1129 (1988).

[17] G. Grüner, Rev. Mod. Phys. **66**, 1 (1994).

[18] E. Fawcett, Rev. Mod. Phys. **60**, 209 (1988).

[19] M. B. Maple, J. W. Chen, Y. Dalichaouch, T. Kohara, C. Rossel, M. S. Torikachvili, M. W. McElfresh, and J. D. Thompson, Phys. Rev. Lett. **56**, 185 (1986).

[20] U. Walter, C.-K. Loong, M. Loewenhaupt, and W. Schlabitz, Phys. Rev. B **33**, 7875 (1986).

[21] S. L. Cooper, M. V. Klein, M. B. Maple, and M. S. Torikachvili, Phys. Rev. B **36**, 5743 (1987).

[22] M. F. Hundley, L. C. Bourne, A. Zettl, C. Rossel, and M. B. Maple, Solid State Commun. **62**, 603 (1987).

[23] P. Steiner, L. Degiorgi, M.B. Maple, and P. Wachter, Physica B **218**, 173 (1995).

[24] St. Thieme, L. Degiorgi, P. Wachter, Y. Dalichaouch, and M. B. Maple, Physica B **223&224**, 192 (1996).

[25] A. de Visser, F. E. Kayzel, A. A. Menovsky, J. J. M. Franse, J. van den Berg, and G. J. Nieuwenhuys, Phys. Rev. B **34**, 8168 (1986).

[26] T. Kohara, Y. Kohori, K. Asayama, Y. Kitaoka, M.B. Maple, and M.S. Torikachvili, Solid State Commun. **59**, 603 (1986).

[27] J. Schoenes, C. Schönengberger, J. J. M. Franse, and A. A. Menovsky, Phys. Rev. B **35**, 5375 (1987).

[28] C. Broholm, J. K. Kjems, W. J. L. Buyers, P. Matthews, T. T. M. Palstra, A. A. Menovsky, and J. A. Mydosh, Phys. Rev. Lett. **58**, 1467 (1987).

[29] D. E. MacLaughlin, D. W. Cooke, R. H. Heffner, R. L. Hutson, M. W. McElfresh, M. E. Schillaci, H. D. Rempp, J. L. Smith, J. O. Willis, E. Zirngiebl, C. Boekema, R. L. Lichti, and J. Oostens, Phys. Rev. B **37**, 3153 (1988).

[30] E. Holland-Moritz, W. Schlabitz, M. Loewenhaupt, and U. Walter, Phys. Rev. B **39**, 551 (1989).

[31] C. Broholm, H. Lin, P. T. Matthews, T. E. Mason, W. J. L. Buyers, M. F. Collins, A. A. Menovsky, J. A. Mydosh, and J. K. Kjems, Phys. Rev. B **43**, 12809 (1991).

[32] E. D. Isaacs, D. B. McWhan, R. N. Kleiman, D. J. Bishop, G. E. Ice, P. Zschack, B. D. Gaulin, T. E. Mason, J. D. Garrett, and W. J. L. Buyers, Phys. Rev. Lett. **65**, 3185 (1990).

[33] A. P. Ramirez, P. Coleman, P. Chandra, E. Brück, A. A. Menovsky, Z. Fisk, and E. Bucher, Phys. Rev. Lett. **68**, 2680 (1992).

[34] M. B. Walker, W. J. L. Buyers, Z. Tun, W. Que, A. A. Menovsky, and J. D. Garrett, Phys. Rev. Lett. **71**, 2630 (1993).

[35] T. E. Mason, W. J. L. Buyers, T. Petersen, A. A. Menovsky, and J. D. Garrett, J. Phys.: Condens. Matter **7**, 5089 (1995).

[36] W. J. L. Buyers, Physica B **223&224**, 9-14 (1996).

[37] J. G. Rodrigo, F. Guinea, S. Vieira, and F. G. Aliev, Phys. Rev. B **55**, 14318 (1997).

[38] G. M. Luke, A. Keren, L. P. Le, Y. J. Uemura, W. D. Wu, D. Bonn, L. Taillefer, J. D. Garrett, and Y. Ōnuki, Hyperfine Interact. **85**, 397 (1994).

[39] O. O. Bernal, B. Becker, J. A. Mydosh, G. J. Nieuwenhuys, A. A. Menovsky, P. M. Paulus, H. B. Brom, D. E. MacLaughlin, and H. G. Lukefahr, Physica B **281&282**, 236 (2000).

[40] O. O. Bernal, C. Rodrigues, A. Martinez, H. G. Lukefahr, D. E. MacLaughlin, A. A. Menovsky and J. A. Mydosh, Phys. Rev. Lett. **87**, 196402 (2001).

[41] O. O. Bernal, J. Mydosh, D. E. MacLaughlin, H. Lukefahr, and A. A. Menovsky, Physica B **312&313**, 501 (2002).

[42] C. R. Wiebe, G. M. Luke, Z. Yamani, A. A. Menovsky, and W. J. L. Buyers, Phys. Rev. B **69**, 132418 (2004).

[43] C. R. Wiebe, J. A. Janik, G. J. MacDougall, G. M. Luke, J. D. Garrett, H. D. Zhou, Y.-J. Jo, L. Balicas, Y. Qiu, J. R. D. Copley, Z. Yamani, and W. J. L. Buyers, Nat. Phys. **3**, 96 (2007).

[44] S. Saitoh, S. Takagi, M. Yokoyama, and H. Amitsuka, J. Phys. Soc. Jpn. **74**, 2209 (2005).

[45] S. Takagi, S. Ishihara, S. Saitoh, H. Sasaki, H. Tanida, M. Yokoyama, and H. Amitsuka, J. Phys. Soc. Jpn. **76**, 033708 (2007).

[46] R. Bel, H. Jin, K. Behnia, J. Flouquet, and P. Lejay, Phys. Rev. B **70**, 220501 (2004).

[47] K. Behnia, R. Bel, Y. Kasahara, Y. Nakajima, H. Jin, H. Aubin, K. Izawa, Y. Matsuda, J. Flouquet, Y. Haga, Y. Ōnuki, and P. Lejay, Phys. Rev. Lett. **94**, 156405 (2005).

[48] P. A. Sharma, N. Harrison, M. Jaime, Y. S. Oh, K. H. Kim, C. D. Batista, H. Amitsuka, and J. A. Mydosh, Phys. Rev. Lett. **97**, 156401 (2006).

[49] W. K. Kwok, L. E. DeLong, G. W. Crabtree, D. G. Hinks, and R. Joynt, Phys. Rev. B **41**, 11649 (1990).

[50] K. Behnia, D. Jaccard, J. Sierro, P. Lejay, and J. Flouquet, Physica C **196**, 57 (1992).

[51] K. Hasselbach, J. R. Kirtley, and P. Lejay, Phys. Rev. B **46**, 5826 (1992).

[52] P. Visani, Y. Dalichaouch, M. A. Lopez de la Torre, B. W. Lee, C. L. Seaman, and M. B. Maple, Phys. Rev. B **49**, 4376 (1994).

[53] J. P. Brison, N. Keller, P. Lejay, A. Huxley, L. Schmidt, A. Buzdin, N. R. Bernhoeft, I. Mineev, A. N. Stepanov, J. Flouquet, D. Jaccard, S. R. Julian, and G. G. Lonzarich, Physica B **199&200**, 70 (1994).

[54] J. P. Brison, N. Keller, A. Vernière, P. Lejay, L. Schmidt, A. Buzdin, J. Flouquet, S. R. Julian, and G. G. Lonzarich, Physica C **250**, 128 (1995).

[55] N. H. van Dijk, A. de Visser, J. J. M. Franse, and A. A. Menovsky, Phys. Rev. B **51**, 12665 (1995).

[56] K. Matsuda, Y. Kohori, and T. Kohara, J. Phys. Soc. Jpn. **65**, 679, (1995).

[57] K. Tenya, M. Ikeda, T. Tayama, K. Kuwahara, H. Amitsuka, T. Sakakibara, E. Yamamoto, K. Maezawa, N. Kimura, R. Settai, Y. Onuki, Physica B **230-232**, 345 (1997).

[58] Y. Kasahara, T. Iwasawa, H. Shishido, T. Shibauchi, K. Behnia, Y. Haga, T. D. Matsuda, Y. Onuki, M. Sigrist, and Y. Matsuda, Phys. Rev. Lett. **99**, 116402 (2007).

[59] T. Sakakibara, A. Yamada, J. Custers, K. Yano, T. Tayama, H. Aoki, and K. Machida, J. Phys. Soc. Jpn. **76**, 051004 (2007).

[60] K. Yano, T. Sakakibara, T. Tayama, M. Yokoyama, H. Amitsuka, Y. Homma, P. Miranović, M. Ichioka, Y. Tsutsumi, and K. Machida, Phys. Rev. Lett. **100**, 017004 (2008).

[61] R. Okazaki, Y. Kasahara, H. Shishido, M. Konczykowski, K. Behnia, Y. Haga, T. D. Matsuda, Y. Onuki, T. Shibauchi, and Y. Matsuda, Phys. Rev. Lett. **100**, 037004 (2008).

[62] M.A. López de la Torre, S. Vieira, R. Villar, M. B. Maple, and M.S. Torikachvili, Physica B **165&166**, 385 (1990).

[63] K. Hasselbach, P. Lejay, and J. Flouquet, Phys. Lett. A **156**, 313 (1991).

[64] A. P. Ramirez, T. Siegrist, T. T. M. Palstra, J. D. Garrett, E. Bruck, A. A. Menovsky, and J. A. Mydosh, Phys. Rev. B **44**, 5392 (1991).

[65] S. B. Roy, A. K. Pradhan, and P. Chaddah, J. Phys.: Condens. Matter **6**, 253 (1994).

[66] J.-G. Park, H.-C. Ri, K. Kuwahara, and H. Amitsuka, J. Magn. Magn. Mater. **177-181**, 455 (1998).

[67] B. Fåk, C. Vettier, J. Flouquet, F. Bourdarot, S. Raymond, A. Vernière, P. Lejay, Ph. Boutrouille, N.R. Bernhoeft, S.T. Bramwell, R.A. Fisher, and N.E. Phillips, J. Magn. Magn. Mater. **154**, 339 (1996).

[68] J.-G. Park, K. A. McEwen, S. de Brion, G. Chouteau, H. Amitsuka, and T. Sakakibara, J. Phys.: Condens. Matter **9**, 3065 (1997).

[69] O. O. Bernal, M. E. Moroz, K. Ishida, H. Murakawa, A. P. Reyes, P. L. Kuhns, D. E. MacLaughlin, J. A. Mydosh, and T. J. Gortenmulder, Physica B **378-380**, 574 (2006).

[70] P. Santini and G. Amoretti, Phys. Rev. Lett. **73**, 1027 (1994).

[71] P. Santini, Phys. Rev. B **57**, 5191 (1998).

[72] A. Kiss and P. Fazekas, Phys. Rev. B **71**, 054415 (2005).

[73] P. Chandra, P. Coleman, J. A. Mydosh, and V. Tripathi, Nature **417**, 831 (2002).

[74] J. A. Mydosh, P. Chandra, P. Coleman, and V. Tripathi, Acta Phys. Pol. B **34**, 0659 (2003).

[75] V. Tripathi, P. Chandra, and P. Coleman, J. Phys.: Condens. Matter **17**, 5825 (2005).

[76] V. P. Mineev and M. E. Zhitomirsky, Phys. Rev. B **72**, 014432 (2005).

[77] C. M. Varma and L. Zhu, Phys. Rev. Lett. **96**, 036405 (2006).

[78] F. R. de Boer, J. J. M. Franse, E. Louis, A. A. Menovsky, J. A. Mydosh, T. T. M. Palstra, U. Rauchschwalbe, W. Schlabitz, F. Steglich, and A. de Visser, Physica **138B**, 1 (1986).

[79] E. Louis, A. de Visser, A. Menovsky and J. J. M. Franse, Physica **144B**, 48 (1986).

[80] Y. Ōnuki, T. Yamazaki, I. Ukon, T. Omi, K. Shibutani, T. Komatsubara, I. Sakamoto, Y. Sugiyama, R. Onodera, K. Yonemitsu, A. Umezawa, W. K. Kwok, G. W. Crabtree, and D. G. Hinks, Physica **148B**, 29 (1987).

[81] R. A. Fisher, S. Kim, Y. Wu, N. E. Phillips, M. W. McElfresh, M. S. Torikachvili, and M. B. Maple, Physica B **163**, 419 (1990).

[82] M. W. McElfresh, J. D. Thompson, J. O. Willis, M. B. Maple, T. Kohara, and M. S. Torikachvili, Phys. Rev. B **35**, 43 (1987).

[83] Y. Uwatoko, K. Iki, G. Oomi, Y. Ōnuki, and T. Komatsubara, Physica B **177**, 147 (1992).

[84] M. Ido, Y. Segawa, H. Amitsuka, and Y. Miyako, J. Phys. Soc. Jpn. **62**, 2962 (1993).

[85] J. P. Brison, N. Keller, P. Lejay, A. Huxley, L. Schmidt, A. Buzdin, N. R. Bernhoeft, I. Mineev, A. N. Stepanov, J. Flouquet, D. Jaccard, S. R. Julian, and G. G. Lonzarich, Physica B **199&200**, 70 (1994).

[86] K. Bakker, A. de Visser, E. Brück, A. A. Menovsky, and J. J. M. Franse, J. Magn. Magn. Mater. **108**, 63 (1992).

[87] A. Guillaume, B. Salce, J. Flouquet, and P. Lejay, Physica B **259-261**, 652 (1999).

[88] H. Amitsuka, M. Sato, N. Metoki, M. Yokoyama, K. Kuwahara, T. Sakakibara, H. Morimoto, S. Kawarazaki, Y. Miyako, and J. A. Mydosh, Phys. Rev. Lett. **83**, 5114 (1999).

[89] K. Matsuda, Y. Kohori, T. Kohara, K. Kuwahara and H. Amitsuka, Phys. Rev. Lett. **87**, 087203 (2001).

[90] K. Matsuda, Y. Kohori, T. Kohara, H. Amitsuka, K. Kuwahara, and T. Matsumoto, J. Phys.: Condens. Matter **15**, 2363 (2003).

[91] H. Amitsuka, K. Tenya, M. Yokoyama, A. Schenck, D. Andreica, F. N. Gygax, A. Amato, Y. Miyako, Ying Kai Huang, J. A. Mydosh, Physica B **326**, 418 (2003).

[92] A. Amato, M. J. Graf, A. de Visser, H. Amitsuka, D. Andreica, and A. Schenck, J. Phys.: Condens. Matter **16**, S4403 (2004).

[93] G. Motoyama, T. Nishioka, and N. K. Sato, Phys. Rev. Lett. **90**, 166402 (2003).

[94] S. Uemura, G. Motoyama, Y. Oda, T. Nishiokak, and N. K. Sato, J. Phys. Soc. Jpn. **74**, 267 (2005).

[95] N. K. Sato, S. Uemura, G. Motoyama, and T. Nishioka, Physica B **378-380**, 576 (2006).

[96] F. Bourdarot, B. Fåk, V. P. Mineev, M. E. Zhitomirsky, N. Kernavanois, S. Raymond, F. Lapierre, P. Lejay, and J. Flouquet, Physica B **350**, e179 (2004).

[97] F. Bourdarot, A. Bombardi, P. Burlet, M. Enderle, J. Flouquet, P. Lejay, N. Kernavanois, V. P. Mineev, L. Paolasini, M. E. Zhitomirsky, and B. Fåk, Physica B **359-361**, 986 (2005).

[98] M. Yokoyama, H. Amitsuka, K. Tenya, K. Watanabe, S. Kawarazaki, H. Yoshizawa, and J. A. Mydosh, Phys. Rev. B **72**, 214419 (2005).

[99] C. Pfleiderer, J. A. Mydosh, and M. Vojta, Phys. Rev. B **74**, 104412 (2006).

[100] G. Knebel, K. Izawa, F. Bourdarot, E. Hassinger, B. Salce, D. Aoki, and J. Flouquet, J. Magn. Magn. Mater. **310**, 195 (2007).

[101] H. Amitsuka, K. Matsuda, I. Kawasaki, K. Tenya, M. Yokoyama, C. Sekine, N. Tateiwa, T. C. Kobayashi, S. Kawarazaki, and H. Yoshizawa, J. Magn. Magn. Mater. **310**, 214 (2007).

[102] K. Matsuda, M. Yokoyama, K. Tenya, H. Amitsuka, and H. Yoshizawa, J. Magn. Magn. Mater. **310**, 337 (2007).

[103] E. Hassinger, G. Knebel, K. Izawa, P. Lejay, B. Salce, and J. Flouquet, Phys. Rev. B **77**, 115117 (2008).

[104] M. Nakashima, H. Ohkuni, Y. Inada, R. Settai, Y. Haga, E. Yamamoto, and Y. Ōnuki, J. Phys.: Condens. Matter **15**, S2011 (2003).

[105] K. Tenya, I. Kawasaki, K. Tameyasu, S. Yasuda, M. Yokoyama, H. Amitsuka, N. Tateiwa, and T. C. Kobayashi, Physica B **359-361**, 1135 (2005).

[106] J. R. Jeffries, N. P. Butch, B. T. Yukich, and M. B. Maple, Phys. Rev. Lett. **99**, 217207 (2007).

[107] J. R. Jeffries, N. P. Butch, B. T. Yukich, and M. B. Maple, J. Phys.: Condens. Matter **20**, 095225 (2008).

[108] Y. J. Jo, L. Balicas, C. Capan, K. Behnia, P. Lejay, J. Flouquet, J. A. Mydosh, and P. Schlottmann, Phys. Rev. Lett. **98**, 166404 (2007).

[109] H. Amitsuka, K. Matsuda, M. Yokoyama, I. Kawasaki, S. Takayama, Y. Ishihara, K. Tenya, N. Tateiwa, T. C. Kobayashi, and H. Yoshizawa, Physica B **403**, 925 (2008).

[110] N. P. Butch, J. R. Jeffries, D. A. Zocco, and M. B. Maple, submitted to Phys. Rev. B (2008).

[111] A. de Visser, F. R. de Boer, A. A. Menovsky and J. J. M. Franse, Solid State Commun. **64**, 527 (1987).

[112] K. Bakker, A. de Visser, A. A. Menovsky and J .J. M. Franse, Physica B **186-188**, 720 (1993).

[113] K. Sugiyama, M. Nakashima, H. Ohkuni, K. Kindo, Y. Haga, T. Honma, E. Yamamoto, and Y. Ōnuki, J. Phys. Soc. Jpn. **68**, 3394 (1999).

[114] T. Inoue, K. Kindo, H. Okuni, K. Sugiyama, Y. Haga, E. Yamamoto, T. C. Kobayashi, Y. Uwatoko, and Y. Onuki, Physica B **294-295**, 271 (2001).

[115] F. Bourdarot, B. Fåk, K. Habicht, and K. Prokeš, Phys. Rev. Lett. **90**, 067203 (2003).

[116] M. Jaime, K. H. Kim, G. Jorge, S. McCall, and J. A. Mydosh, Phys. Rev. Lett. **89**, 287201 (2002).

[117] J. S. Kim, D. Hall, P. Kumar, and G. R. Stewart, Phys. Rev. B **67**, 014404 (2003).

[118] N. Harrison, M. Jaime, and J. A. Mydosh, Phys. Rev. Lett. **90**, 096402 (2003).

[119] N. Harrison, K.H. Kim, M. Jaime, and J.A. Mydosh, Physica B **346-347**, 92 (2004).

[120] A. Suslov, J. B. Ketterson, D. G. Hinks, D. F. Agterberg, and B. K. Sarma, Phys. Rev. B **68**, 020406R (2003).

[121] K. H. Kim, N. Harrison, M. Jaime, G. S. Boebinger, and J. A. Mydosh, Phys. Rev. Lett. **91**, 256401 (2003).

[122] K. H. Kim, N. Harrison, H. Amitsuka, G. A. Jorge, M. Jaime, and J. A. Mydosh, Phys. Rev. Lett. **93**, 206402 (2004).

[123] A.V. Silhanek, N. Harrison, C. D. Batista, M. Jaime, A. Lacerda, H. Amitsuka, and J. A. Mydosh, Phys. Rev. Lett. **95**, 026403 (2005).

[124] Y. S. Oh, Kee Hoon Kim, P. A. Sharma, N. Harrison, H. Amitsuka, and J. A. Mydosh, Phys. Rev. Lett. **98**, 106401 (2007).

[125] K. H. Kim, Y. S. Oh, P. A. Sharma, N. Harrison, H. Amitsuka, and J. A. Mydosh, Physica B **403**, 721 (2008).

[126] S. Francoual, N. P. Butch, N. Harrison, M. Jaime, A. Lacerda, and M. B. Maple, unpublished.

[127] H. Ohkuni, T. Ishida, Y. Inada, Y. Haga, E. Yamamoto, Y. Ōnuki, and S. Takahashi, J. Phys. Soc. Jpn. **66**, 945 (1997).

[128] C. Bergemann, S. R. Julian, G. J. McMullan, B. K. Howard, G. G. Lonzarich, P. Lejay, J. P. Brison, J. Flouquet, Physica B **230-232**, 348 (1997).

[129] H. Ohkuni, Y. Inada, Y. Tokiwa, K. Sakurai, R. Settai,T. Honma,Y. Haga, E. Yamamoto, Y. Onuki, H. Yamagami, S. Takahashi, and T. Yanagisawa, Phil. Mag. B **79**, 1045 (1999).

[130] Y. Inada and Y. Ōnuki, Low Temp. Phys. **25**, 573 (1999).

[131] J. D. Denlinger, G.-H. Gweon, J. W. Allen, C. G. Olson, M. B. Maple, J. L. Sarrao, P. E. Armstrong, Z. Fisk, and H. Yamagami, J. Electron Spectrosc. **117-118**, 347 (2001).

[132] Y. Dalichaouch, M. B. Maple, M. S. Torikachvili, and A. L. Giorgi, Phys. Rev. B **39**, 2423 (1989).

[133] Y. Dalichaouch, M. B. Maple, J. W. Chen, T. Kohara, C. Rossel, M. S. Torikachvili, and A. L. Giorgi, Phys. Rev. B **41**, 1829 (1990).

[134] Y. Dalichaouch, M. B. Maple, R. P. Guertin, M. V. Kuric, M. S. Torikachvili, and A. L. Giorgi, Physica B **163**, 113 (1990).

[135] Y. Miyako, T. Kuwai, T. Taniguchi, S. Kawarazaki, H. Amitsuka, and T. Sakakibara, J. Magn. Magn. Mater. **108**, 190 (1992).

[136] Y. Kohori, Y. Noguchi, T. Kohara, K. Asayama, H. Amitsuka, and Y. Miyako, Solid State Commun. 82, 479 (1992).

[137] S. Kawarazaki, Y. Kobashi, T. Taniguchi, Y. Miyako, and H. Amitsuka, J. Phys. Soc. Jpn. **63**, 716 (1994).

[138] M. Yokoyama, H. Amitsuka, S. Itoh, I. Kawasaki, K. Tenya, and H. Yoshizawa, J. Phys. Soc. Jpn. **73**, 545 (2004).

[139] M. Yokoyama, H. Amitsuka, S. Itoh, I. Kawasaki, K. Tenya, and H. Yoshizawa, Physica B **359-361**, 1129 (2005).

[140] M. S. Torikachvili, L. Rebelsky, K. Motoya, S. M. Shapiro, Y. Dalichaouch, and M. B. Maple, Phys. Rev. B **45**, 2262 (1992).

[141] Y. Kohori, Y. Noguchi, T. Kohara, Y. Dalichaouch, M. A. Lopez de la Torre, and M. B. Maple, Physica B **186-188**, 792 (1993).

[142] E. D. Bauer, V. S. Zapf, P.-C. Ho, N. P. Butch, E. J. Freeman, C. Sirvent, and M. B. Maple, Phys. Rev. Lett. **94**, 046401 (2005).

[143] E. D. Bauer, PhD dissertation, University of California, San Diego (2002).

[144] V. V. Krishnamurthy, D. T. Adroja, N. P. Butch, R. Osborn, S. K. Sinha, J. L. Robertson, M. C. Aronson, S. E. Nagler, M. B. Maple, unpublished.

[145] J. Czochralski, Z. Phys. Chem. **92**, 219 (1918).

[146] G. K. Teal and J. B. Little, Phys. Rev. **78**, 647 (1950).

[147] G. K. Teal, M. Sparks, and E. Buehler, Phys. Rev. **81**, 637 (1951).

[148] C. W. Chu, W. L. McMillan, and H. L. Luo, Phys. Rev. B **3**, 3757 (1971).

[149] XLAT - Least Squares Refinement of Cell Constants, B. Rupp, Scripta Metall. **22**, I (1988).

[150] CrystalMaker 7, CrystalMaker Ltd.

[151] OrientExpress 3.3, J. Laugier.

[152] J. R. Jeffries, N. A. Frederick, E. D. Bauer, H. Kimura, V. S. Zapf, K.-D. Hof, T. A. Sayles, and M. B. Maple, Phys. Rev. B **72**, 024551 (2005).

[153] J. Paglione, T. A. Sayles, P.-C. Ho, J. R. Jeffries, and M. B. Maple, Nat. Phys. **3**, 703 - 706 (2007).

[154] R. P. Dickey, V. S. Zapf, P.-C. Ho, E. J. Freeman, N. A. Frederick, and M. B. Maple, Phys. Rev. B **68**, 104404 (2003).

[155] M. Tinkham, *Introduction to Superconductivity*, Second Edition, Dover Publications, 2004.

[156] H. G. Lukefahr, O. O. Bernal, D. E. MacLaughlin, C. L. Seaman, M. B. Maple, and B. Andraka, Phys. Rev. B **52**, 3038 (1995).

[157] K. A. Gschneidner, Jr., J. Magn. Magn. Mater. **47&48**, 57 (1985).

[158] W. J. L. Buyers, J. Magn. Magn. Mater. **47&48**, 602 (1985).

[159] S. Gregory, Phys. Rev. Lett. **39**, 1035 (1977).

[160] Quantum Design MPMS Application Note **1014-210B** (1997).

[161] A. Arrott and J. E. Goldman, Phys. Rev. **108**, 948 (1957).

[162] R. Caciuffo, G. Amoretti, P. Santini, G. H. Lander, J. Kulda, and P. de V. Du Plessis, Phys. Rev. B **59**, 13892 (1999).

[163] A. Arrott and J. E. Noakes, Phys. Rev. Lett. **19**, 786 (1967).

[164] S. Blundell, *Magnetism in Condensed Matter*, Oxford University Press, 2006.

[165] P. M. Chaikin and T. C. Lubensky, *Principles of Condensed Matter Physics*, Cambridge University Press, 2000.

[166] W. M. Yuhasz, N. A. Frederick, P.-C. Ho, N. P. Butch, B. J. Taylor, T. A. Sayles, M. B. Maple, J. B. Betts, A. H. Lacerda, P. Rogl, and G. Giester, Phys. Rev. B **71**, 104402 (2005).

[167] N. P. Butch, W. M. Yuhasz, P.-C. Ho, J. R. Jeffries, N. A. Frederick, T. A. Sayles, X. G. Zheng, M. B. Maple, J. B. Betts, A. H. Lacerda, F. M. Woodward, J. W. Lynn, P. Rogl, and G. Giester, Phys. Rev. B **71**, 214417 (2005).

[168] A. Belayachi, J. L. Dormann, and M Noguès, J. Phys.: Condens. Matter **10**, 1599 (1998).

[169] S. Ubaid-Kassis and A. Schroeder, Physica B **403**, 1325 (2008).

[170] R. B. Laughlin and D. Pines, P. Natl. Acad. Sci. **97**, 28 (2000).

[171] R. B. Laughlin, G. G. Lonzarich, P. Monthoux, and David Pines, Adv. Phys. **50**, 361 (2001).

[172] D. Belitz and T. R. Kirkpatrick, J. Phys.: Condens. Matter **8**, 9707 (1996).

[173] A. Aharoni, J. Magn. Magn. Mater. **58**, 297 (1986).

[174] I. Yeung, R. M. Roshko, and G. Williams, Phys. Rev. B **34**, 3456 (1986).

[175] A. V. Chubukov, C. Pépin, and J. Rech, Phys. Rev. Lett. **92**, 147003 (2004).

[176] D. Belitz, T. R. Kirkpatrick, M. T. Mercaldo, and S. L. Sessions, Phys. Rev. B **63**, 174427 (2001).

[177] D. Belitz, T. R. Kirkpatrick, M. T. Mercaldo, and S. L. Sessions, Phys. Rev. B **63**, 174428 (2001).

[178] I. R. Walker, F. M. Grosche, D. M. Freye, and G. G. Lonzarich, Physica C **282-287**, 303 (1997)

[179] S. S. Saxena, P. Agarwal, K. Ahilan, F. M. Grosche, R. K. W. Haselwimmer, M. J. Steiner, E. Pugh, I. R. Walker, S. R. Julian, P. Monthoux, G. G. Lonzarich, A. Huxley, I. Sheikin, D. Braithwaite, and J. Flouquet, Nature **406**, 587 (2000).

[180] D. Jaccard, A. T. Holmesa, G. Behrb, Y. Inadac, and Y. Onuki, Phys. Lett. A **299**, 282 (2002).

[181] G. R. Stewart and A. L. Giorgi, Solid State Commun. **28**, 969 (1978).